Gravitational Wave Astrophysics: Instrumentation, Detector Characterization, and a Search for Gravitational Signals from Gamma-ray Bursts

Daniel Hoak

Dissertation Presentation - July 28 2015

Highlights of the Thesis

Precision measurements of optical cavities

Optics Express **23** (2015) 19417

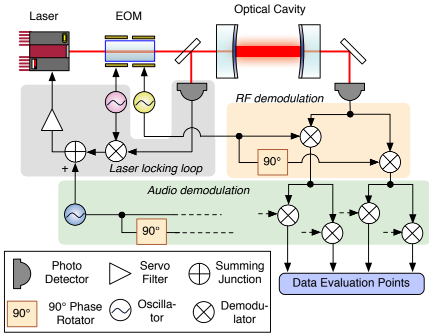

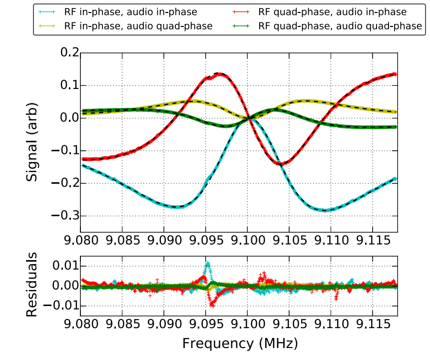

Advanced LIGO Commissioning & Characterization of the H1 OMC

Class. Quantum Gravity **34** 245010 (2015), & OMC paper in prep.

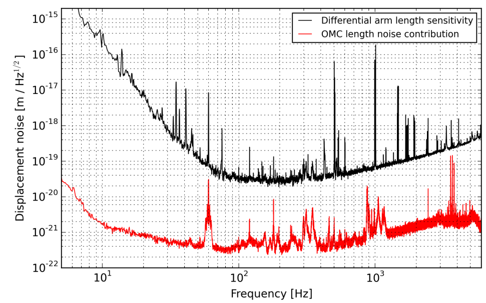

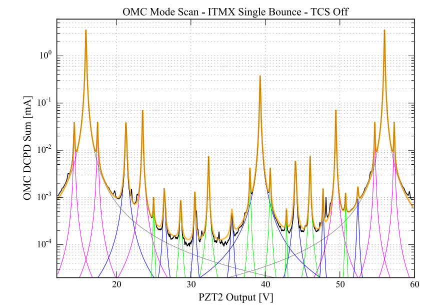

Novel techniques for detector characterization

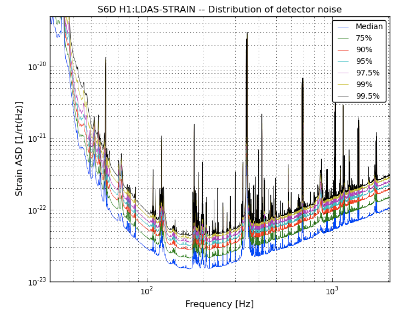

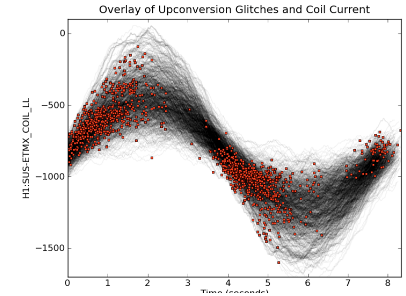

A search for gravitational waves associated with GRBs, and sky localization for potential GW signals

Phys. Rev. D **89** (2014) 122004

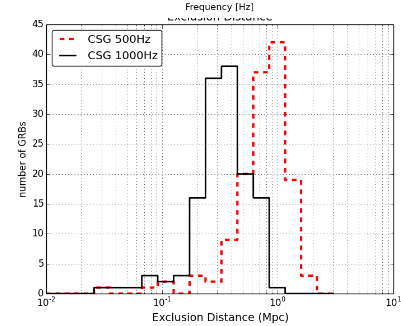

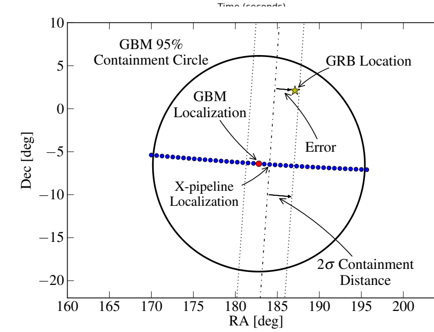

The Detectors: Transducers for Strain, Antennas for GWs

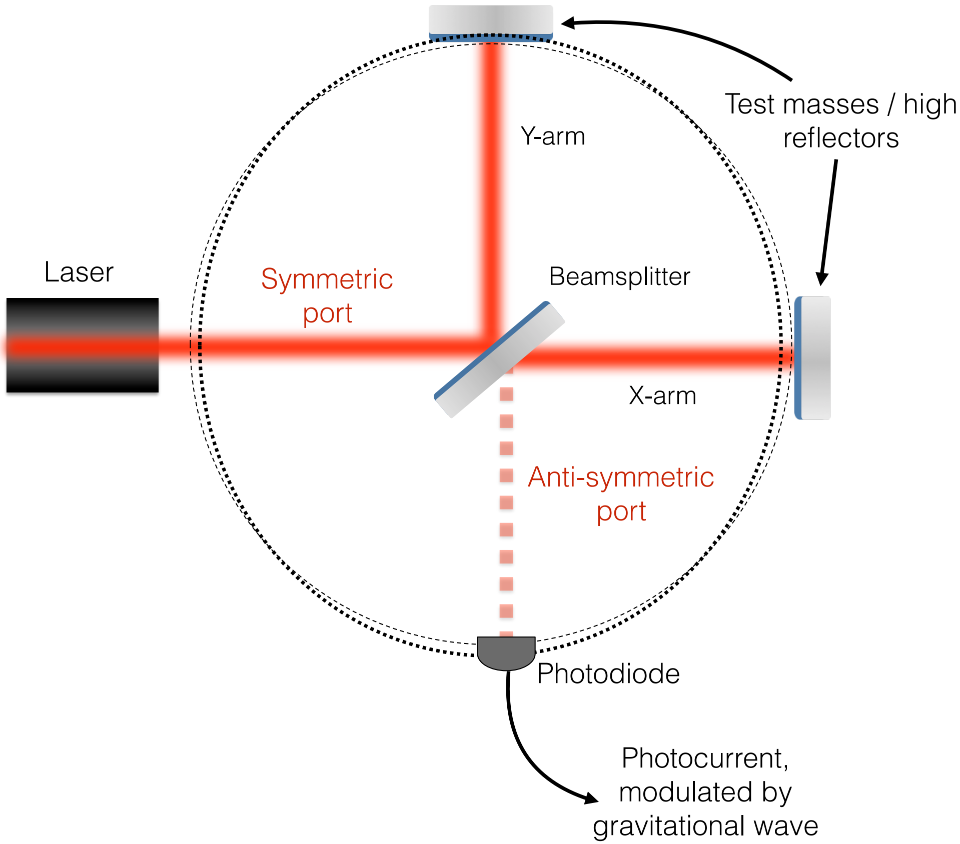

$$\Box \tilde{h}_{\mu\nu} = -\frac{16\pi G}{c^4} T_{\mu\nu}$$

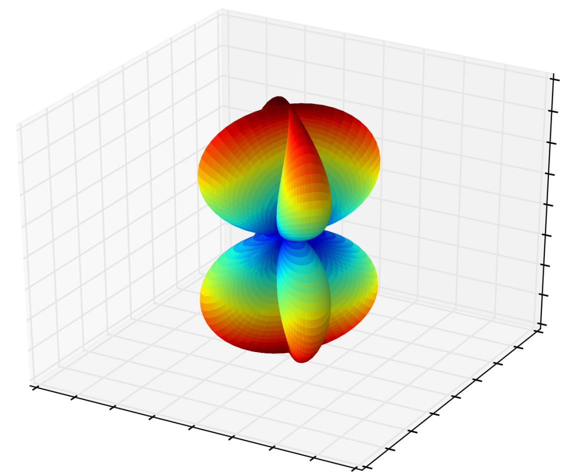

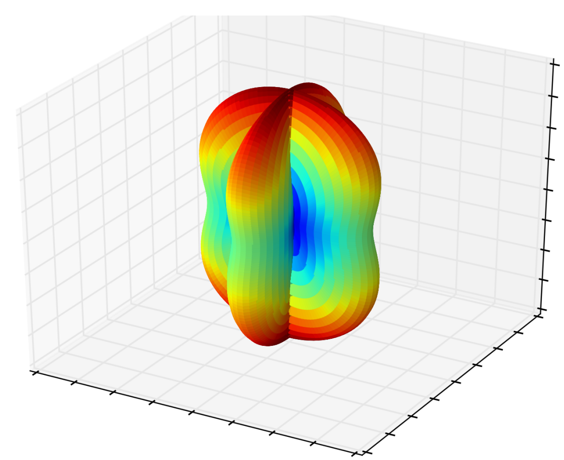

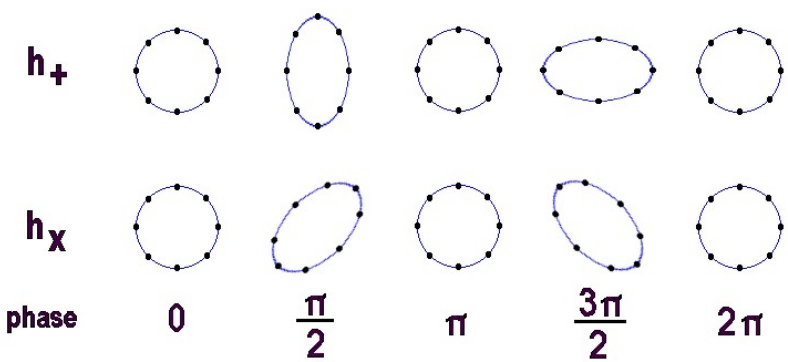

The Global Network of Gravitational Wave Detectors

The Initial Detector Era - Timeline of Observing Runs

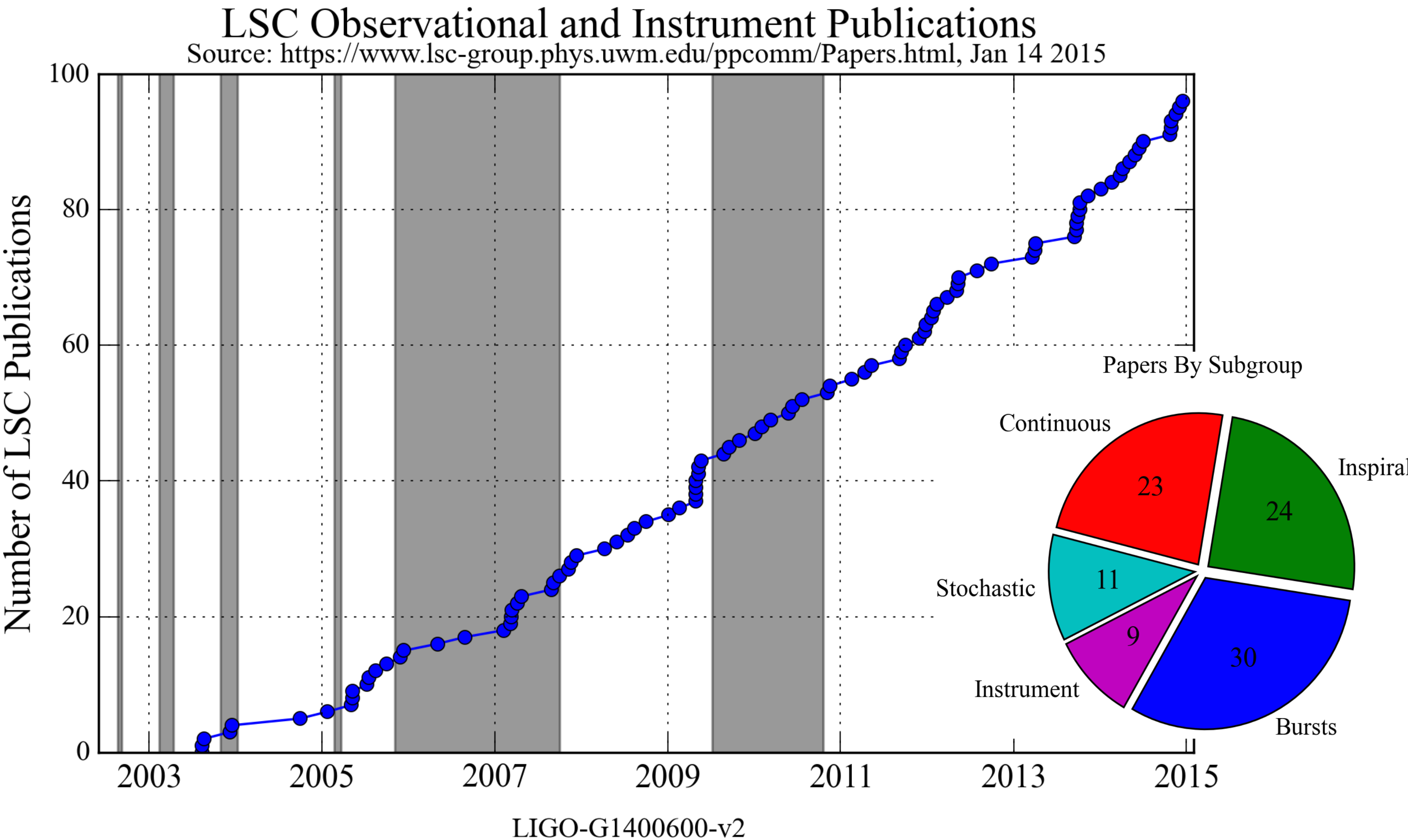

Optics

Optical Resonators

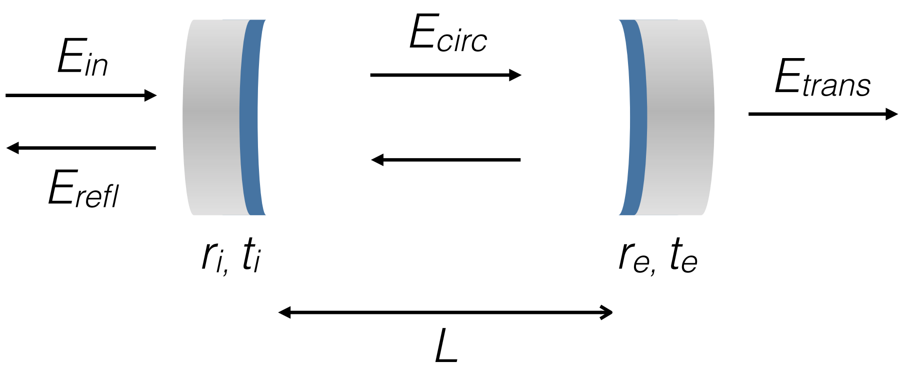

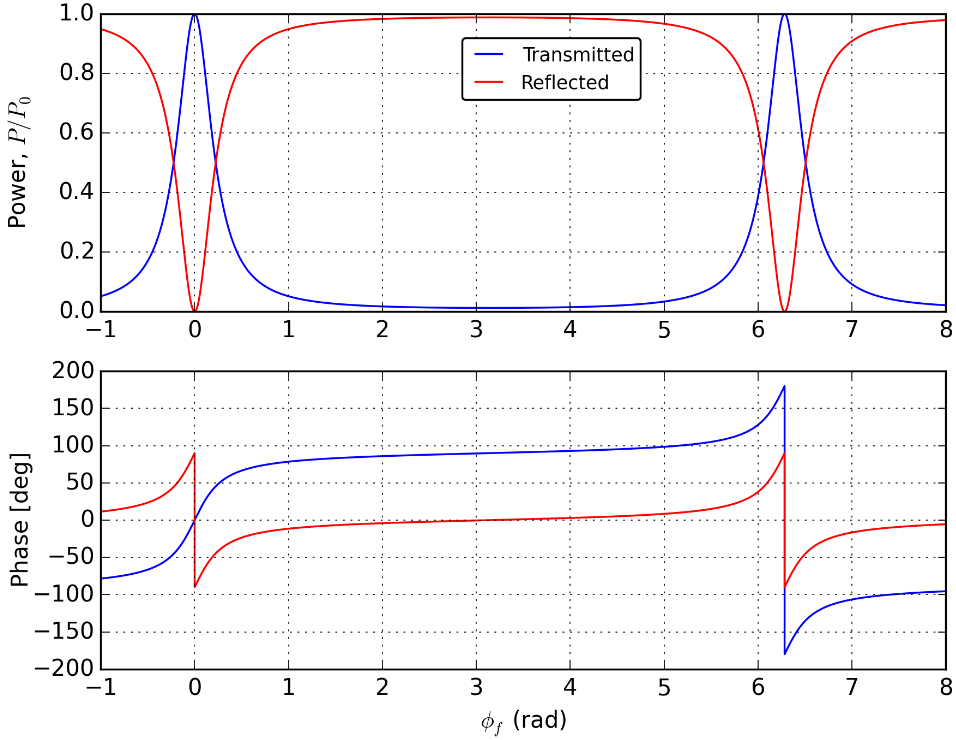

$$E_{refl} = E_0 \frac{(r_e e^{2i\omega L/c} - r_i)}{1 - r_i r_e e^{2i\omega L/c}}$$

$$E_{trans} = E_0 \frac{t_e t_i e^{i\omega L/c}}{1 - r_i r_e e^{2i\omega L/c}}$$

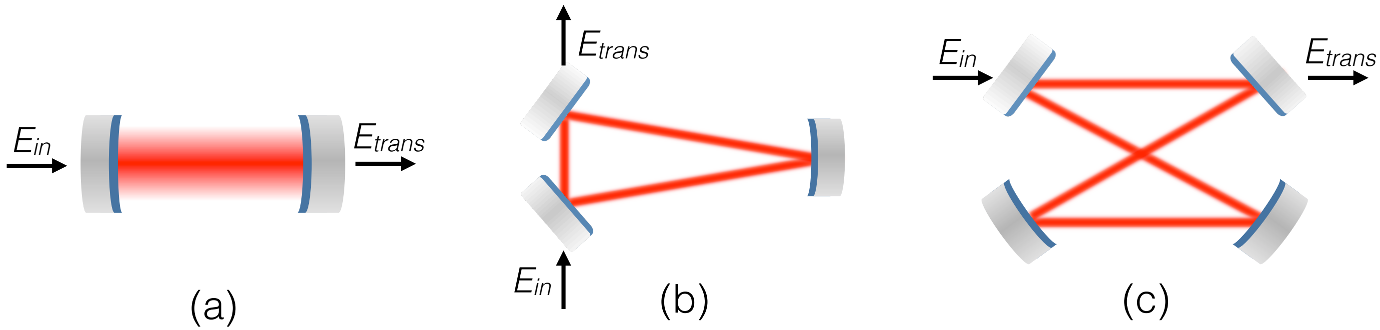

Pound-Drever-Hall Locking

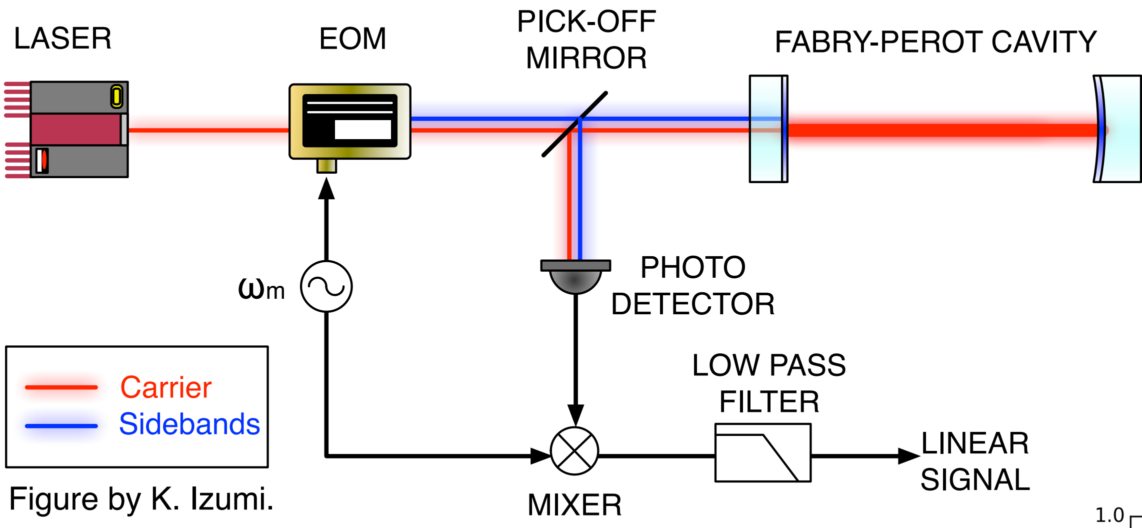

Figure by K. Izumi.

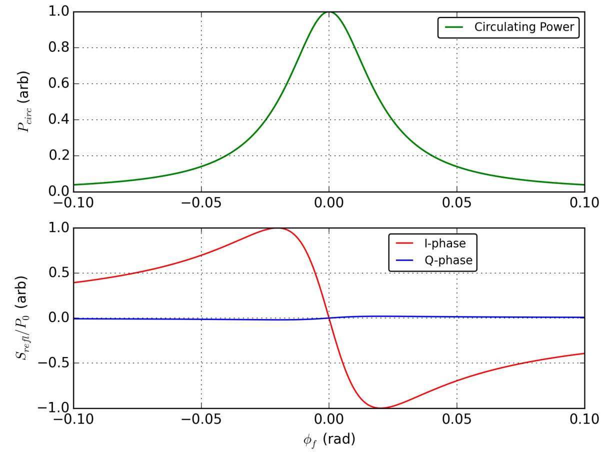

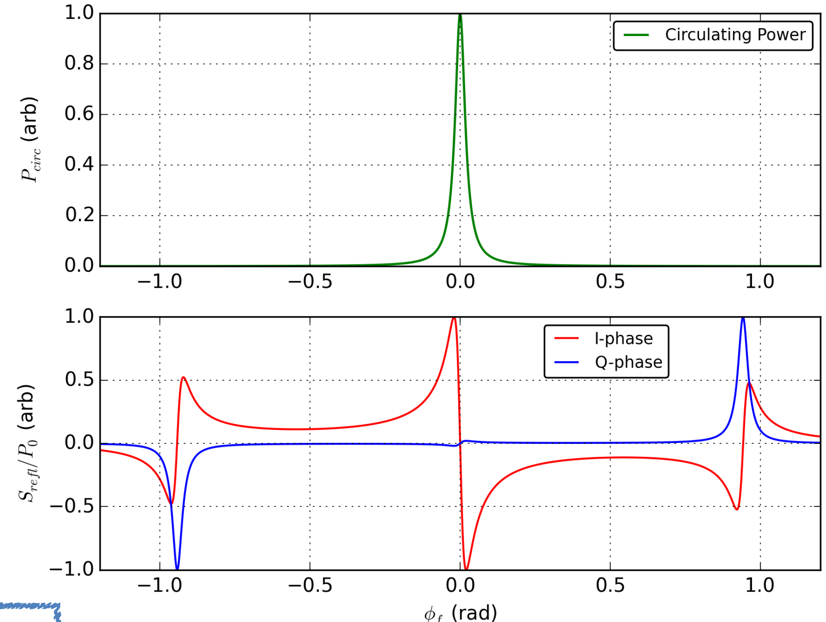

Non-resonant sidebands act as a reference to measure the carrier's phase shift around resonance.

Drever et al., Appl. Phys. B **31** 97 (1983)

$$E_{inc} = E_0 \left[J_0(\Gamma) e^{i\omega_0 t} + J_1(\Gamma) e^{i(\omega_0+\omega_{RF})t} - J_1(\Gamma) e^{i(\omega_0-\omega_{RF})t} \right]$$

$$r(\omega) = \frac{(r_e - r_i) e^{2i\omega L/c}}{1 - r_i r_e e^{2i\omega L/c}}$$

$$P_{refl}(\omega_{RF}) = 2P_0\, J_0(\Gamma) J_1(\Gamma) \Big[\mathrm{Re}[r(\omega_0) r^*(\omega_{RF}) - r^*(\omega_0) r(-\omega_{RF})] \cos\omega_{RF} t$$
$$+ \mathrm{Im}[r(\omega_0) r^*(\omega_{RF}) - r^*(\omega_0) r(-\omega_{RF})] \sin\omega_{RF} t \Big]$$

Double-Modulation Measurement of Optical Cavities

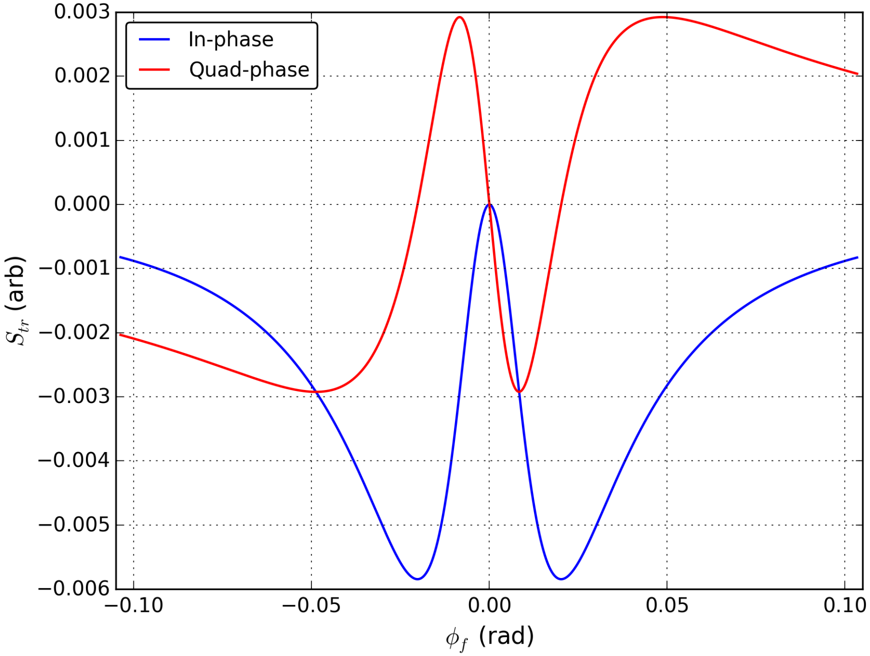

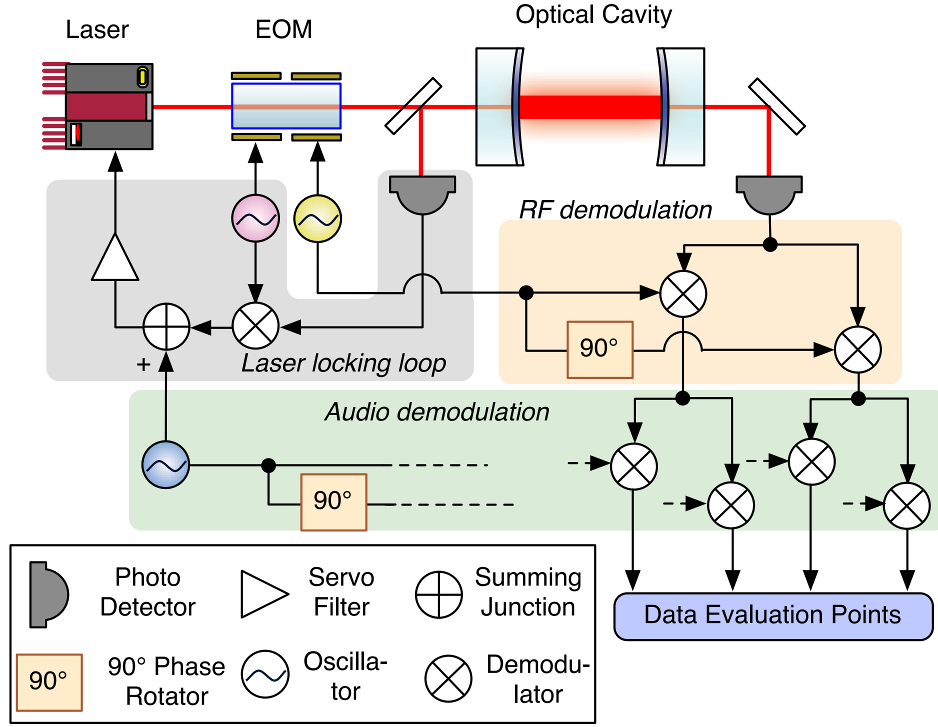

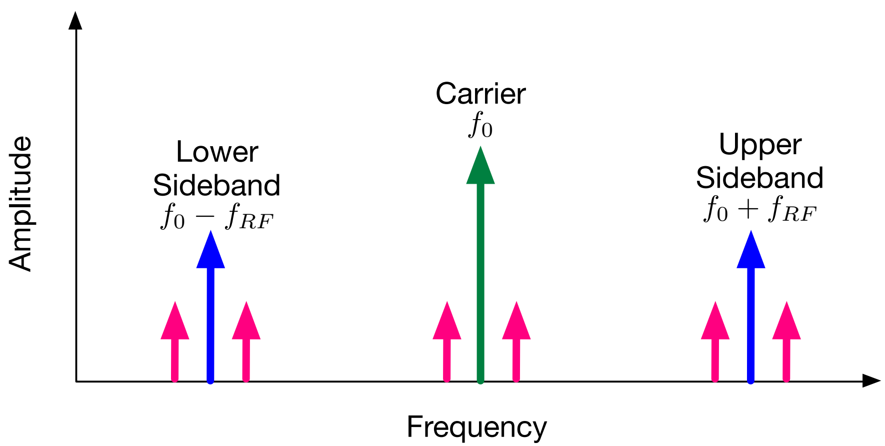

Sys. Uncertainty (Hz)	16 m Cavity Length	16 m Cavity f_{pole}	4 km Cavity Length
Absolute Timing	1	0	1
RAM	≪0.001	≪0.001	≪0.001
RF Modulation Phase	0	48	0
RF Harmonics	0	4	0
Total	±1	±52	±1

Double-Modulation Measurement - Results

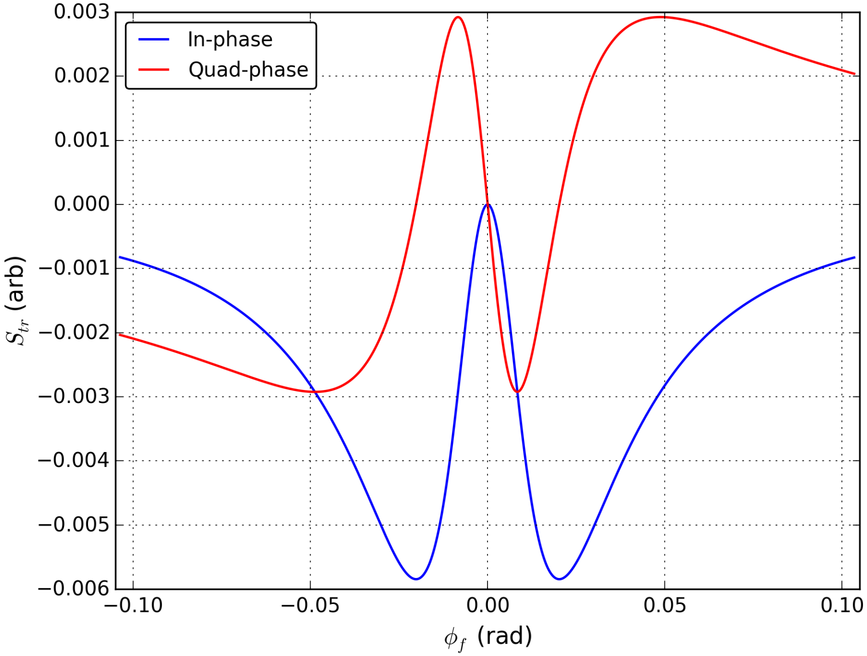

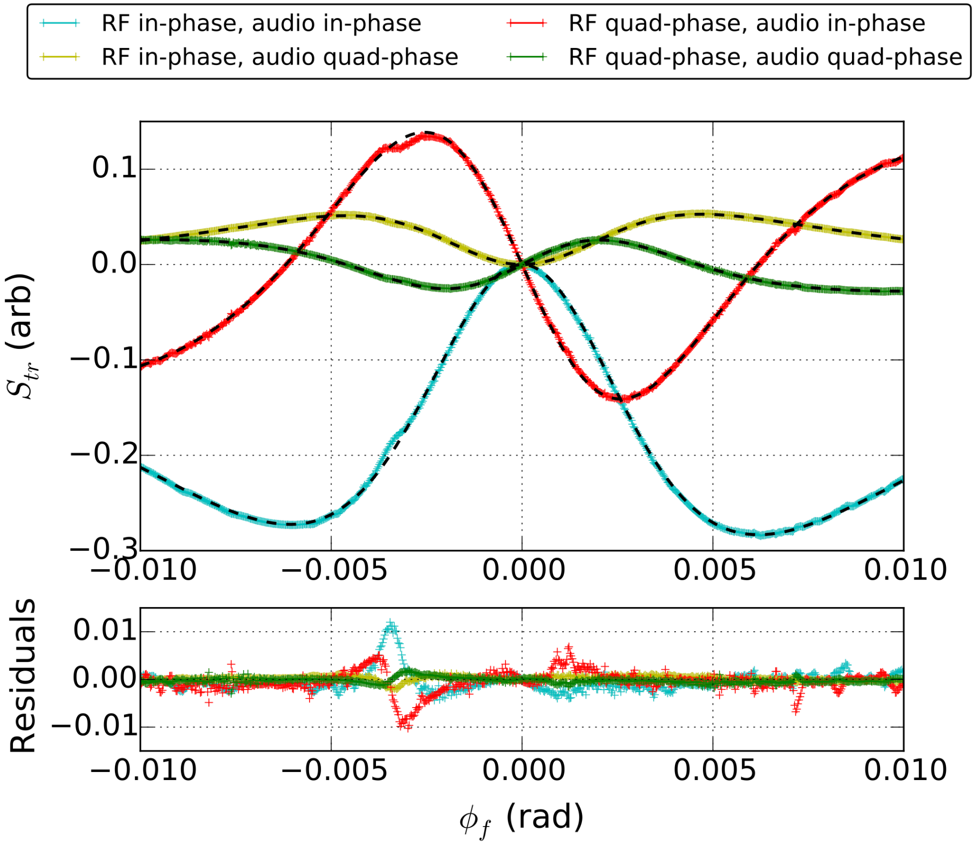

Parameter	Best-Fit Value	Stat. Uncertainty
f_{FSR}	9 100 234 Hz	2 Hz
T (=1-R)	6068 ppm	3 ppm
f_{EOM}	9 113 000 Hz	120 Hz
Q_{EOM}	61.1	0.2
θ_0	54.0°	0.2°
ϕ_0	10.23°	0.08°

Parameter	Measured Value	Stat. Uncertainty	Sys. Uncertainty
Y-arm Length	3994.4692 m	0.2 mm	0.2 mm
IMC Length	16.471701 m	3 μm	1 μm
IMC f_{pole}	8806 Hz	10 Hz	52 Hz

Double-Modulation Measurement - Results

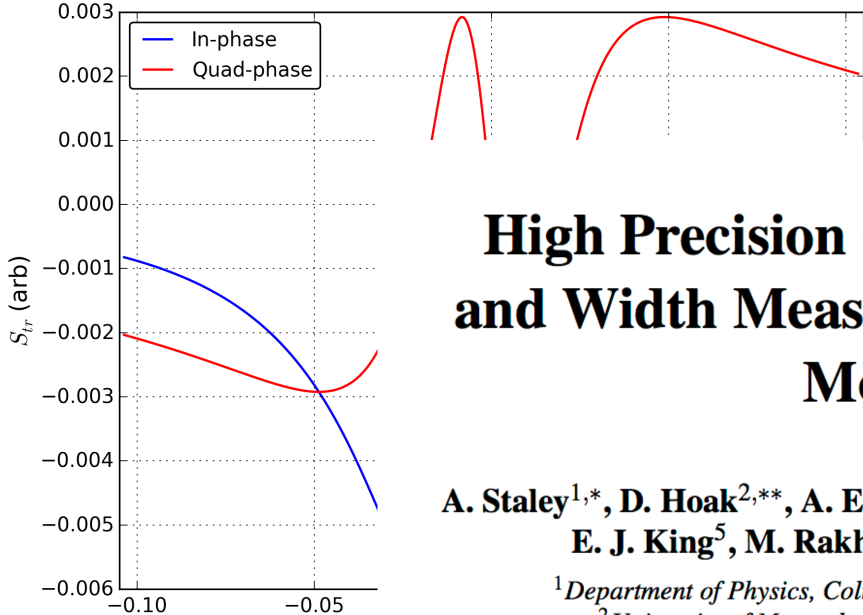

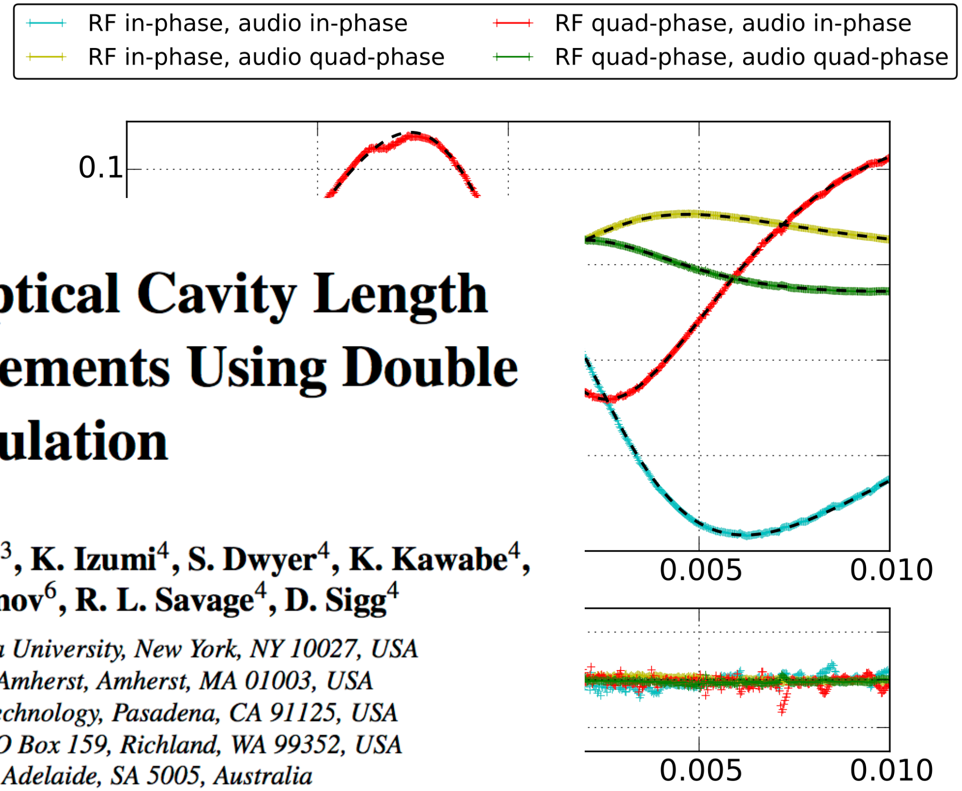

High Precision Optical Cavity Length and Width Measurements Using Double Modulation

A. Staley[1,*], D. Hoak[2,], A. Effler[3], K. Izumi[4], S. Dwyer[4], K. Kawabe[4], E. J. King[5], M. Rakhmanov[6], R. L. Savage[4], D. Sigg[4]**

[1]*Department of Physics, Columbia University, New York, NY 10027, USA*
[2]*University of Massachusetts Amherst, Amherst, MA 01003, USA*
[3]*LIGO, California Institute of Technology, Pasadena, CA 91125, USA*
[4] *LIGO Hanford Observatory, PO Box 159, Richland, WA 99352, USA*
[5]*University of Adelaide, Adelaide, SA 5005, Australia*
[6]*The University of Texas at Brownsville, Brownsville, TX 78520, USA*

[*]*ans2161@columbia.edu*

[**]*dhoak@physics.umass.edu*

Parameter	Best-Fit V	
f_{FSR}	9 100 234	
T (=1-R)	6068	
f_{EOM}	9 113 00	
Q_{EOM}	61.1	0.2
θ_0	54.0°	0.2°
ϕ_0	10.23°	0.08°

		ty	Sys. Uncertainty
Y-arm Length	3994.4692 m	0.2 mm	0.2 mm
IMC Length	16.471701 m	3 μm	1 μm
IMC f_{pole}	8806 Hz	10 Hz	52 Hz

Instrumentation

Advanced LIGO - What Hasn't Been Changed

Advanced LIGO - What Has Been Changed

Larger Mirrors, Larger Beams, Better Coatings

Increased Arm Cavity Finesse

Increased Laser Power

Big Investment in Seismic Isolation and Suspensions

Signal Recycling / Signal Extraction

OMC - rejects the laser field that does not couple to GWs

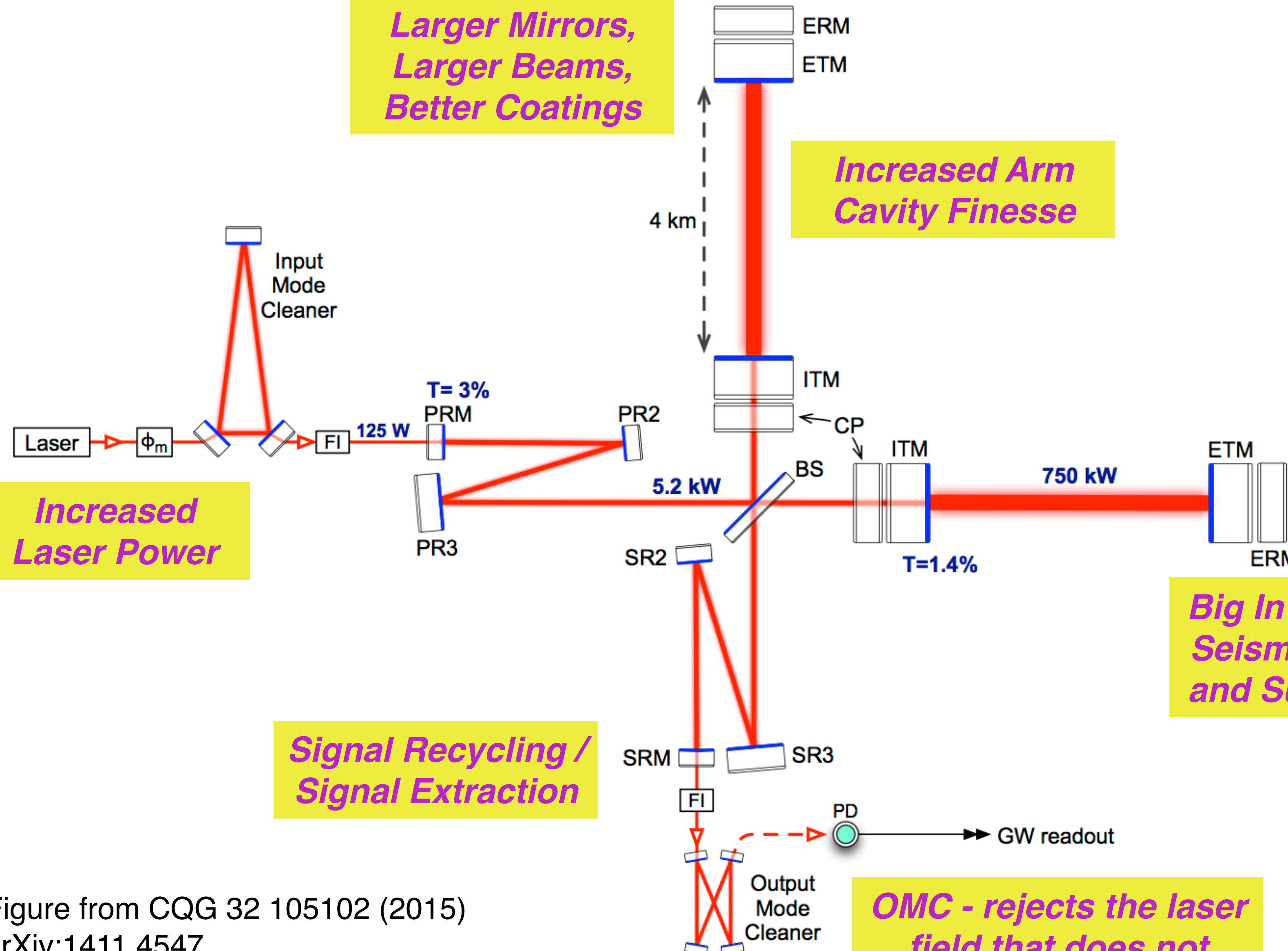

Figure from CQG 32 105102 (2015)
arXiv:1411.4547

Advanced LIGO - What Has Been Changed

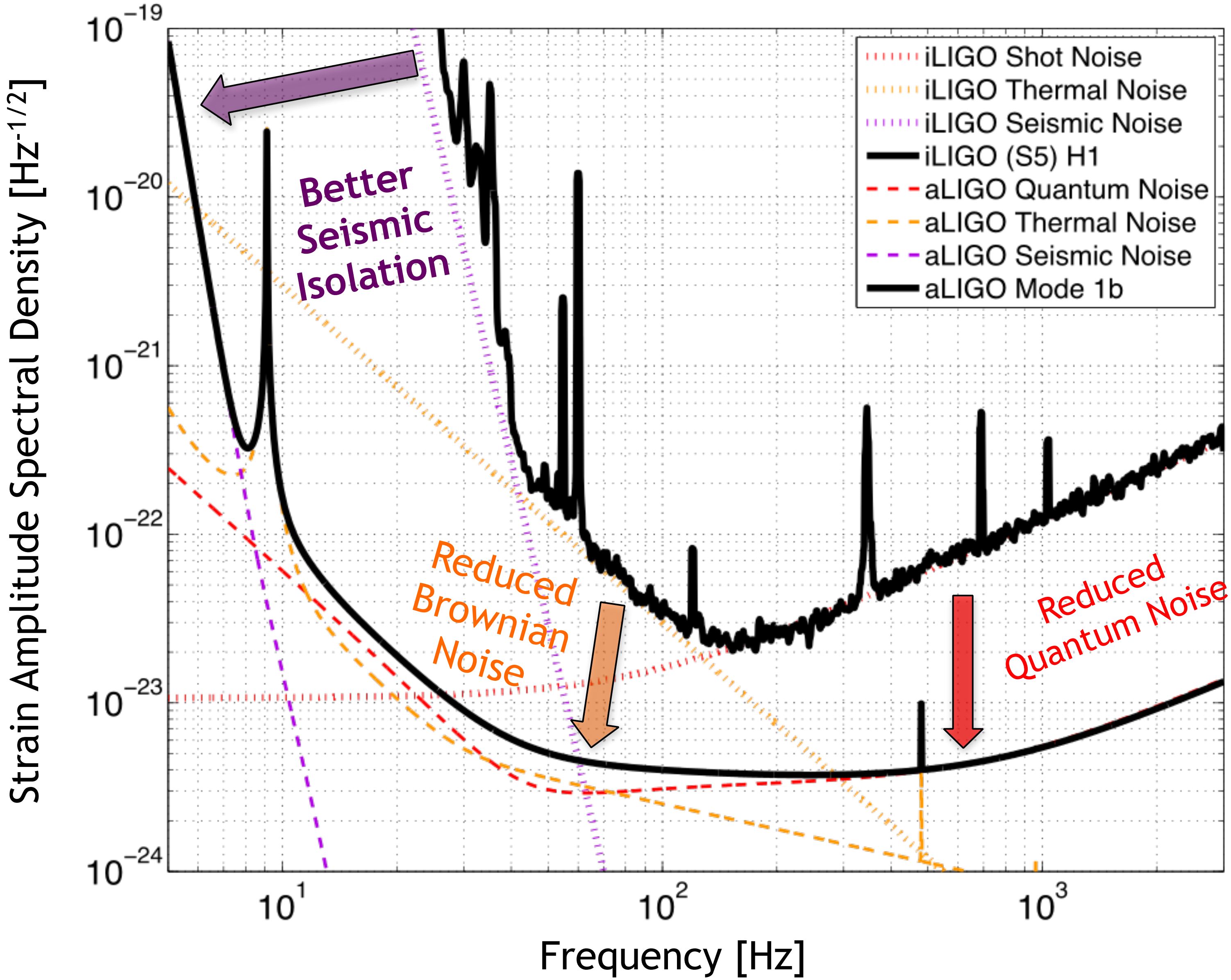

Arm Length Stabilization

LIGO-G1300524

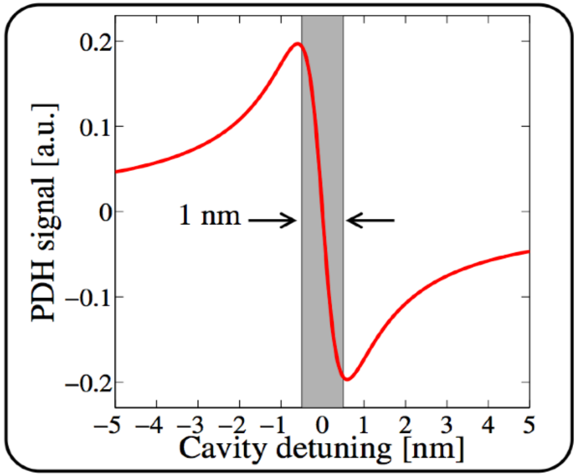

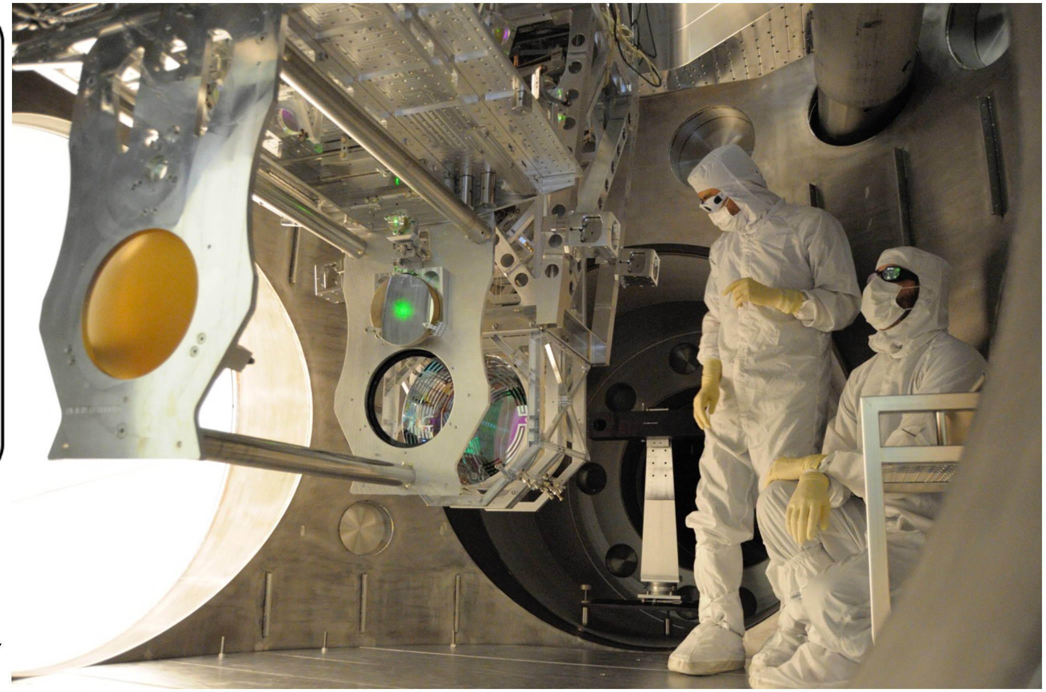

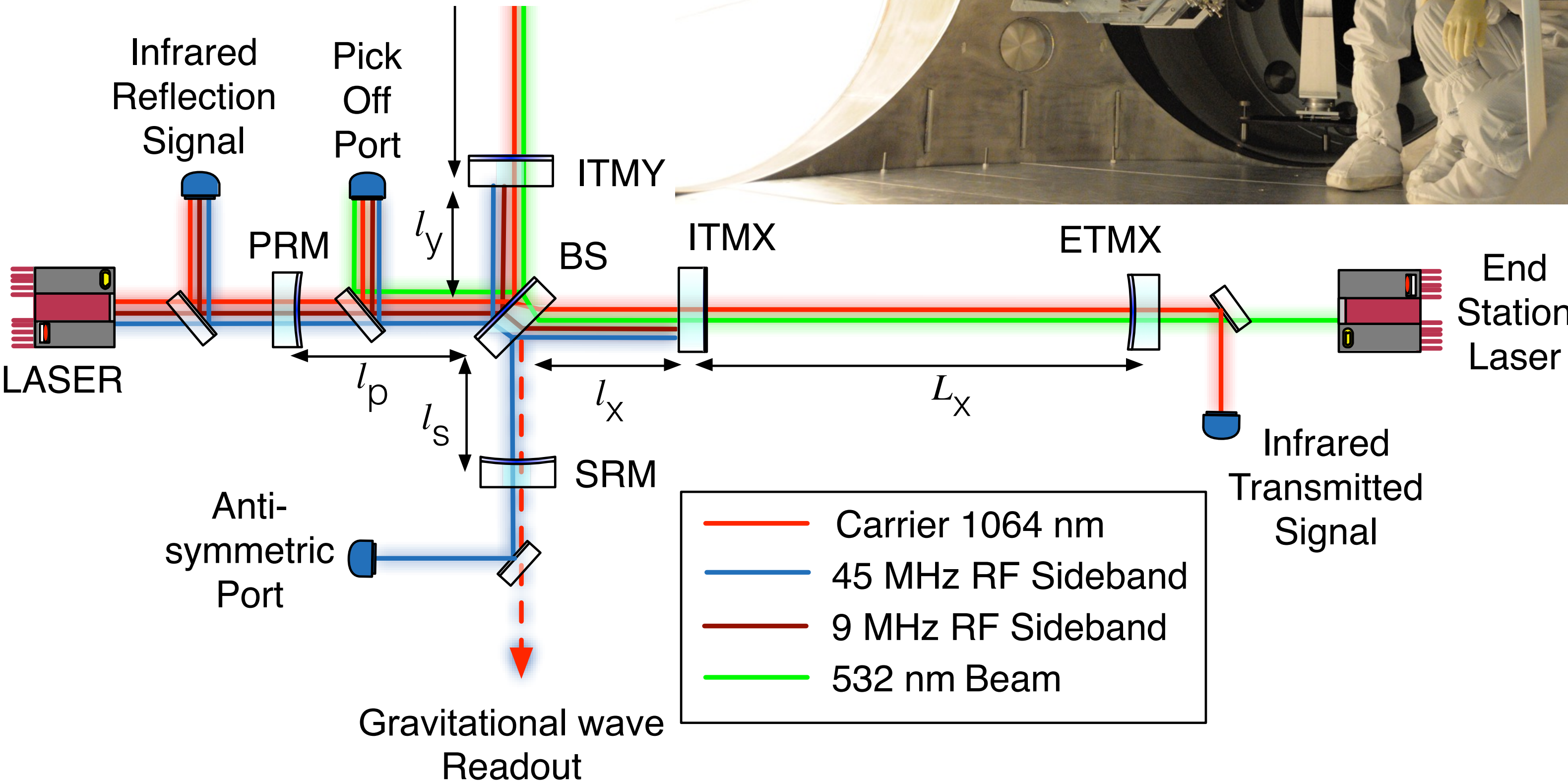

Lock Acquisition

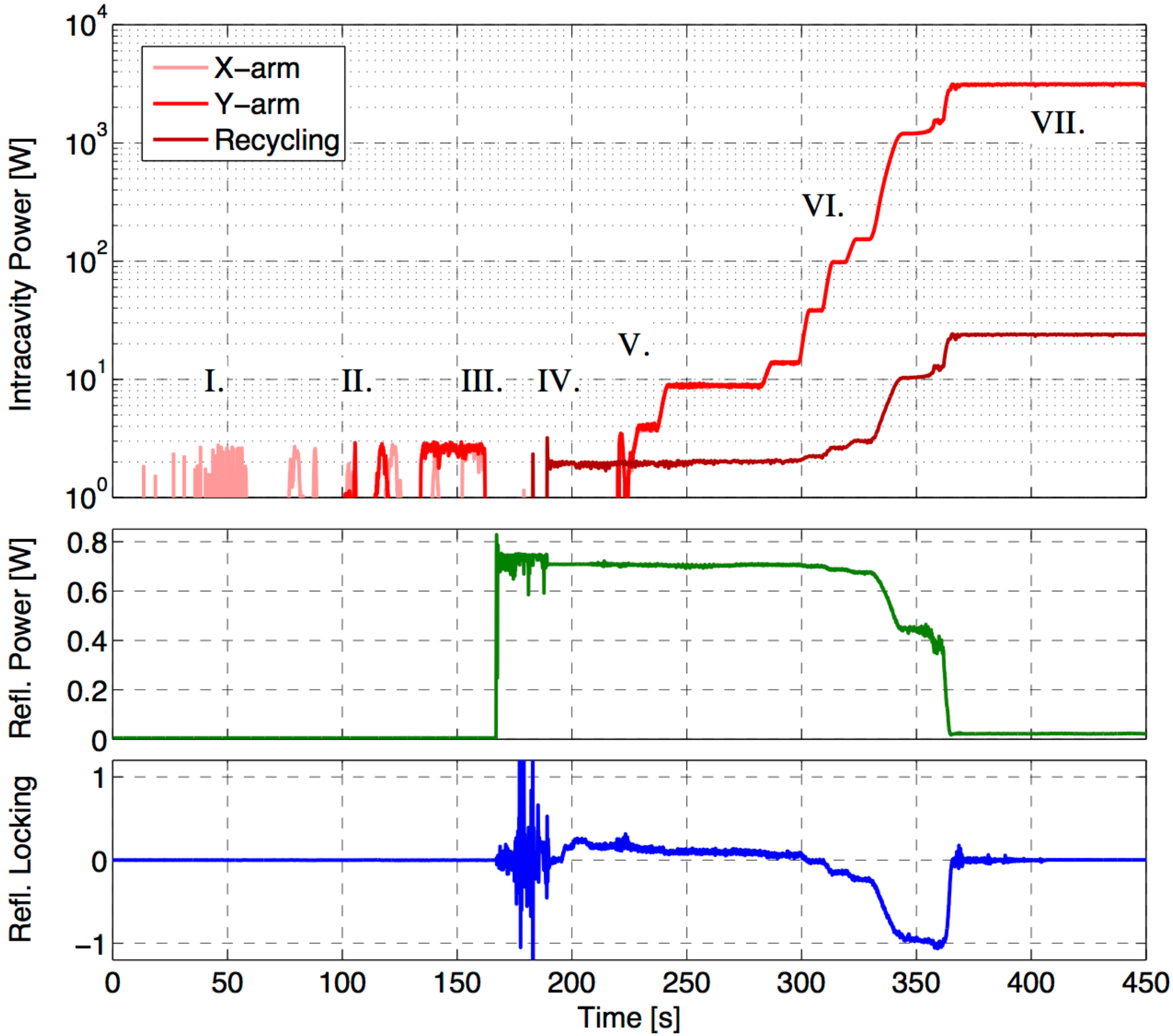

Lock Acquisition

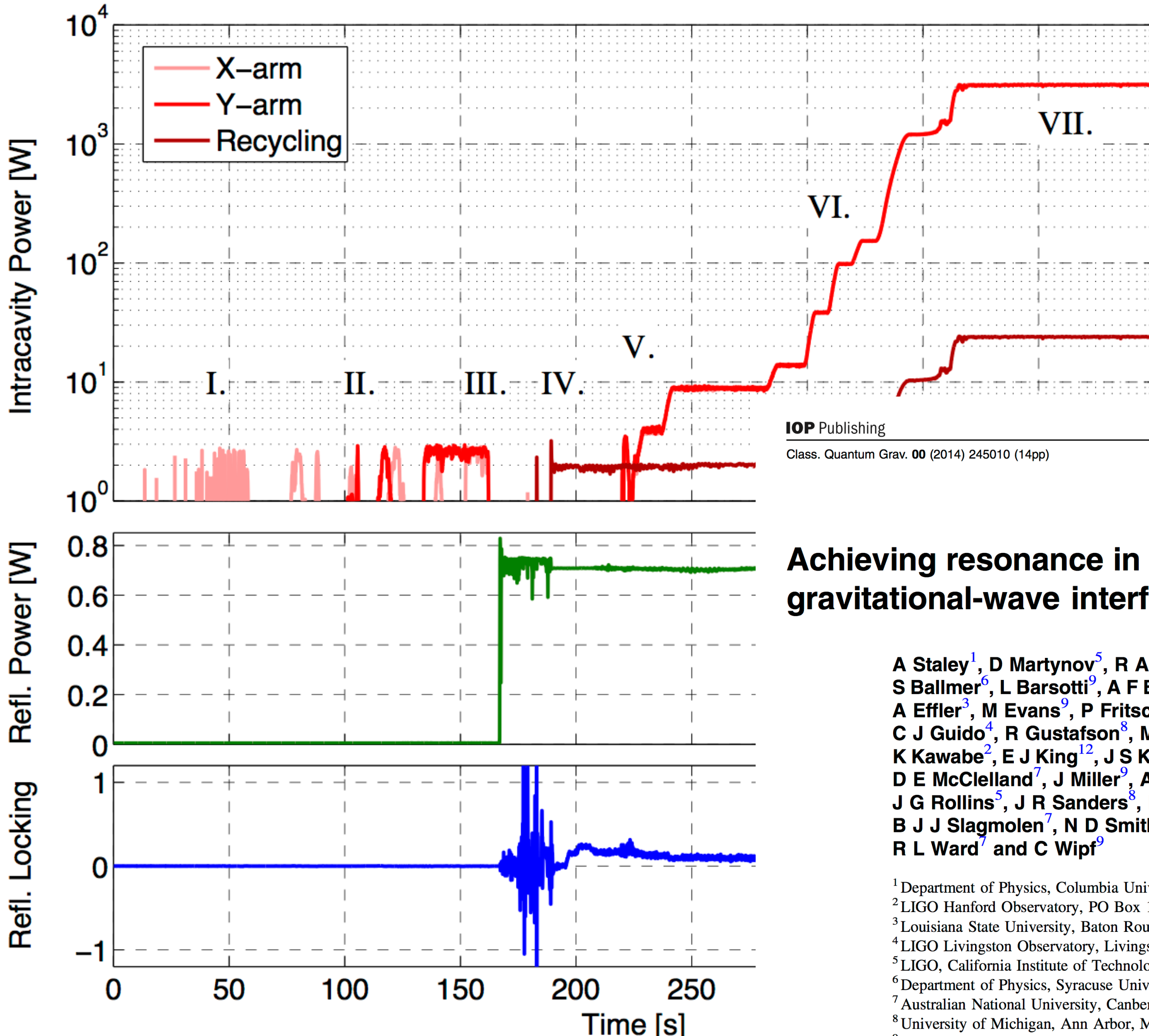

IOP Publishing — Classical and Quantum Gravity

Class. Quantum Grav. **00** (2014) 245010 (14pp) — doi:10.1088/0264-9381/31/24/245010

Achieving resonance in the Advanced LIGO gravitational-wave interferometer

A Staley[1], D Martynov[5], R Abbott[5], R X Adhikari[5], K Arai[5], S Ballmer[6], L Barsotti[9], A F Brooks[5], R T DeRosa[3], S Dwyer[2], A Effler[3], M Evans[9], P Fritschel[9], V V Frolov[4], C Gray[2], C J Guido[4], R Gustafson[8], M Heintze[4], D Hoak[10], K Izumi[2], K Kawabe[2], E J King[12], J S Kissel[2], K Kokeyama[3], M Landry[2], D E McClelland[7], J Miller[9], A Mullavey[3], B O'Reilly[4], J G Rollins[5], J R Sanders[8], R M S Schofield[11], D Sigg[2], B J J Slagmolen[7], N D Smith-Lefebvre[5], G Vajente[5], R L Ward[7] and C Wipf[9]

[1] Department of Physics, Columbia University, New York, NY 10027, USA
[2] LIGO Hanford Observatory, PO Box 159, Richland, WA 99352, USA
[3] Louisiana State University, Baton Rouge, LA 70803, USA
[4] LIGO Livingston Observatory, Livingston, LA 70754, USA
[5] LIGO, California Institute of Technology, Pasadena, CA 91125, USA
[6] Department of Physics, Syracuse University, Syracuse, NY 13244, USA
[7] Australian National University, Canberra, ACT 0200, Australia
[8] University of Michigan, Ann Arbor, MI 48109, USA
[9] LIGO, Massachusetts Institute of Technology, Cambridge, MA 02139, USA
[10] University of Massachusetts Amherst, Amherst, MA 01003, USA
[11] University of Oregon, Eugene, OR 97403, USA
[12] University of Adelaide, Adelaide, SA 5005, Australia

Advanced LIGO - Latest Sensitivity

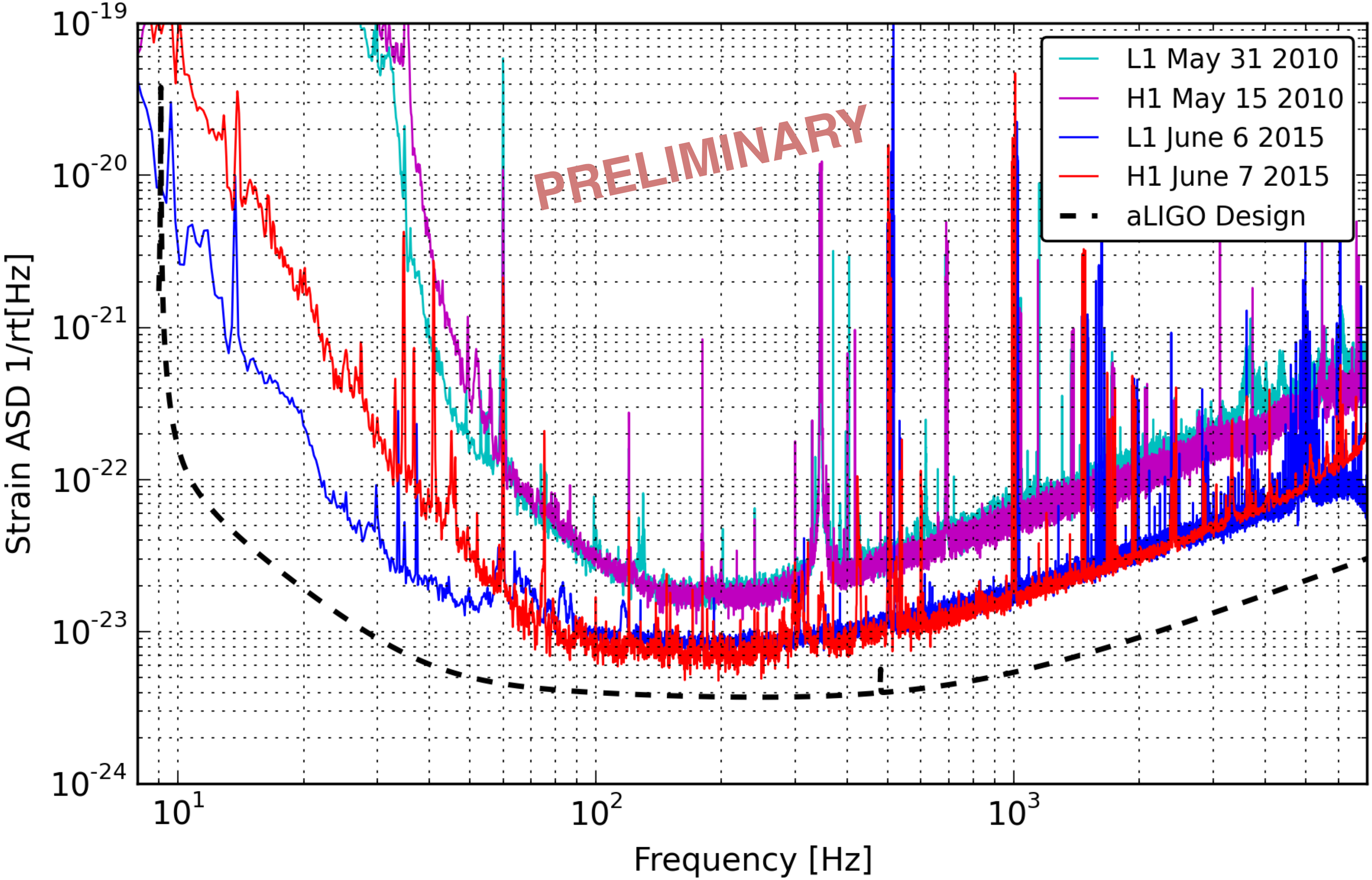

The Output Mode Cleaner

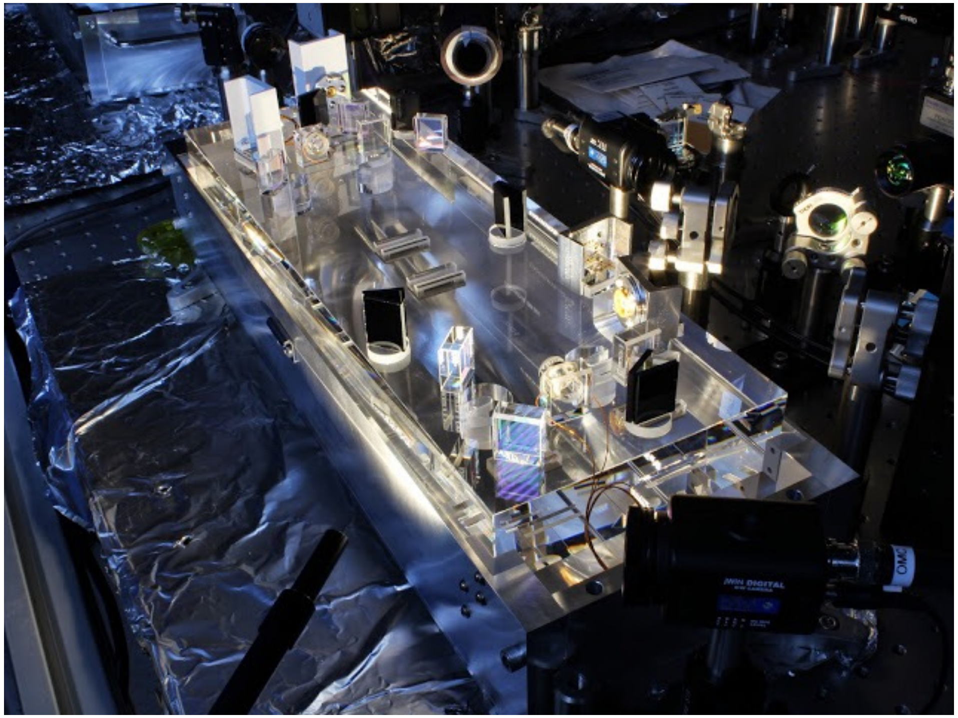

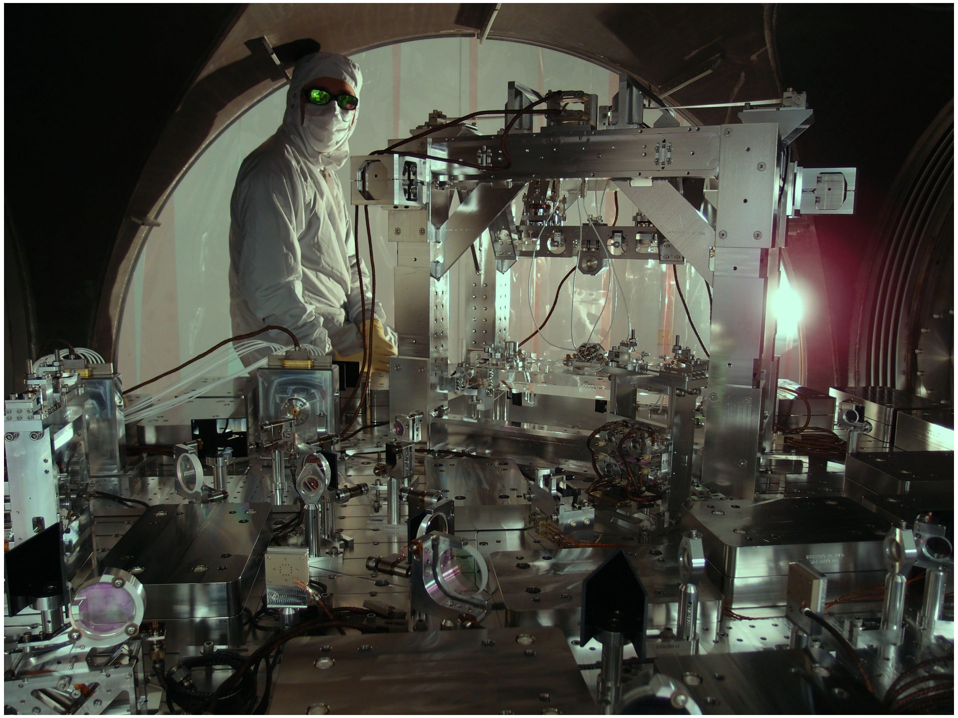

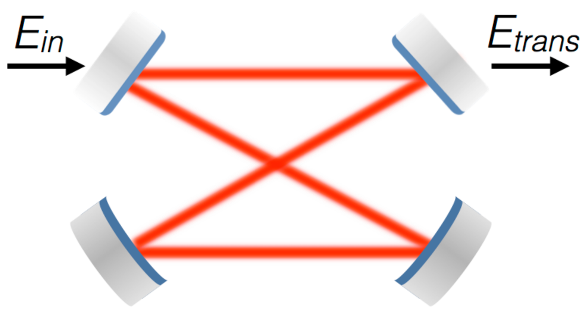

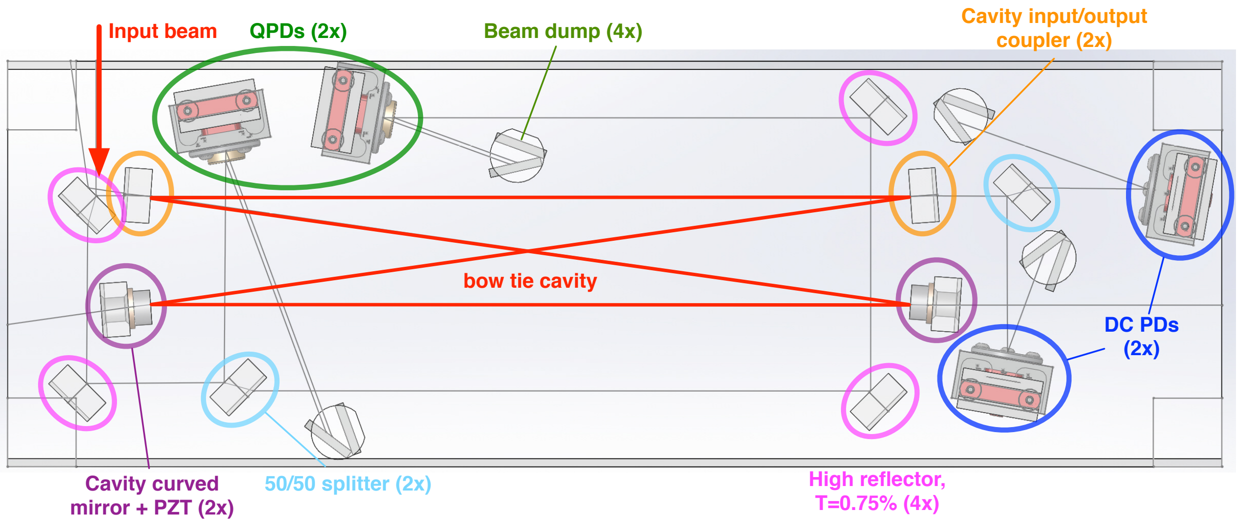

Output Mode Cleaner - Cavity Length Noise

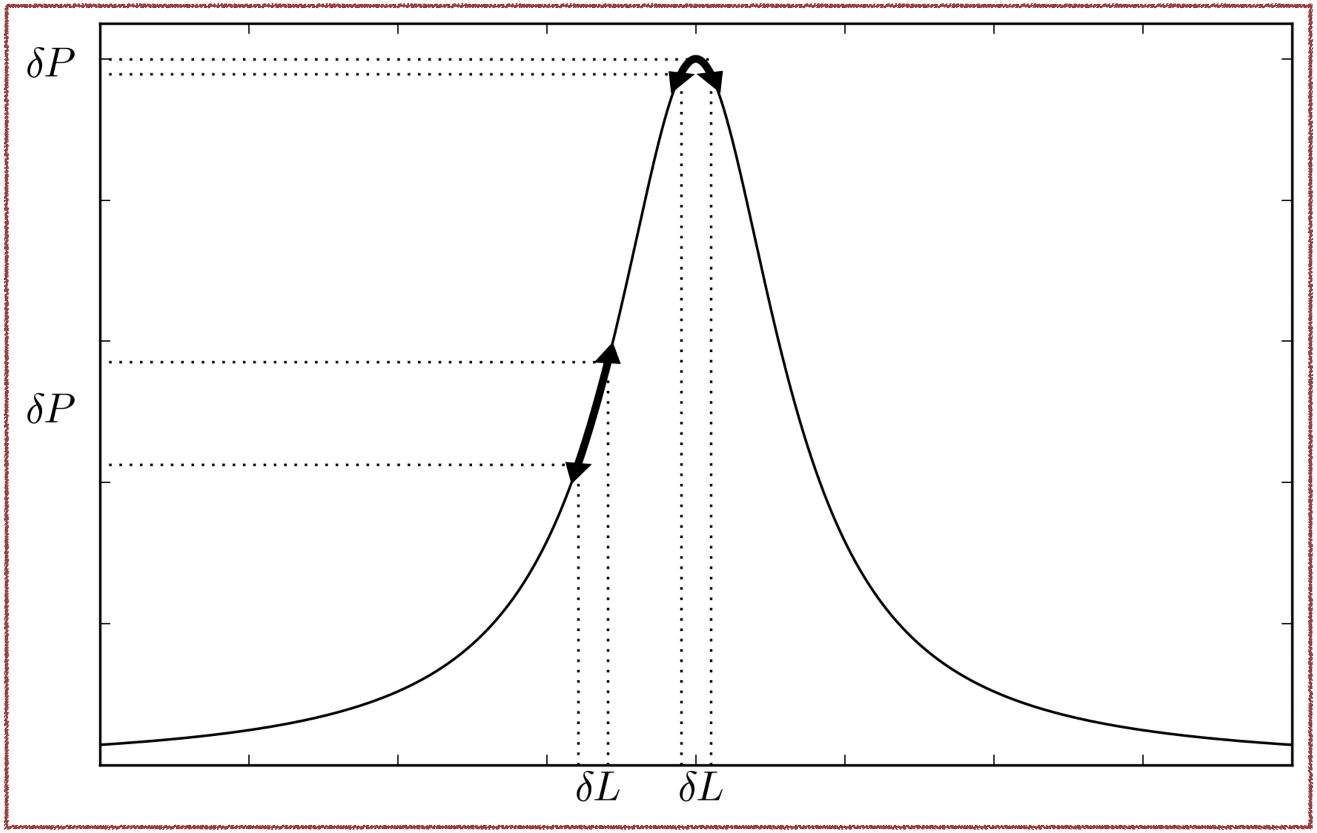

Fluctuations of the OMC length or alignment could generate noise in the transmitted power, and pollute the gravitational wave channel.

We can characterize length noise by locking the OMC with an offset.

Output Mode Cleaner - Cavity Length Noise

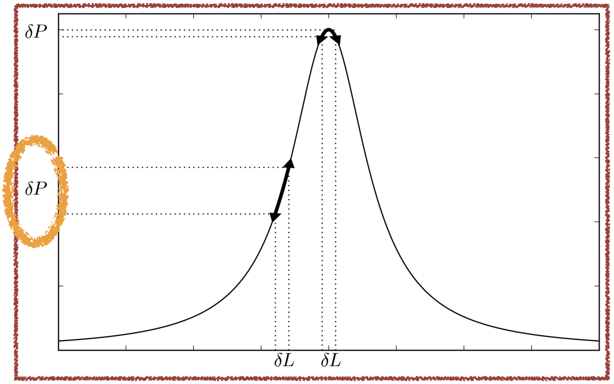

1. Measure power fluctuations while locked on the half-fringe.

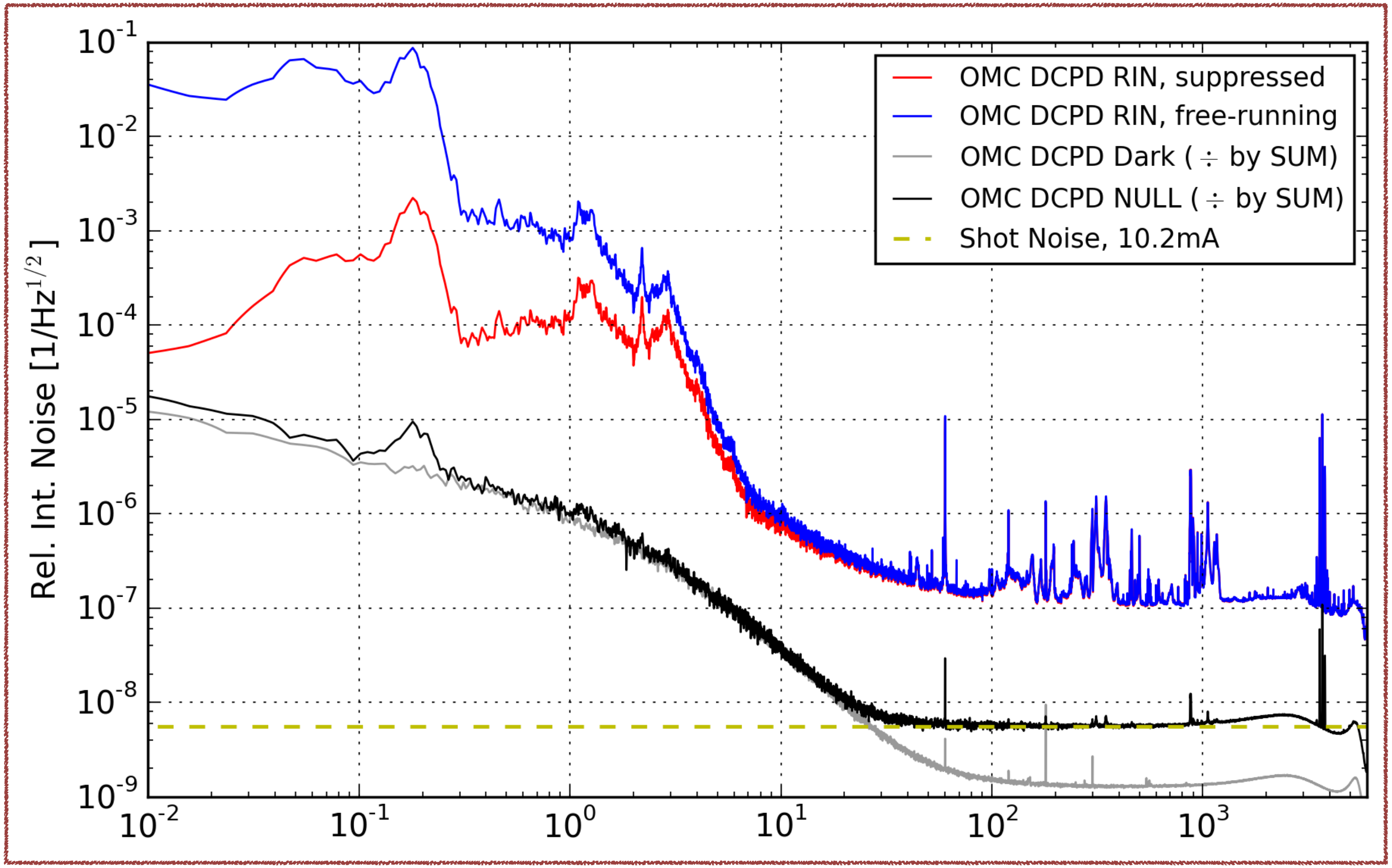

Output Mode Cleaner - Cavity Length Noise

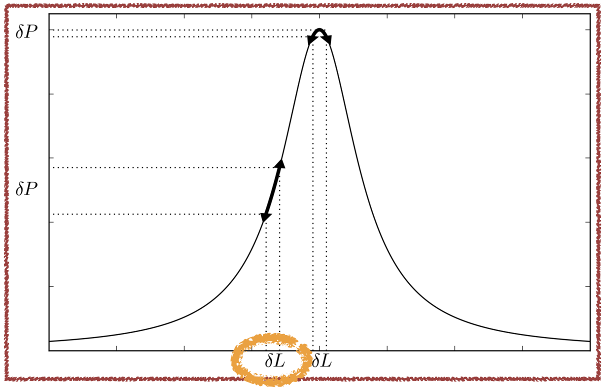

1. Measure power fluctuations while locked on the half-fringe.

2. Convert dP into dL using cavity resonance curve.

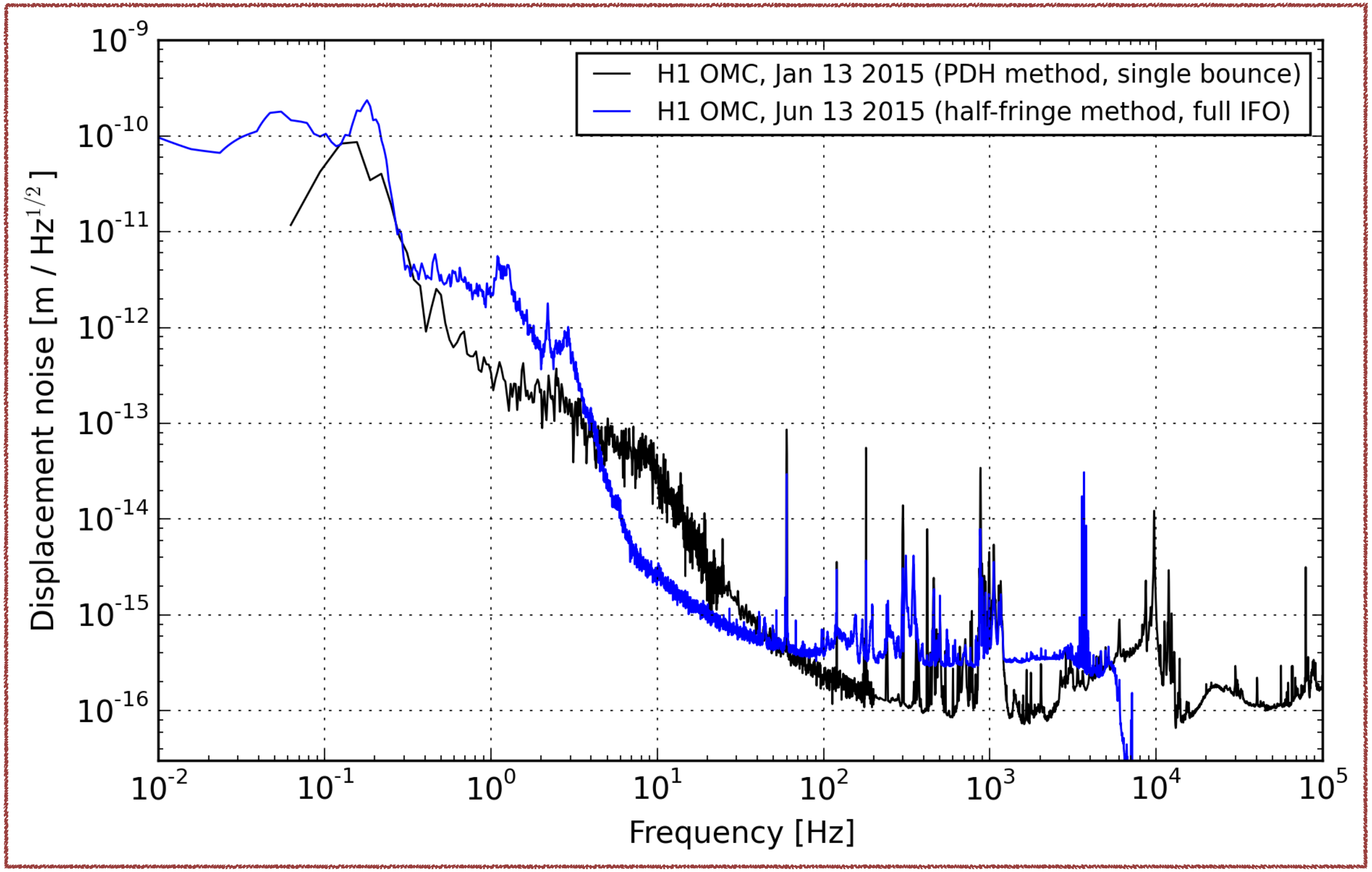

Output Mode Cleaner - Cavity Length Noise

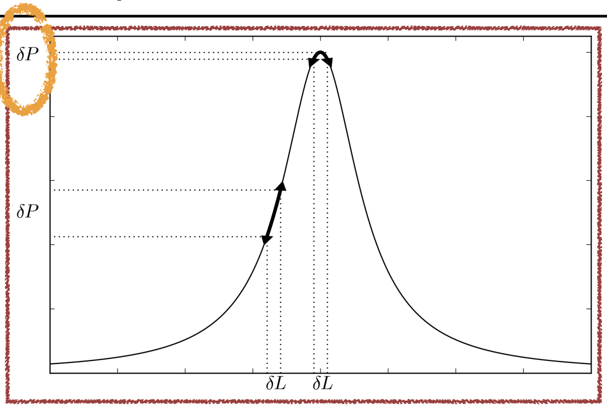

1. Measure power fluctuations while locked on the half-fringe.

2. Convert dP into dL using cavity resonance curve.

3. Calculate quadratic fluctuations in dP due to dL when locked on the full-fringe, and compare to gravitational wave sensitivity.

Divide by arm length to get strain →

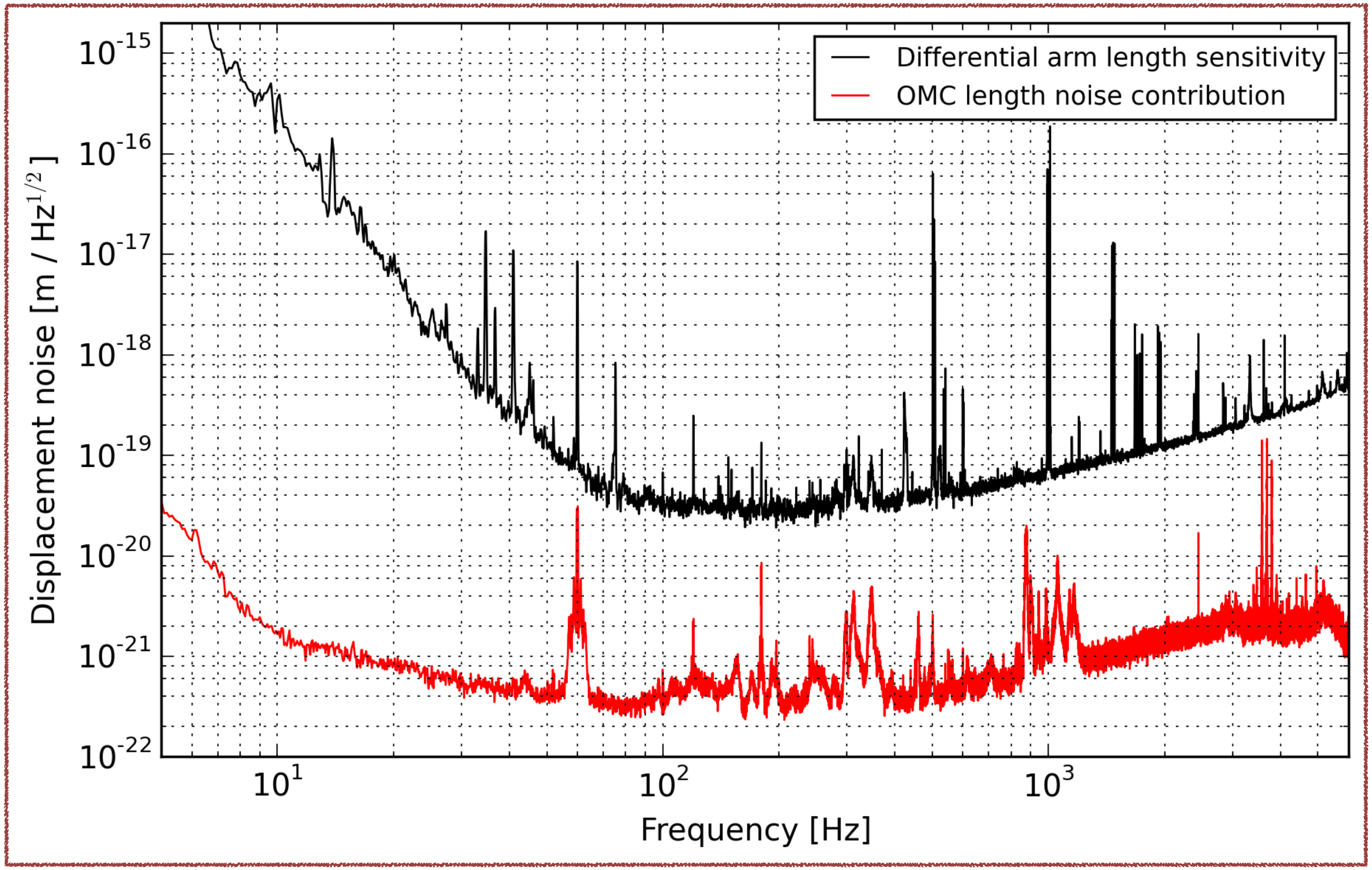

Optical Spectrum Analysis Using the OMC

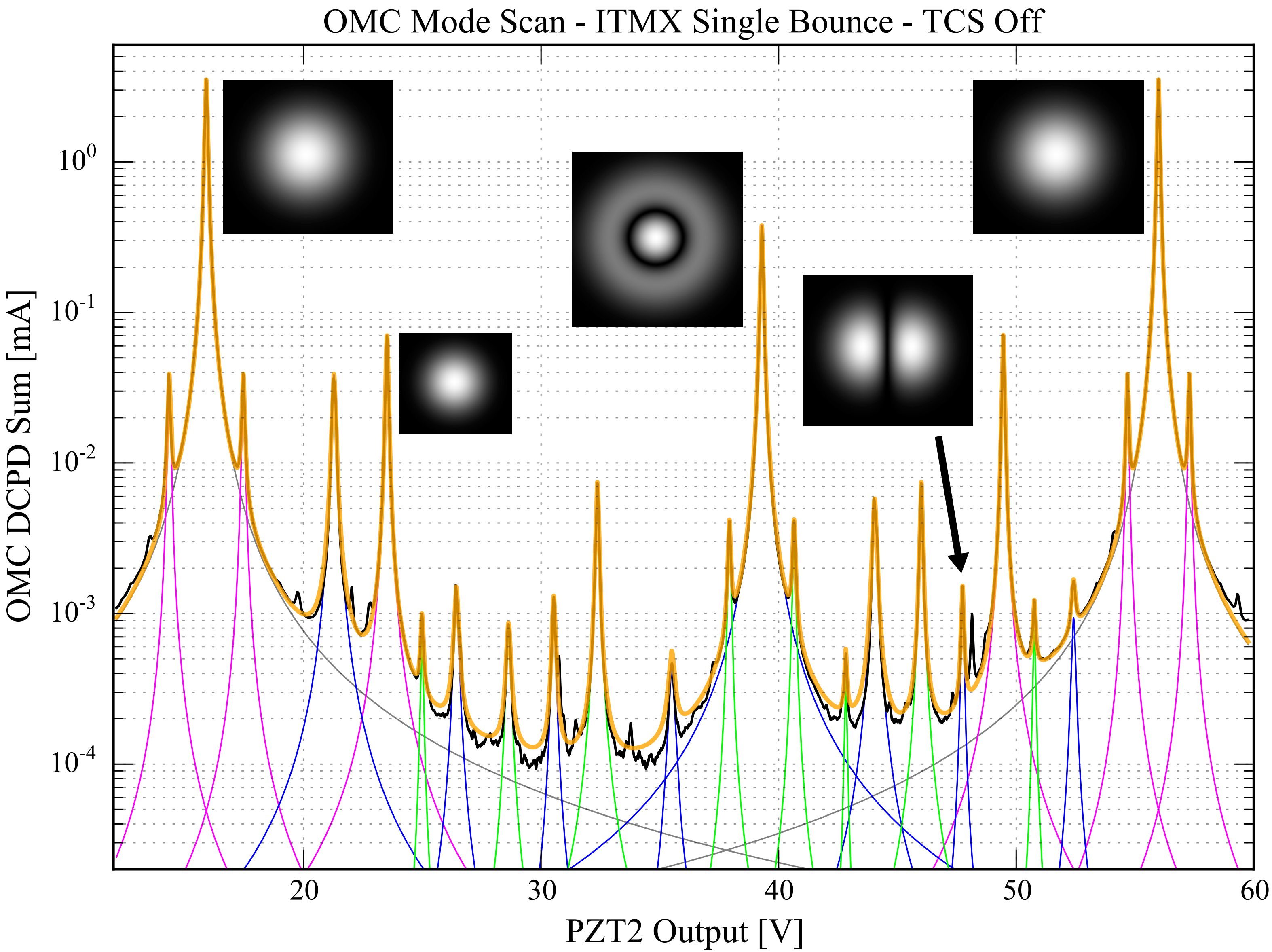

Contrast Defect Measurement

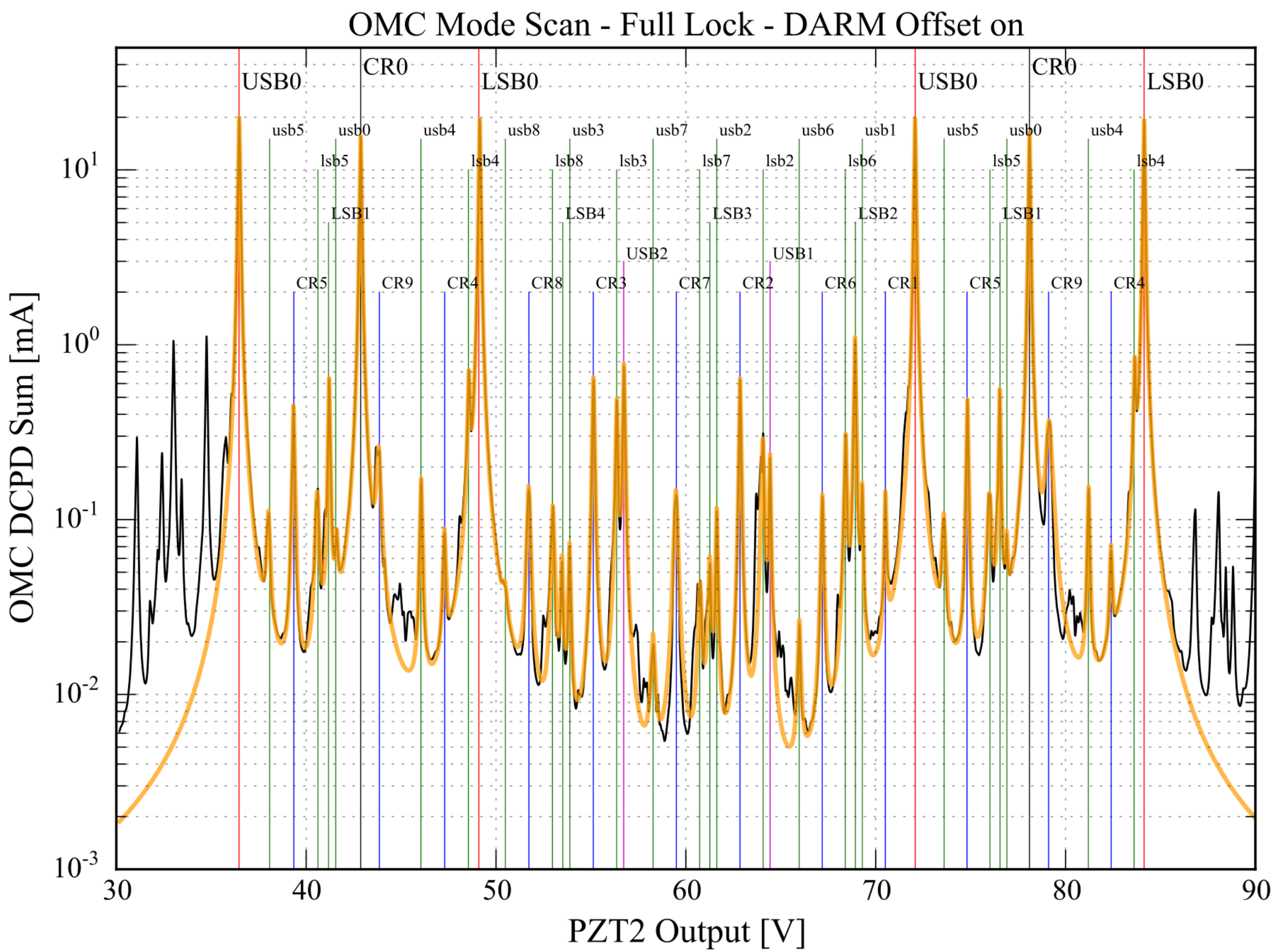

Interferometer Contrast Defect: 140ppm

Detector Characterization

Detector Duty Factor

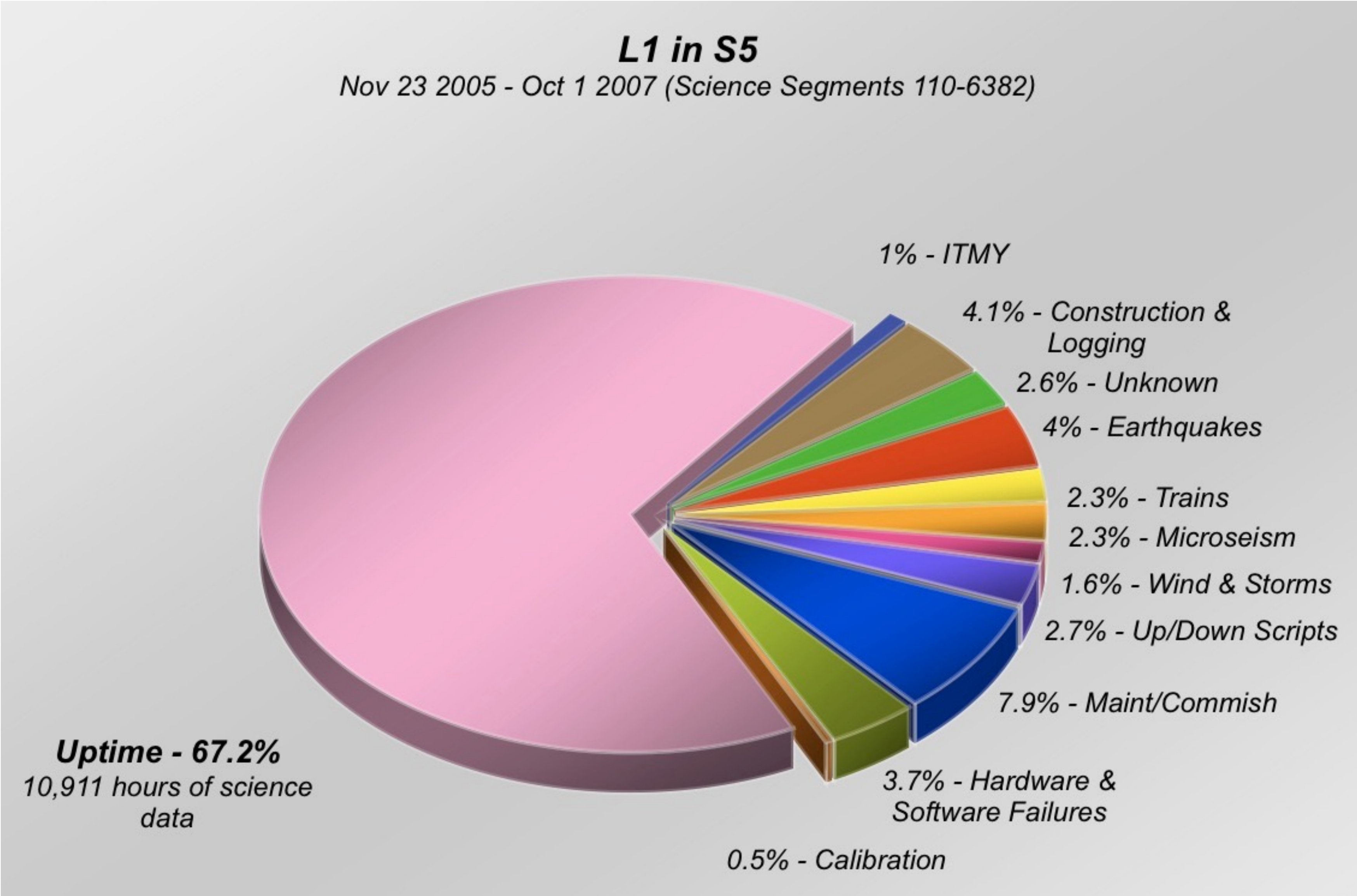

Science Segment Durations

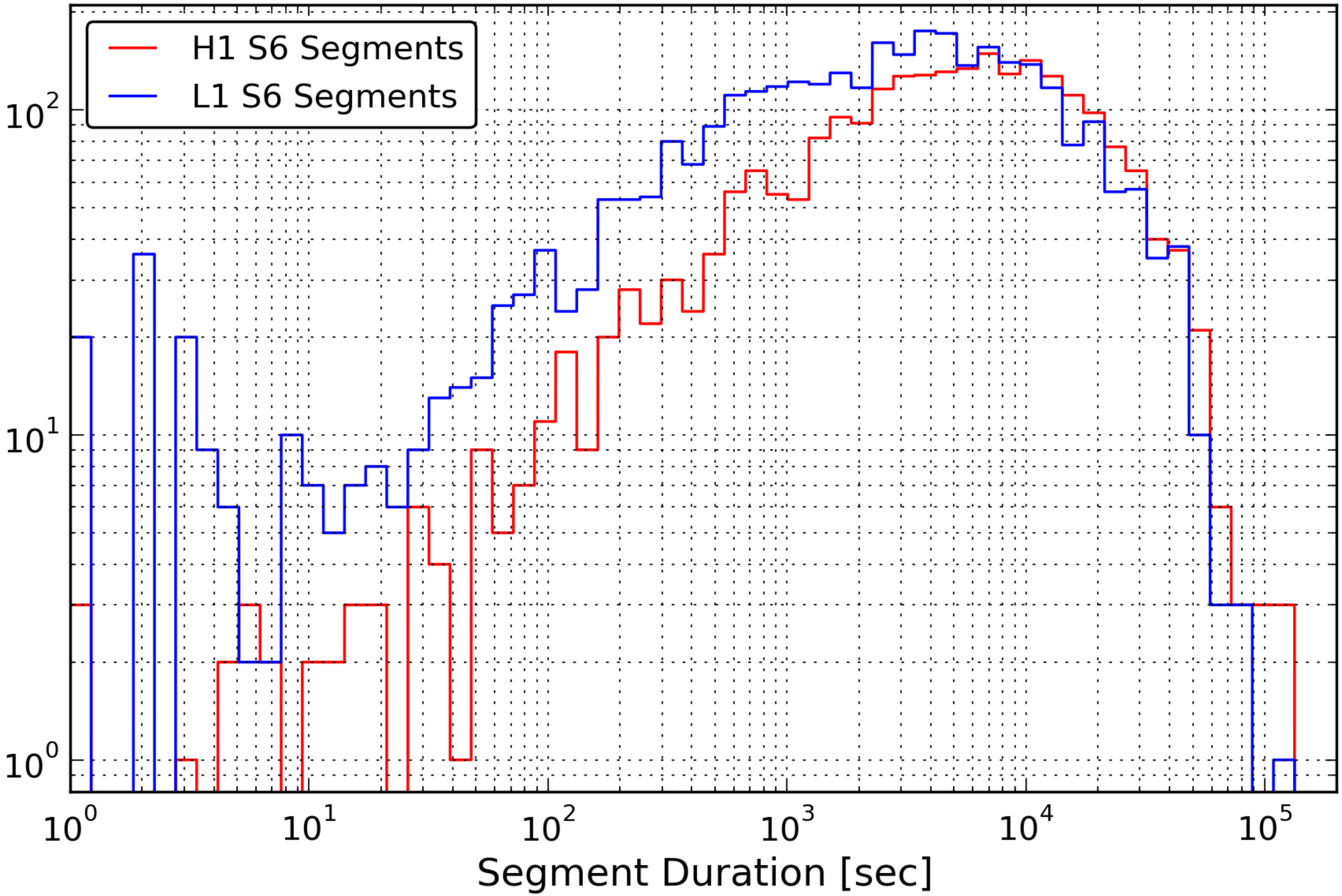

Gaussianity of the Noise

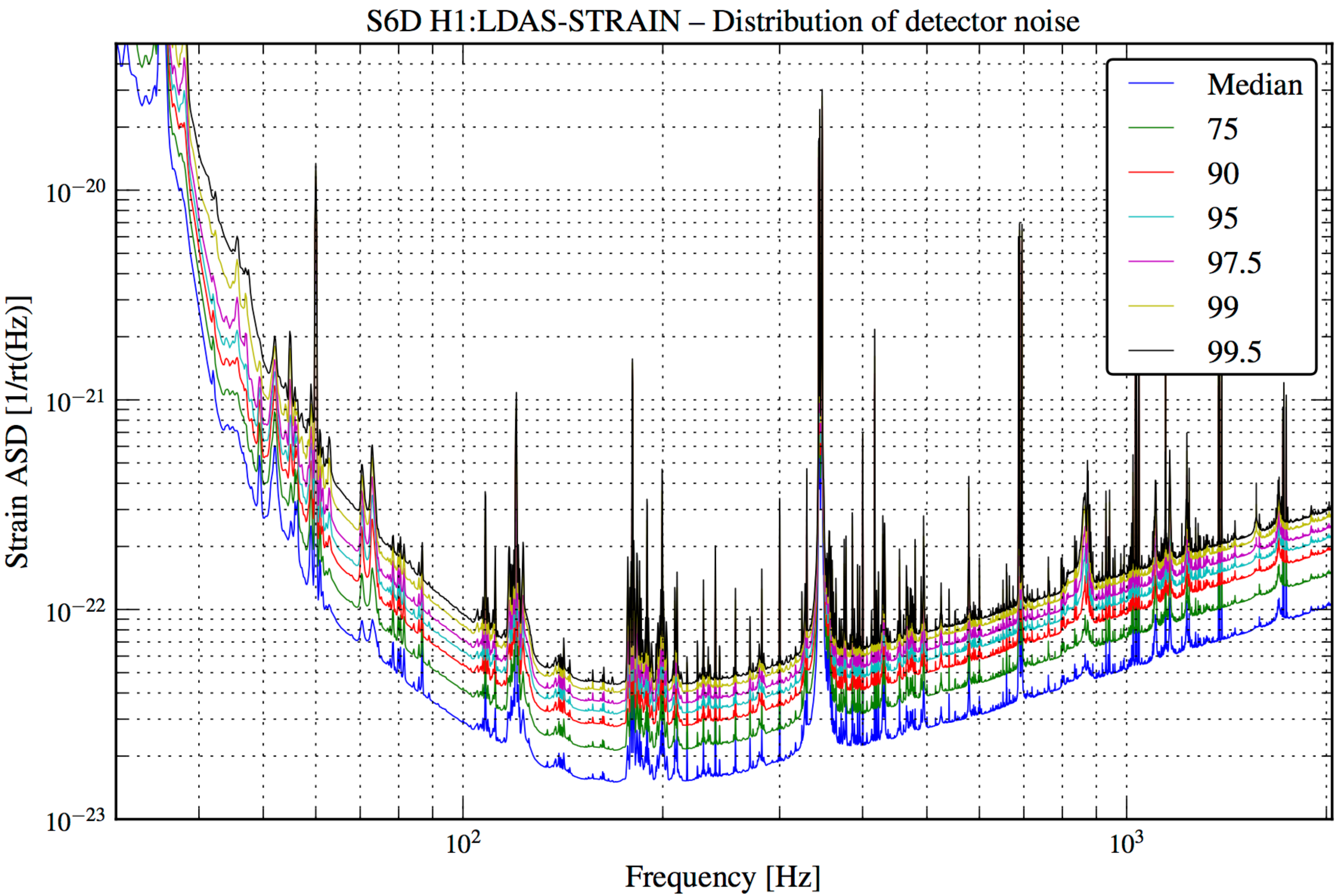

(non)Gaussianity of the Noise

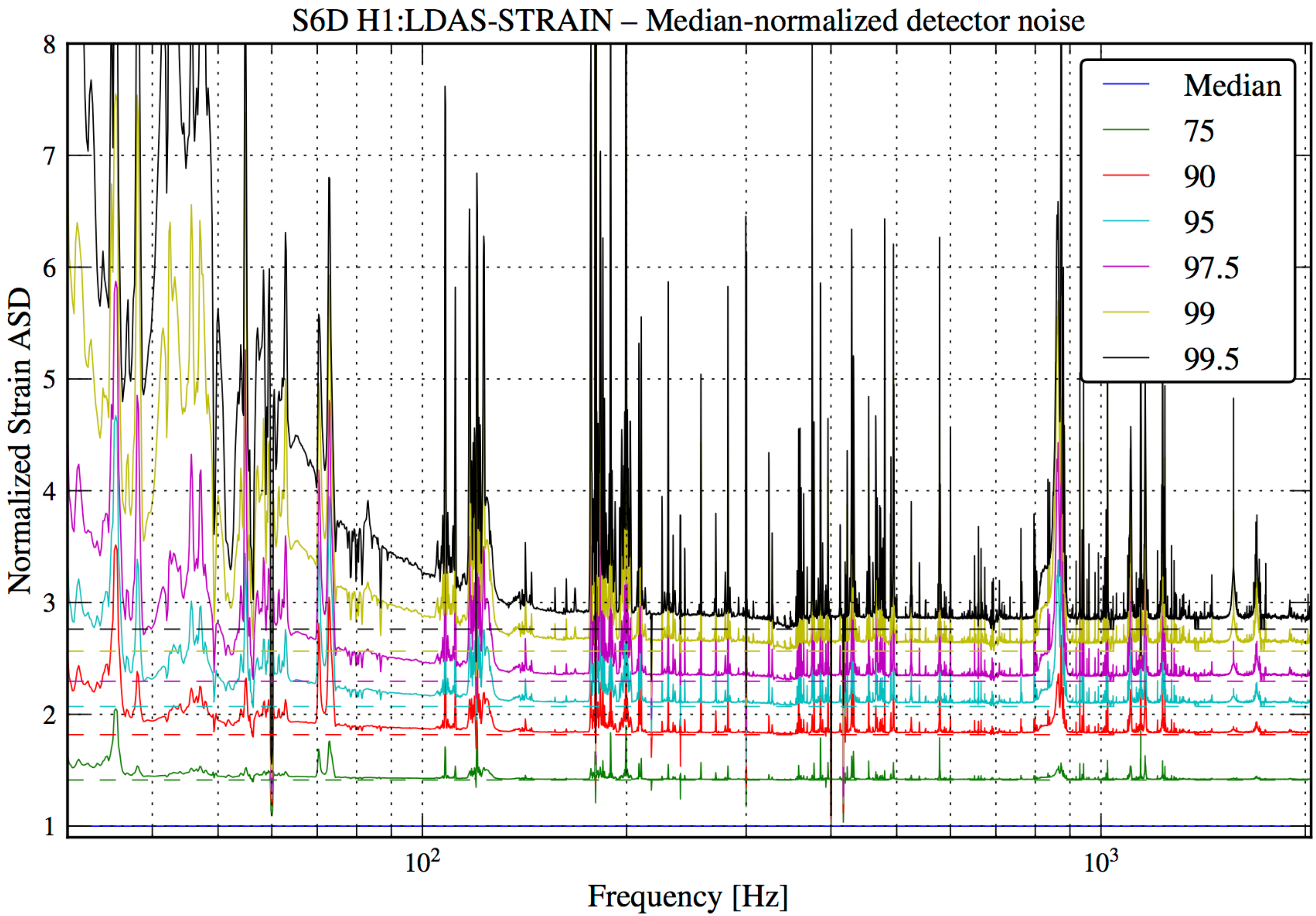

Instrumental Channel Veto - Barkhausen Noise Example

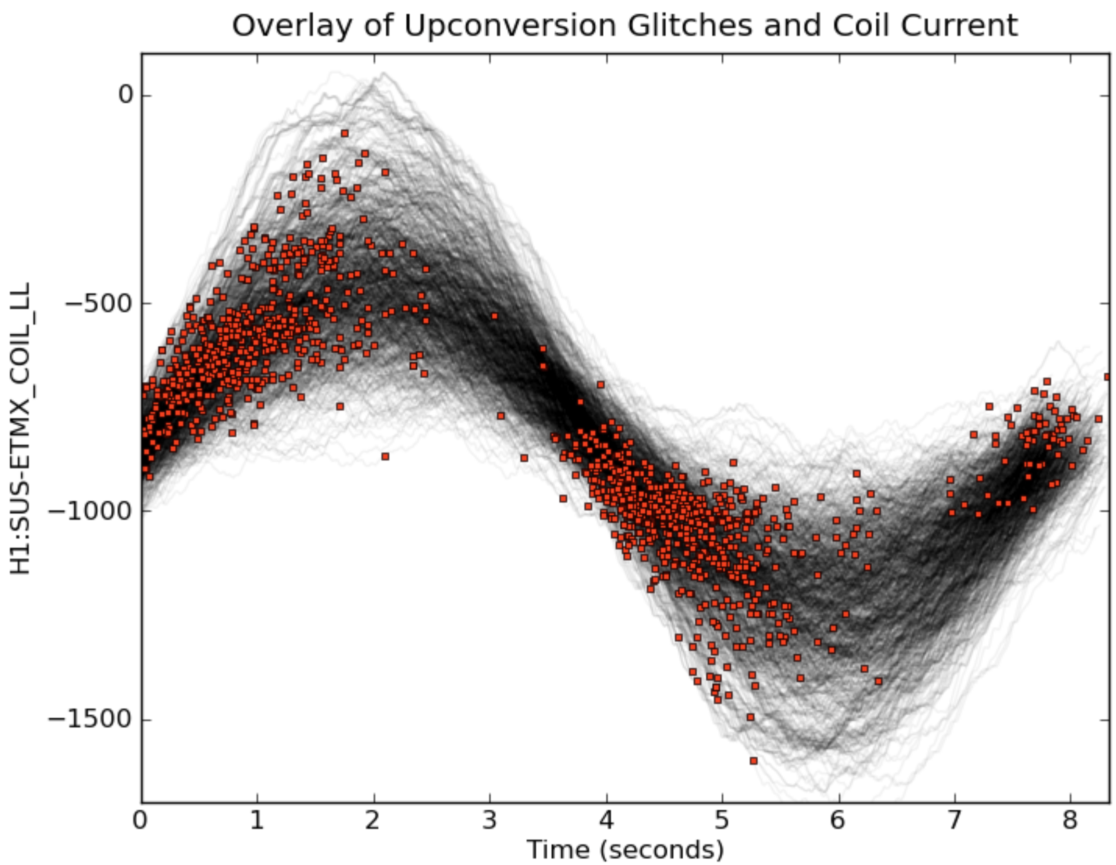

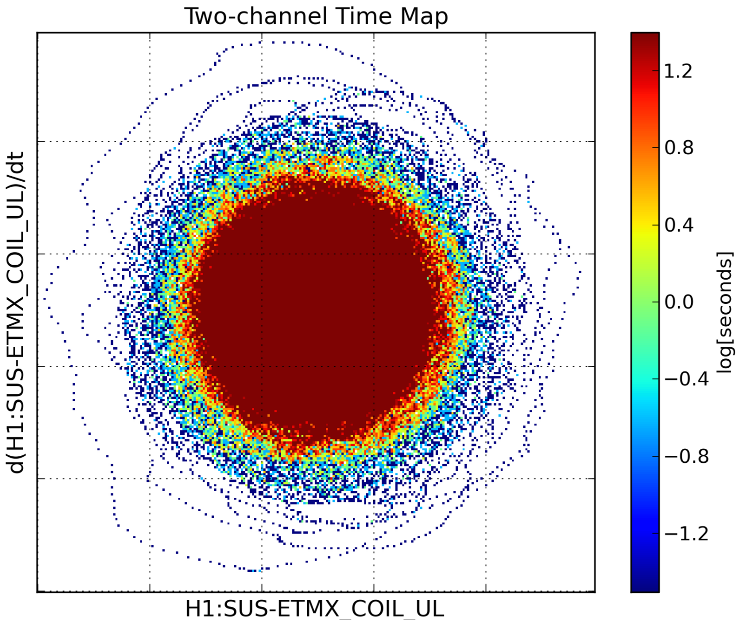

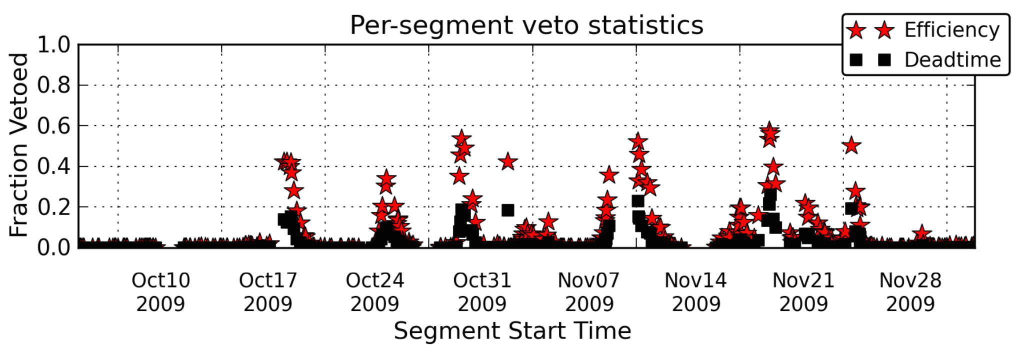

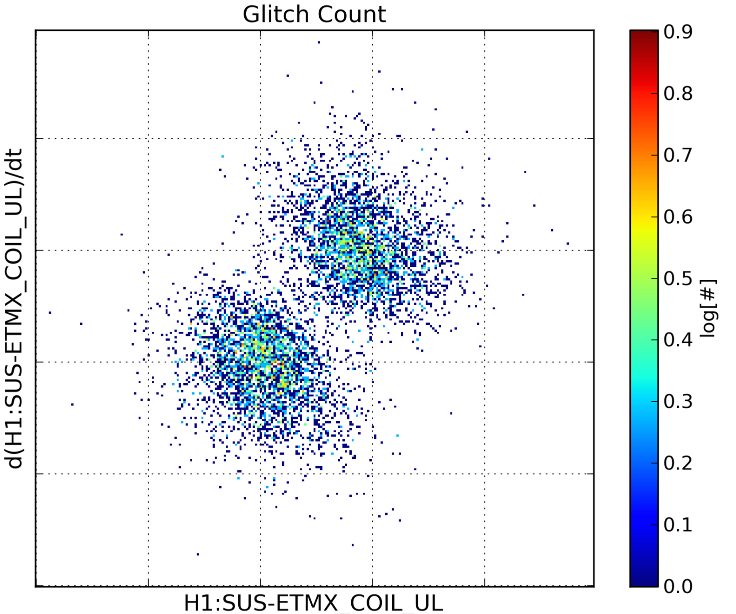

Gamma-ray Bursts

Gravitational Wave Emission from GRB Central Engines

Short GRBs: model is a compact binary coalescence (CBC), either BNS or NS-BH.

GW emission is very strong, esp. from inspiral phase (E_{GW} = 10% of a solar mass). aLIGO detection out to z~0.1 possible.

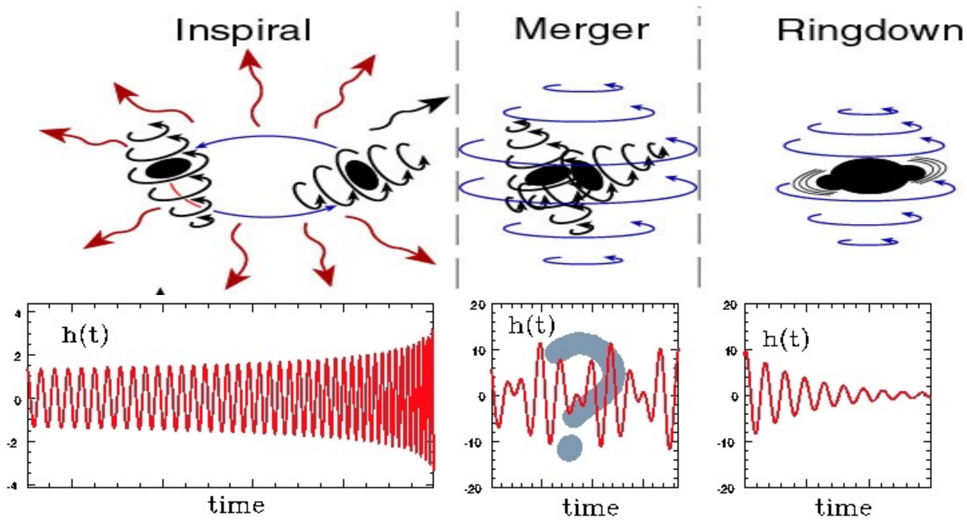

Long GRBs: collapsar model. GW emission is speculative, may be at high energy where detectors are less sensitive. Also, higher redshift.

Potential mechanisms for GW emission are bar mode instabilities, proto-NS oscillations, accretion disk instabilities, and others.

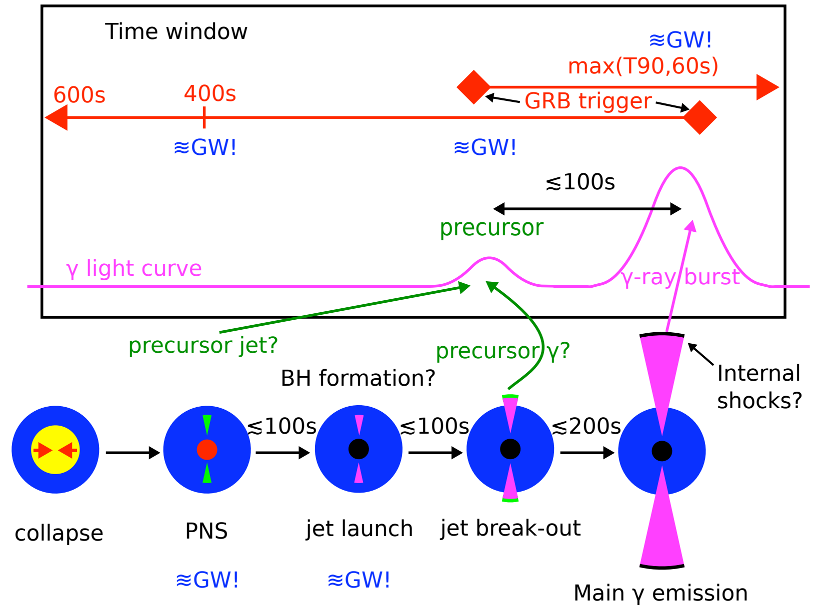

Figure by M. Was.

Coherent Analysis Techniques

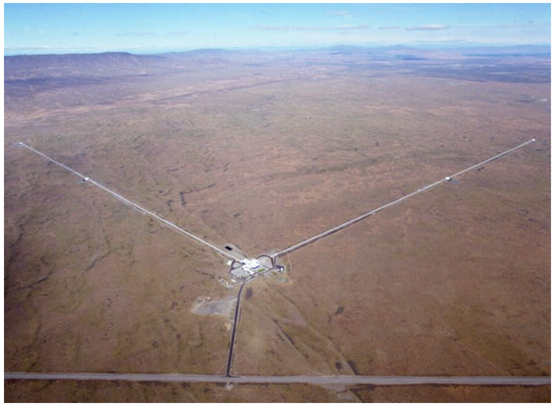

$$\begin{bmatrix} d_1(t) \\ d_2(t) \\ d_3(t) \end{bmatrix} = \begin{bmatrix} F_1^+(\Omega) & F_1^\times(\Omega) \\ F_2^+(\Omega) & F_2^\times(\Omega) \\ F_3^+(\Omega) & F_3^\times(\Omega) \end{bmatrix} \begin{bmatrix} h_+(t) \\ h_\times(t) \end{bmatrix} + \begin{bmatrix} n_1(t) \\ n_2(t) \\ n_3(t) \end{bmatrix}$$

Coherent Analysis Techniques

$$\begin{bmatrix} d_1(t) \\ d_2(t) \\ d_3(t) \end{bmatrix} = \begin{bmatrix} F_1^+(\Omega) & F_1^\times(\Omega) \\ F_2^+(\Omega) & F_2^\times(\Omega) \\ F_3^+(\Omega) & F_3^\times(\Omega) \end{bmatrix} \begin{bmatrix} h_+(t) \\ h_\times(t) \end{bmatrix} + \begin{bmatrix} n_1(t) \\ n_2(t) \\ n_3(t) \end{bmatrix}$$

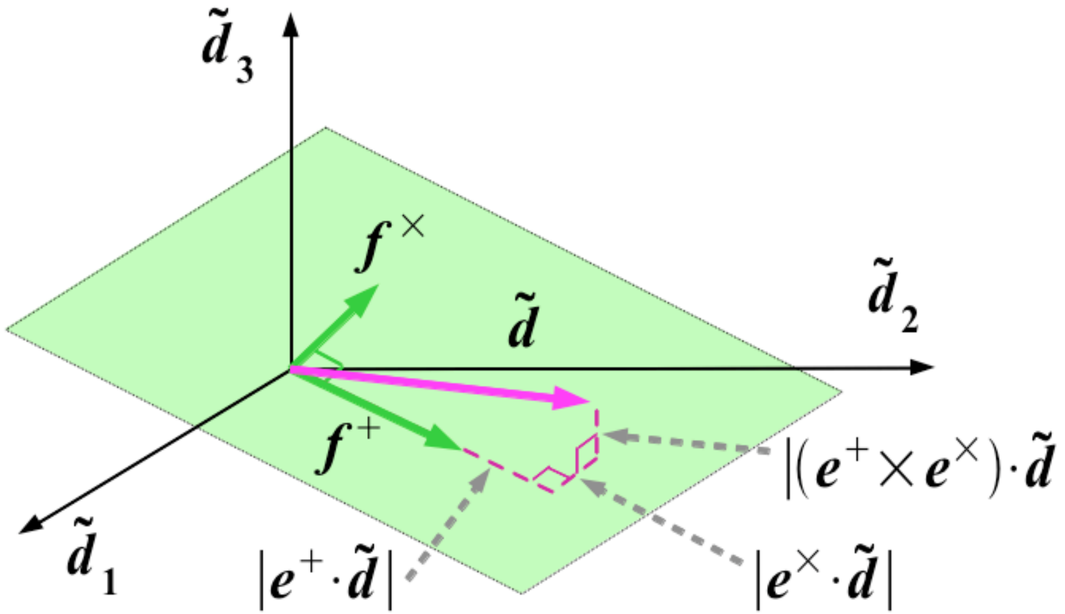

Figure from Sutton et al., New J. Phys. 12 (2010) 053034

True GW signals will lie on the plane generated by the antenna vectors.

Noise transients are independent between detectors and will lie off the signal plane.

Event significance is measured by energy in the signal plane.

Background rejection is performed by comparing signal energy to null energy.

Analysis Procedure

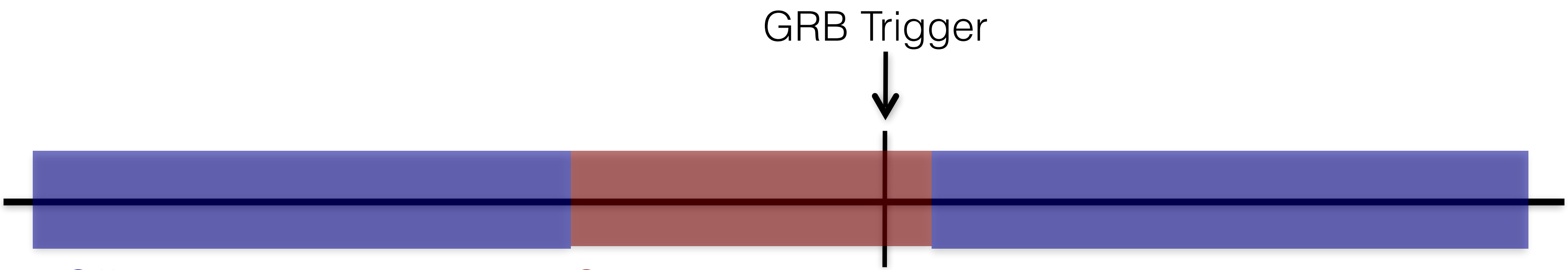

Off-source window:
[-1.5, +1.5] hours around the time of the GRB.

Used for background estimation.

Unphysical time-slides are added to the data to generate additional background events.

On-source window:
Unmodeled search:
[-600, +60] sec

BNS/NSBH search:
[-5, +1] sec

Simulated GW signals are used to tune cut thresholds, calculate upper limits. Simulation parameters are varied to account for systematic uncertainties.

Open-box data:
On-source events with detection statistic > 99% of the background events are considered detection candidates.

What A Detection Looks Like

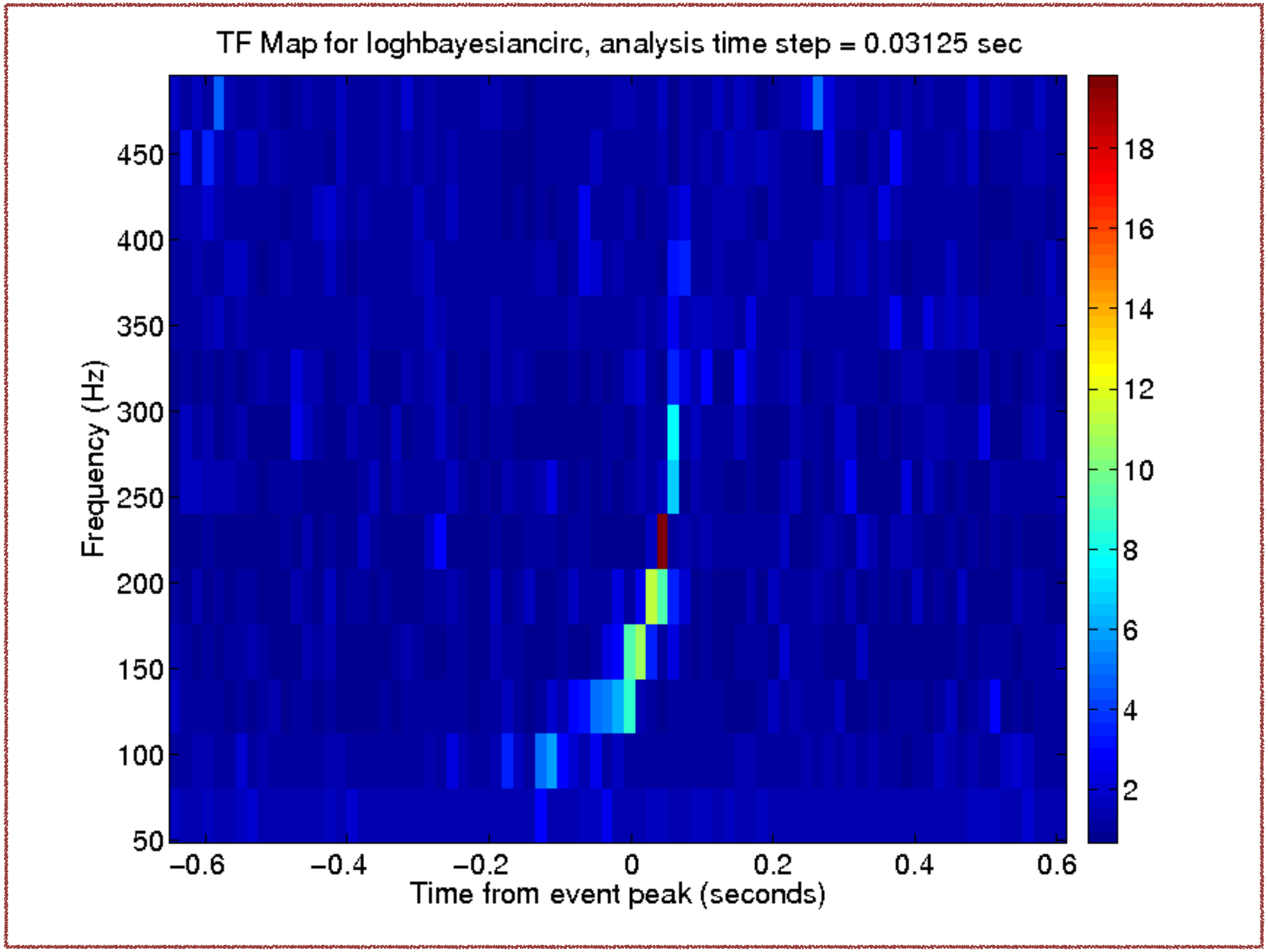

What A Detection Looks Like

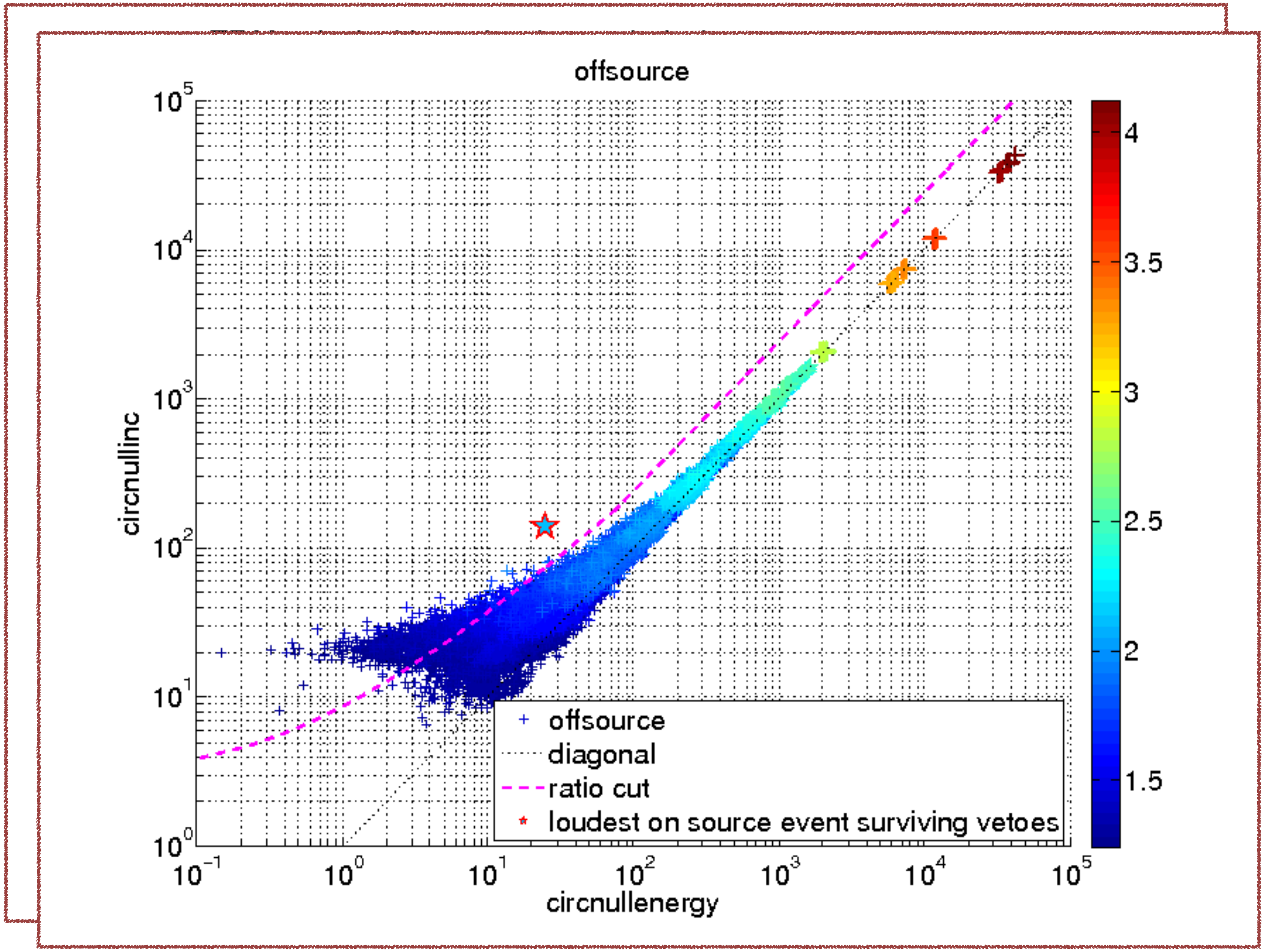

What A Detection Looks Like

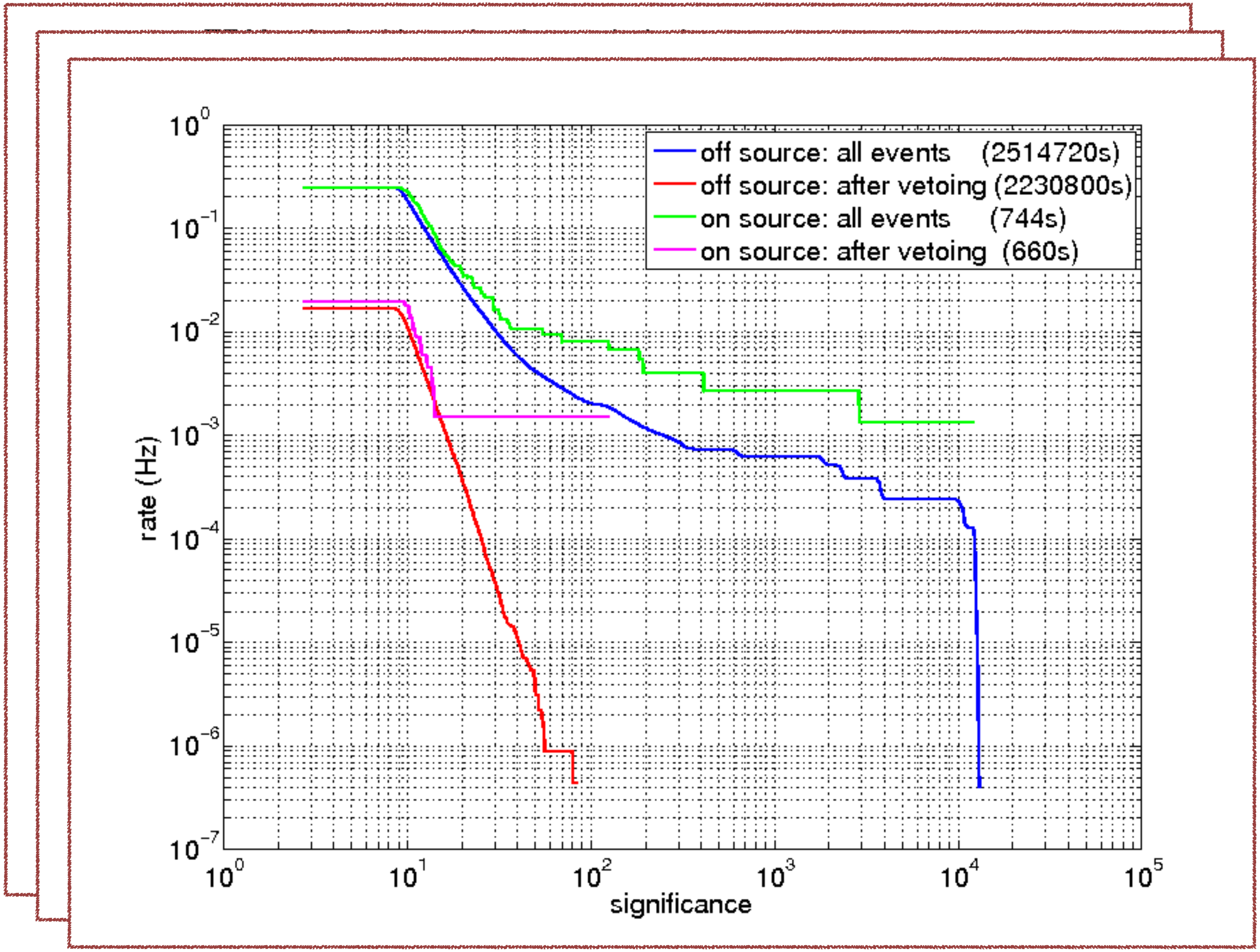

The loudest event in the on-source is assigned a p-value.

The GEO-GRBs Search - Methods

152 GRBs between 2007 and 2011.

All use 2-detector network: GEO 600 and one other observatory.

Challenges for the search: GEO's best sensitivity is 500Hz and higher.

We use an extended search band compared to most recent GW-GRB analyses, 64-1792Hz.

The high-frequency search band requires a different approach to GRBs with large sky position uncertainty.

Use a linear grid of search points on the sky for GRBs with localization uncertainty > 1 degree.

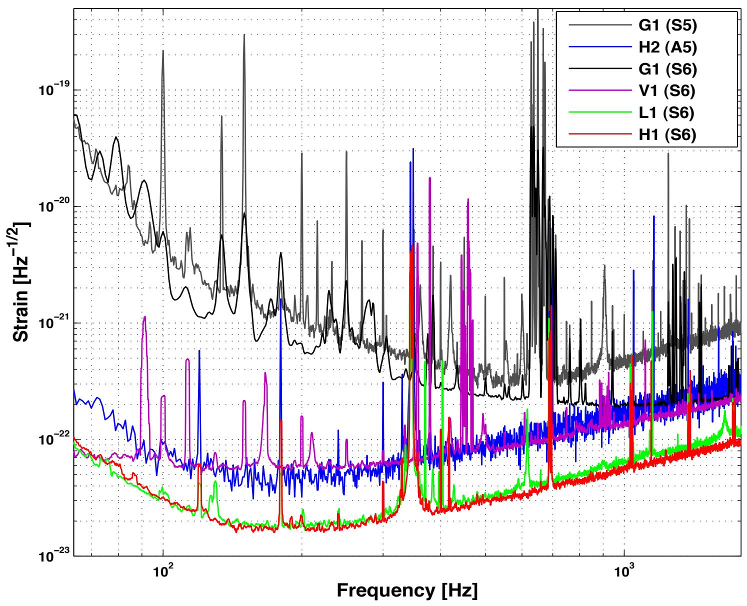

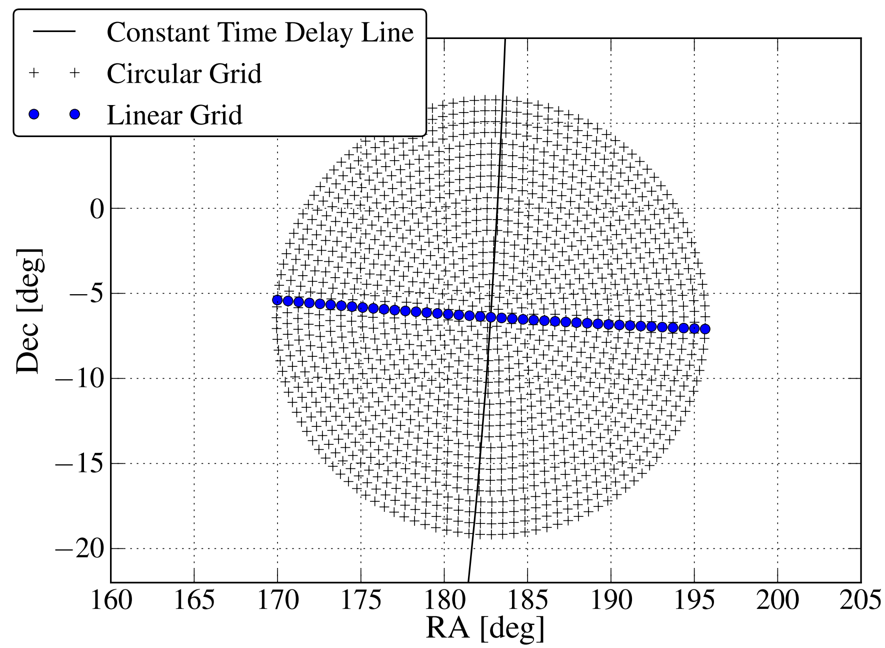

The GEO-GRBs Search - Results

We analyzed each of the 152 GRBs independently. For *Fermi* events, with rough sky localization, we used the linear grid to reduce the computational cost.

Some of the analysis results showed we were insensitive to GW signals, due to unlucky sky location or poor sensitivity.

129 GRB events had good sensitivity to gravitational waves.

None of these GRBs had significant events in the on-source window.

The population as a whole did not have a statistically significant population of low-probability events, after weighting for sensitivity.

Probability that results were consistent with background: 19.3%.

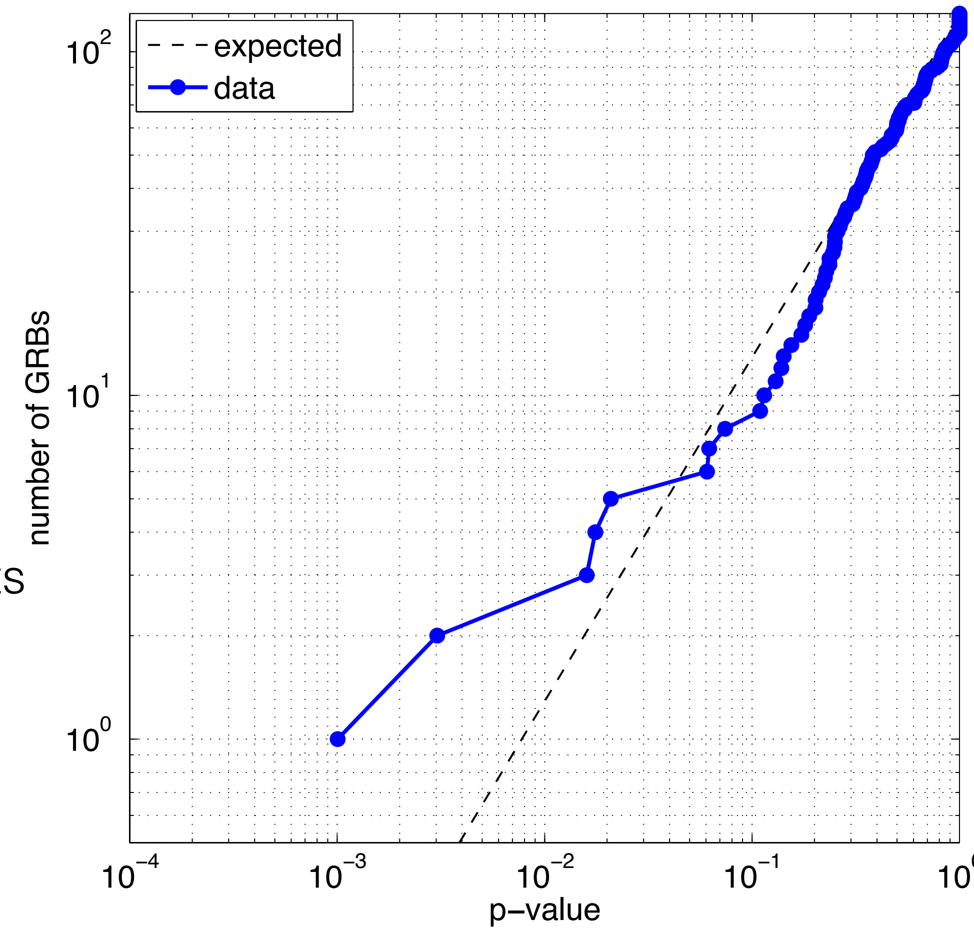

Statistical Significance of the Results

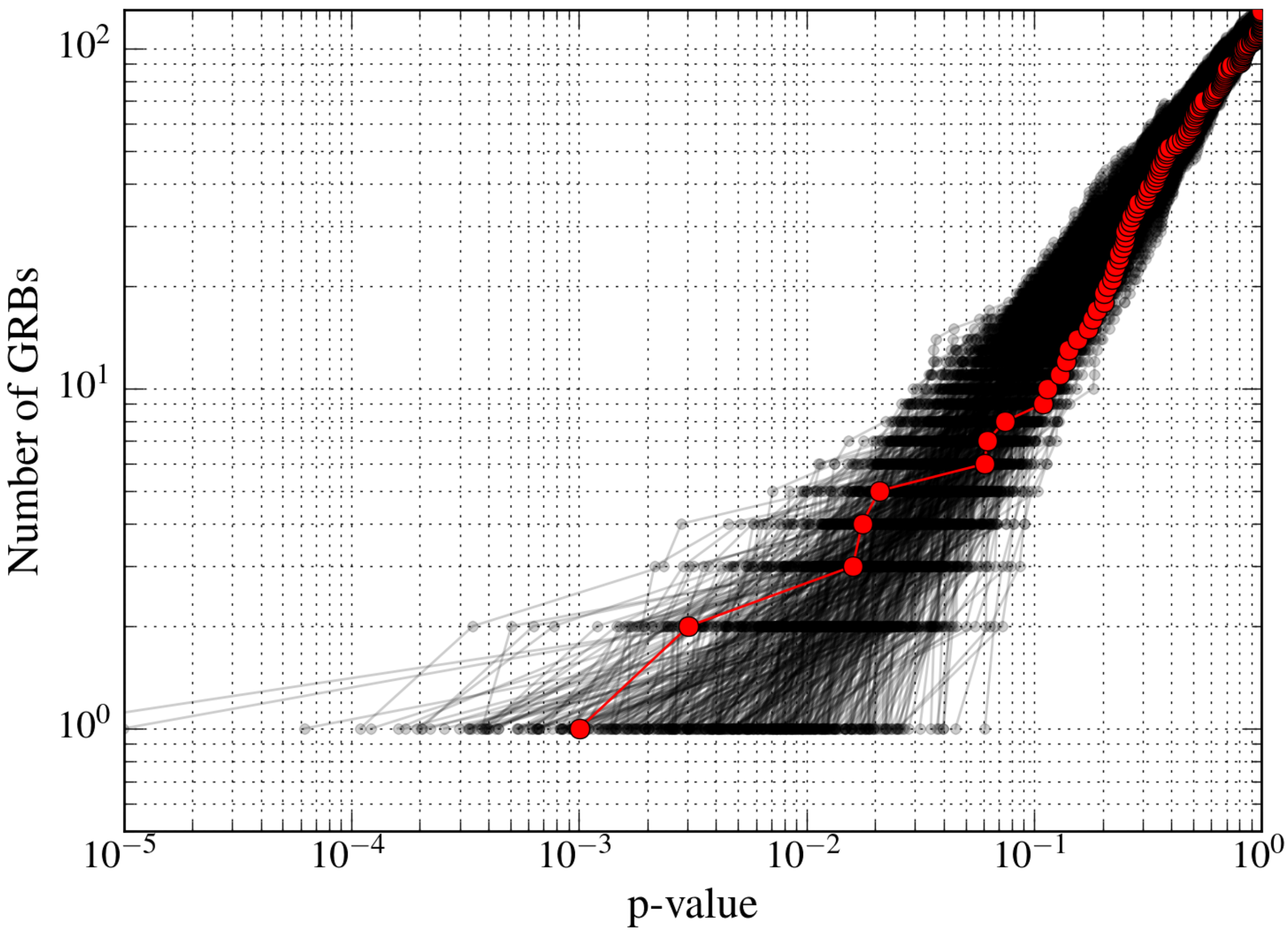

The GEO-GRBs Search - Upper Limits

We used simulated gravitational waveforms to measure the search sensitivity.

These signals were used to place upper limits on the amplitude of generic narrowband, short-duration signals.

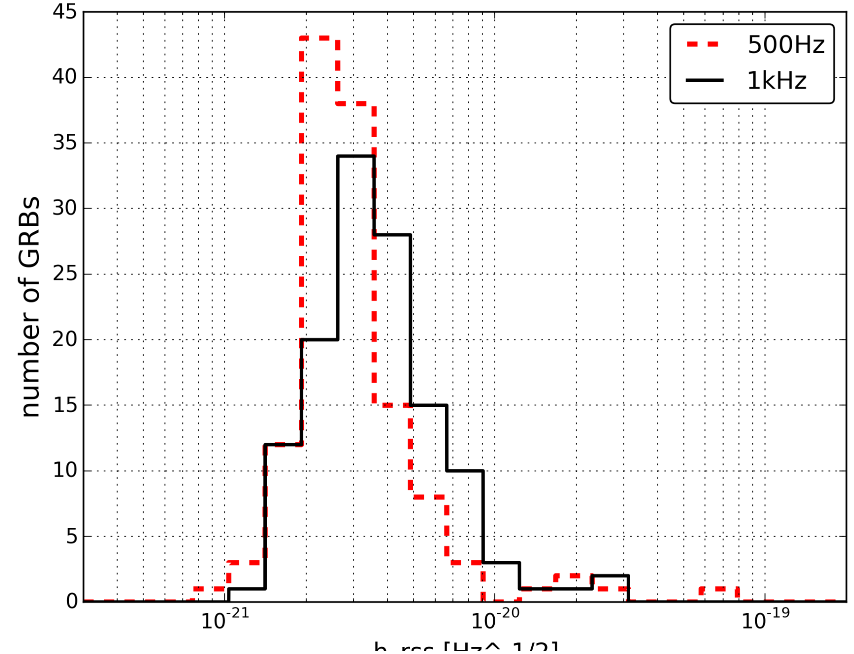

Using a model for energy emitted to gravitational waves, can set a lower limit on distance to the source.

For an optimistic emission energy, our limits were O(1) Mpc.

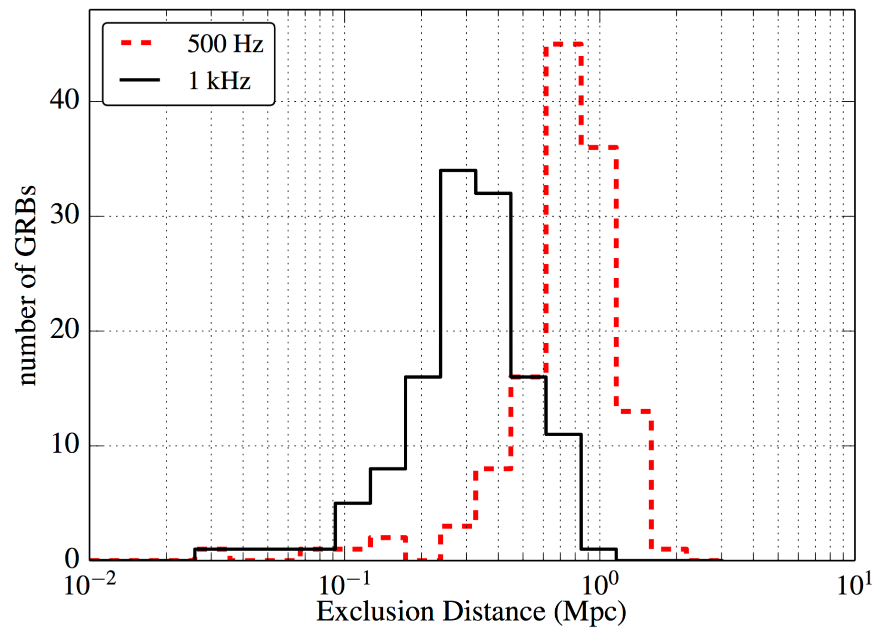

The sensitivity of the search was limited by our detector network. Advanced detectors could improve limits by 20x.

The GEO-GRBs Search - Upper Limits

We used simulated gr
to measure the search

These signals were us
limits on the amplitude
narrowband, short-dur

Using a model for ene
gravitational waves, ca
distance to the source

For an optimistic emis
were O(1) Mpc.

The sensitivity of the s
our detector network.
could improve limits by 20x.

PHYSICAL REVIEW D **89,** 122004 (2014)

Methods and results of a search for gravitational waves associated with gamma-ray bursts using the GEO 600, LIGO, and Virgo detectors

J. Aasi,[1] B. P. Abbott,[1] R. Abbott,[1] T. Abbott,[2] M. R. Abernathy,[1] F. Acernese,[3,4] K. Ackley,[5] C. Adams,[6] T. Adams,[7] P. Addesso,[8] R. X. Adhikari,[1] C. Affeldt,[9] M. Agathos,[10] N. Aggarwal,[11] O. D. Aguiar,[12] P. Ajith,[13] A. Alemic,[14] B. Allen,[9,15,16] A. Allocca,[17,18] D. Amariutei,[5] M. Andersen,[19] R. A. Anderson,[1] S. B. Anderson,[1] W. G. Anderson,[15] K. Arai,[1] M. C. Araya,[1] C. Arceneaux,[20] J. S. Areeda,[21] S. Ast,[16] S. M. Aston,[6] P. Astone,[22] P. Aufmuth,[16] H. Augustus,[23] C. Aulbert,[9] B. E. Aylott,[23] S. Babak,[24] P. T. Baker,[25] G. Ballardin,[26] S. W. Ballmer,[14] J. C. Barayoga,[1] M. Barbet,[5] B. C. Barish,[1] D. Barker,[27] F. Barone,[3,4] B. Barr,[28] L. Barsotti,[11] M. Barsuglia,[29] M. A. Barton,[27] I. Bartos,[30] R. Bassiri,[19] A. Basti,[31,18] J. C. Batch,[27] J. Bauchrowitz,[9] Th. S. Bauer,[10] C. Baune,[9] V. Bavigadda,[26] B. Behnke,[24] M. Bejger,[32] M. G. Beker,[10] C. Belczynski,[33] A. S. Bell,[28] C. Bell,[28] G. Bergmann,[9] D. Bersanetti,[34,35] A. Bertolini,[10] J. Betzwieser,[6] I. A. Bilenko,[36] G. Billingsley,[1] J. Birch,[6] S. Biscans,[11] M. Bitossi,[18] C. Biwer,[14] M. A. Bizouard,[37] E. Black,[1] J. K. Blackburn,[1] L. Blackburn,[38] D. Blair,[39] S. Bloemen,[10,40] O. Bock,[9] T. P. Bodiya,[11] M. Boer,[41] G. Bogaert,[41] C. Bogan,[9] C. Bond,[23] F. Bondu,[42] L. Bonelli,[31,18] R. Bonnand,[43] R. Bork,[1] M. Born,[9] V. Boschi,[18] Sukanta Bose,[44,45] L. Bosi,[46] C. Bradaschia,[18] P. R. Brady,[15,47] V. B. Braginsky,[36] M. Branchesi,[48,49] J. E. Brau,[50] T. Briant,[51] D. O. Bridges,[6] A. Brillet,[41] M. Brinkmann,[9] V. Brisson,[37] A. F. Brooks,[1] D. A. Brown,[14] D. D. Brown,[23] F. Brückner,[23] S. Buchman,[19] A. Buikema,[11] T. Bulik,[33] H. J. Bulten,[52,10] A. Buonanno,[53] R. Burman,[39] D. Buskulic,[43] C. Buy,[29] L. Cadonati,[54,7] G. Cagnoli,[55] J. Cain,[20] J. Calderón Bustillo,[56] E. Calloni,[57,4] J. B. Camp,[38] P. Campsie,[28] K. C. Cannon,[58] B. Canuel,[26] J. Cao,[59] C. D. Capano,[53] F. Carbognani,[26] L. Carbone,[23] S. Caride,[60] G. Castaldi,[8] S. Caudill,[15] M. Cavaglià,[20] F. Cavalier,[37] R. Cavalieri,[26] C. Celerier,[19] G. Cella,[18] C. Cepeda,[1] E. Cesarini,[61] R. Chakraborty,[1] T. Chalermsongsak,[1] S. J. Chamberlin,[15] S. Chao,[62] P. Charlton,[63] E. Chassande-Mottin,[29] X. Chen,[39] Y. Chen,[64] A. Chincarini,[35] A. Chiummo,[26] H. S. Cho,[65] M. Cho,[53] J. H. Chow,[66] N. Christensen,[67] Q. Chu,[39] S. S. Y. Chua,[66] S. Chung,[39] G. Ciani,[5] F. Clara,[27] D. E. Clark,[19] J. A. Clark,[54] J. H. Clayton,[15] F. Cleva,[41] E. Coccia,[68,69] P.-F. Cohadon,[51] A. Colla,[70,22] C. Collette,[71] M. Colombini,[46] L. Cominsky,[72] M. Constancio, Jr.,[12] A. Conte,[70,22] D. Cook,[27] T. R. Corbitt,[2] N. Cornish,[25] A. Corsi,[73] C. A. Costa,[12] M. W. Coughlin,[74] J.-P. Coulon,[41] S. Countryman,[30] P. Couvares,[14] D. M. Coward,[39] M. J. Cowart,[6] D. C. Coyne,[1] R. Coyne,[73] K. Craig,[28] J. D. E. Creighton,[15] R. P. Croce,[8] S. G. Crowder,[75] A. Cumming,[28] L. Cunningham,[28] E. Cuoco,[26] C. Cutler,[64] K. Dahl,[9] T. Dal Canton,[9] M. Damjanic,[9] S. L. Danilishin,[39] S. D'Antonio,[61] K. Danzmann,[16,9] V. Dattilo,[26] H. Daveloza,[76] M. Davier,[37] G. S. Davies,[28] E. J. Daw,[77] R. Day,[26] T. Dayanga,[44] D. DeBra,[19] G. Debreczeni,[78] J. Degallaix,[55] S. Deléglise,[51] W. Del Pozzo,[23] W. Del Pozzo,[10] T. Denker,[9] T. Dent,[9] H. Dereli,[41] V. Dergachev,[1] R. De Rosa,[57,4] R. T. DeRosa,[2] R. DeSalvo,[8] S. Dhurandhar,[45] M. Díaz,[76] J. Dickson,[66] L. Di Fiore,[4] A. Di Lieto,[31,18] I. Di Palma,[9] A. Di Virgilio,[18] V. Dolique,[55] E. Dominguez,[79] F. Donovan,[11] K. L. Dooley,[9] S. Doravari,[6] R. Douglas,[28] T. P. Downes,[15] M. Drago,[80,81] R. W. P. Drever,[1] J. C. Driggers,[1] Z. Du,[59] M. Ducrot,[43] S. Dwyer,[27] T. Eberle,[9] T. Edo,[77] M. Edwards,[7] A. Effler,[2] H.-B. Eggenstein,[9] P. Ehrens,[1] J. Eichholz,[5] S. S. Eikenberry,[5] G. Endrőczi,[78] R. Essick,[11] T. Etzel,[1] M. Evans,[11] T. Evans,[6] M. Factourovich,[30] V. Fafone,[68,61] S. Fairhurst,[7] X. Fan,[28] Q. Fang,[39] S. Farinon,[35] B. Farr,[82] W. M. Farr,[23] M. Favata,[83] D. Fazi,[82] H. Fehrmann,[9] M. M. Fejer,[19] D. Feldbaum,[5,6] F. Feroz,[74] I. Ferrante,[31,18] E. C. Ferreira,[12] F. Ferrini,[26] F. Fidecaro,[31,18] L. S. Finn,[84] I. Fiori,[26] R. P. Fisher,[14] R. Flaminio,[55] N. Fotopoulos,[1] J.-D. Fournier,[41] S. Franco,[37] S. Frasca,[70,22] F. Frasconi,[18] M. Frede,[9] Z. Frei,[85] A. Freise,[23] R. Frey,[50] T. T. Fricke,[9] P. Fritschel,[11] V. V. Frolov,[6] P. Fulda,[5] M. Fyffe,[6] J. R. Gair,[74] L. Gammaitoni,[86,46] S. Gaonkar,[45] F. Garufi,[57,4] N. Gehrels,[38] G. Gemme,[35] B. Gendre,[41] E. Genin,[26] A. Gennai,[18] S. Ghosh,[10,40] J. A. Giaime,[6,2] K. D. Giardina,[6] A. Giazotto,[18] C. Gill,[28] J. Gleason,[5] E. Goetz,[9] R. Goetz,[5] L. Gondan,[85] G. González,[2] N. Gordon,[28] M. L. Gorodetsky,[36] S. Gossan,[64] S. Goßler,[9] R. Gouaty,[43] C. Gräf,[28] P. B. Graff,[38] M. Granata,[55] A. Grant,[28] S. Gras,[11] C. Gray,[27] R. J. S. Greenhalgh,[87] A. M. Gretarsson,[88] P. Groot,[40] H. Grote,[9] K. Grover,[23] S. Grunewald,[24] G. M. Guidi,[48,49] C. J. Guido,[6] K. Gushwa,[1] E. K. Gustafson,[1] R. Gustafson,[60] J. Ha,[89] E. D. Hall,[1] W. Hamilton,[2] D. Hammer,[15] G. Hammond,[28] M. Hanke,[9] J. Hanks,[27] C. Hanna,[90,84] M. D. Hannam,[7] J. Hanson,[6] K. Haris,[98] J. Harms,[1] G. M. Harry,[91] I. W. Harry,[14] E. D. Harstad,[50] M. Hart,[28] M. T. Hartman,[5] C.-J. Haster,[23] K. Haughian,[28] A. Heidmann,[51] M. Heintze,[5,6] H. Heitmann,[41] P. Hello,[37] G. Hemming,[26] M. Hendry,[28] I. S. Heng,[28] A. W. Heptonstall,[1] M. Heurs,[9] M. Hewitson,[9] S. Hild,[28] D. Hoak,[54] K. A. Hodge,[1] D. Hofman,[55] K. Holt,[6] P. Hopkins,[7] T. Horrom,[92] D. Hoske,[93] D. J. Hosken,[93] J. Hough,[28] E. J. Howell,[39] Y. Hu,[28] E. Huerta,[14] B. Hughey,[88] S. Husa,[56] S. H. Huttner,[28] M. Huynh,[15] T. Huynh-Dinh,[6] A. Idrisy,[84] D. R. Ingram,[27] R. Inta,[84] G. Islas,[21] T. Isogai,[11] A. Ivanov,[1] B. R. Iyer,[94] K. Izumi,[27] M. Jacobson,[1] H. Jang,[95] P. Jaranowski,[96] Y. Ji,[59] F. Jiménez-Forteza,[56] W. W. Johnson,[2] D. I. Jones,[97] G. Jones,[7] R. Jones,[28] R. J. G. Jonker,[10] L. Ju,[39] P. Kalmus,[1] V. Kalogera,[82] S. Kandhasamy,[20] G. Kang,[95] J. B. Kanner,[1] J. Karlen,[54] M. Kasprzack,[37,26] E. Katsavounidis,[11] W. Katzman,[6] H. Kaufer,[16] S. Kaufer,[16] T. Kaur,[39] K. Kawabe,[27] F. Kawazoe,[9] F. Kéfélian,[41] G. M. Keiser,[19] D. Keitel,[9] D. B. Kelley,[14] W. Kells,[1] D. G. Keppel,[9] A. Khalaidovski,[9] F. Y. Khalili,[36] E. A. Khazanov,[99] C. Kim,[89,95] K. Kim,[100] N. G. Kim,[95] N. Kim,[19] S. Kim,[95] Y.-M. Kim,[65] E. J. King,[93] P. J. King,[1] D. L. Kinzel,[6] J. S. Kissel,[27] S. Klimenko,[5]

1550-7998/2014/89(12)/122004(17) 122004-1

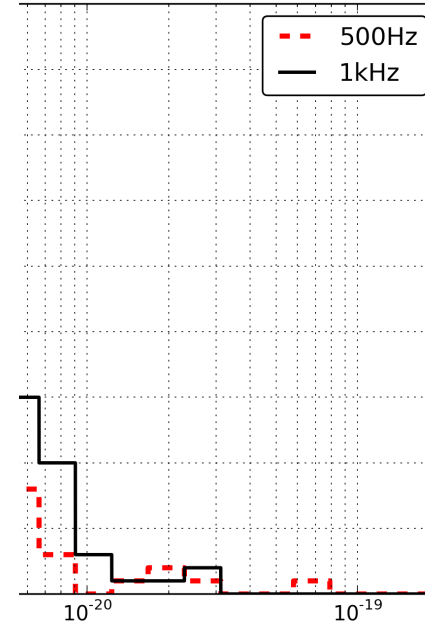

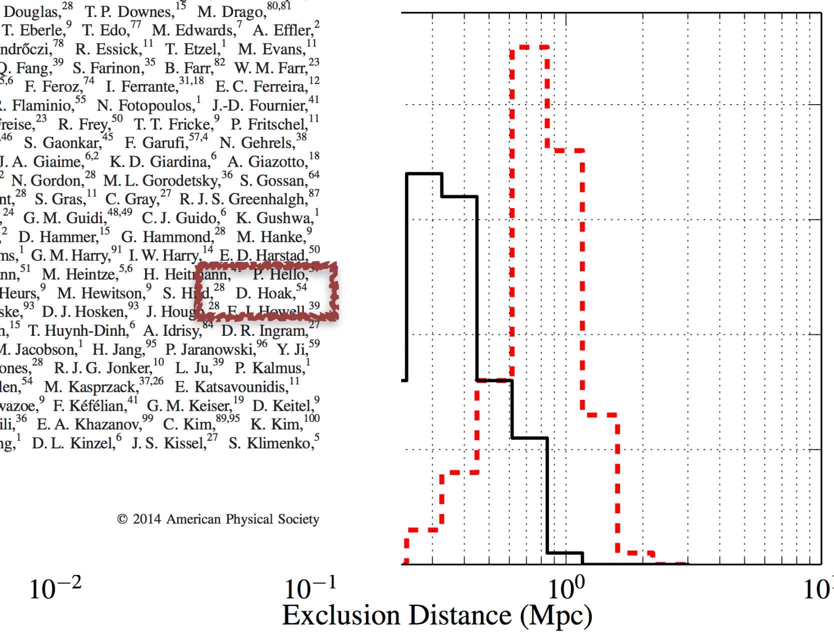

Sky Localization

Hard to improve upon gamma-ray satellite localizations (even *Fermi* GBM)

Some hope for CBC or high-frequency bursts (due to likelihood maximization across sky locations / time-of-flight)

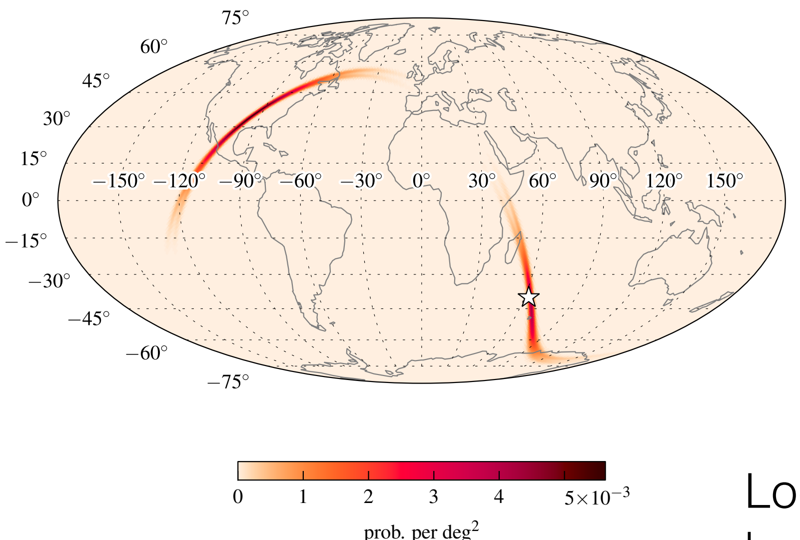

Figure from Singer, Price et al., Ap. J. 795 (2014) 105, **arXiv:1404.5623**

See also Essick et al., **arXiv:1409.2435**

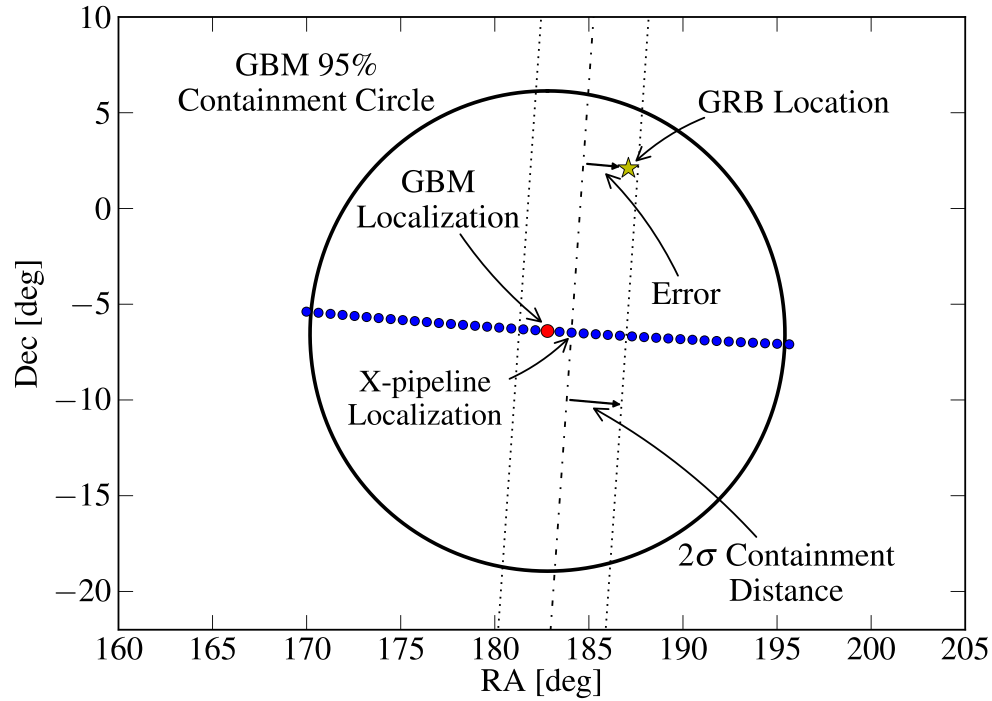

Figure from **arXiv:1405.1053**

Localization capabilities of GW detector networks have been carefully studied for all-sky CBC and unmodeled searches - less so for triggered searches.

Sky Localization - Results

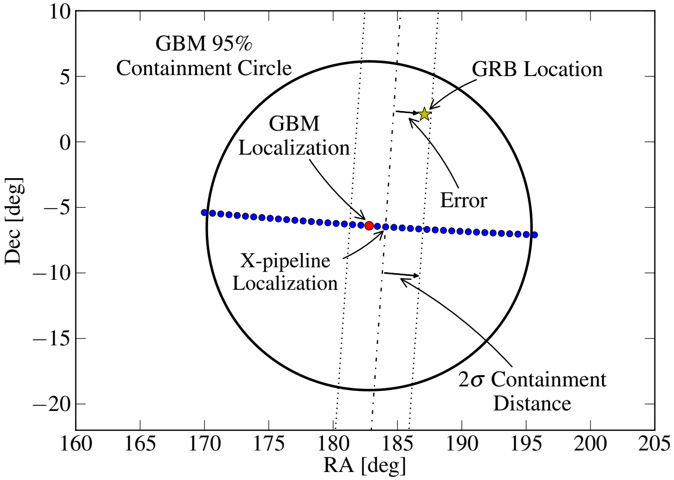

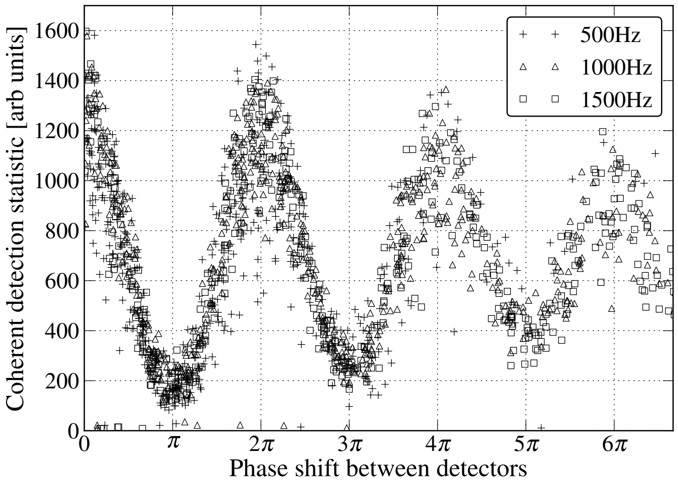

For H1-V1 detector pair:

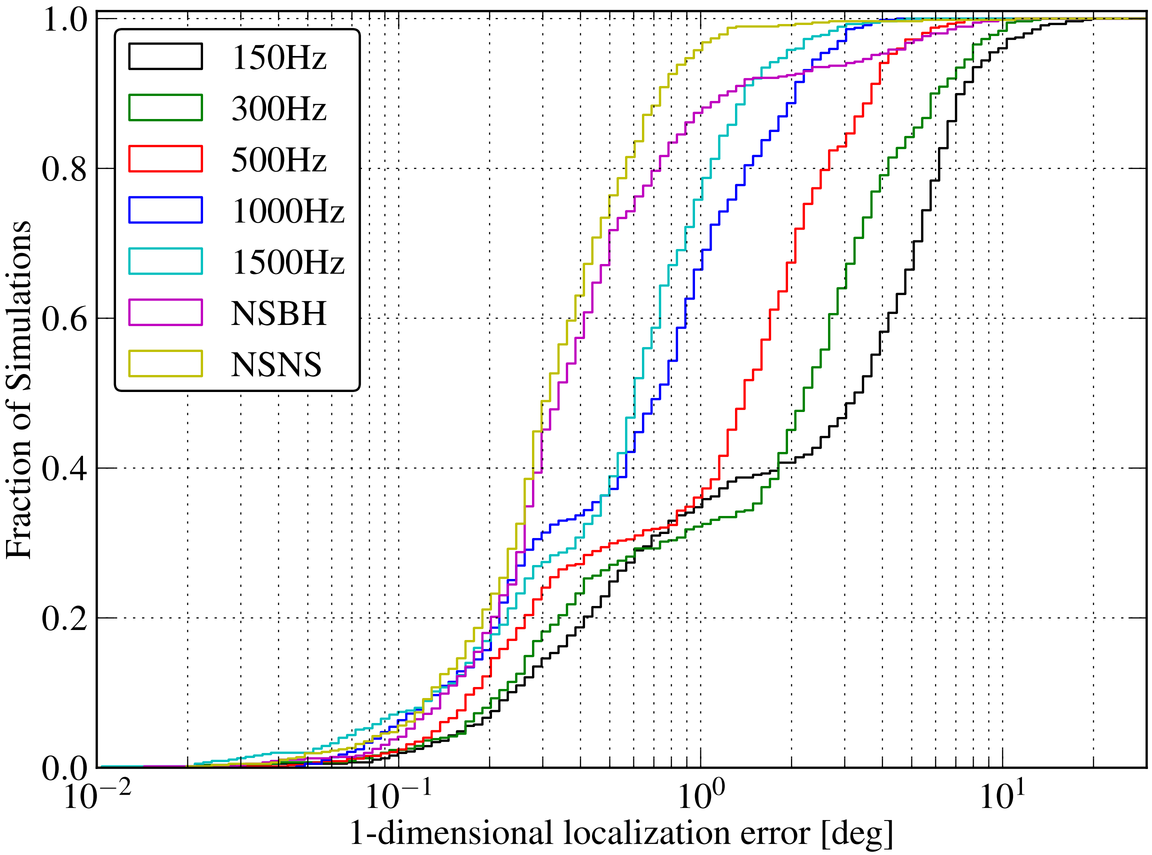

Conclusion

Prospects for Detection

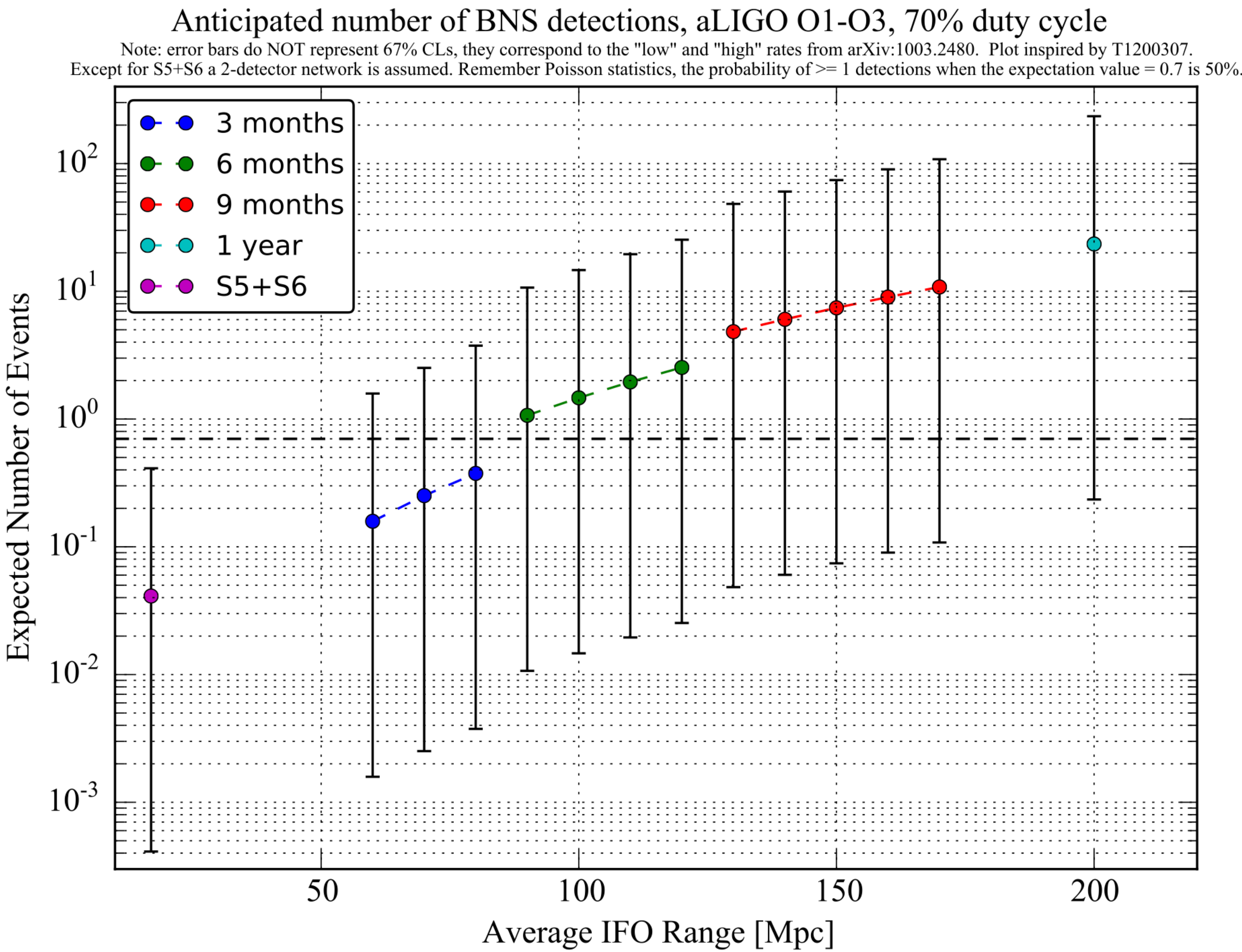

The end is not in sight!

Supplemental Slides

The Initial Detector Era - Results Highlights

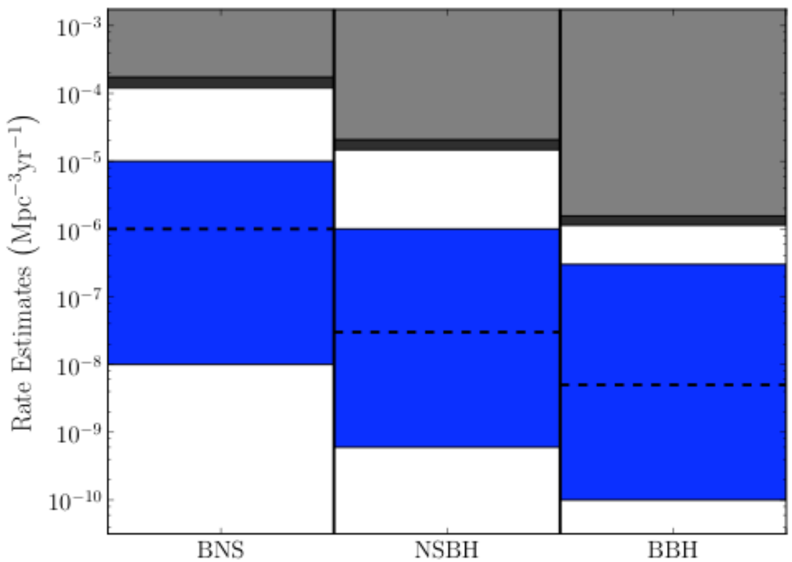

arXiv:1111.7314

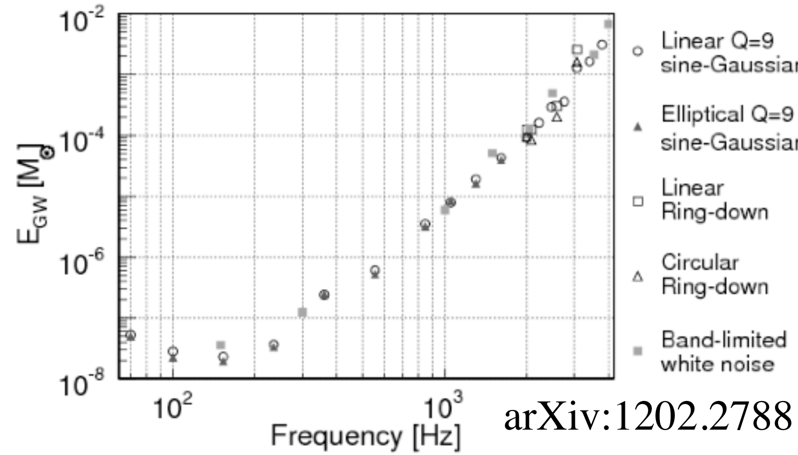

arXiv:1202.2788

arXiv:1207.7176

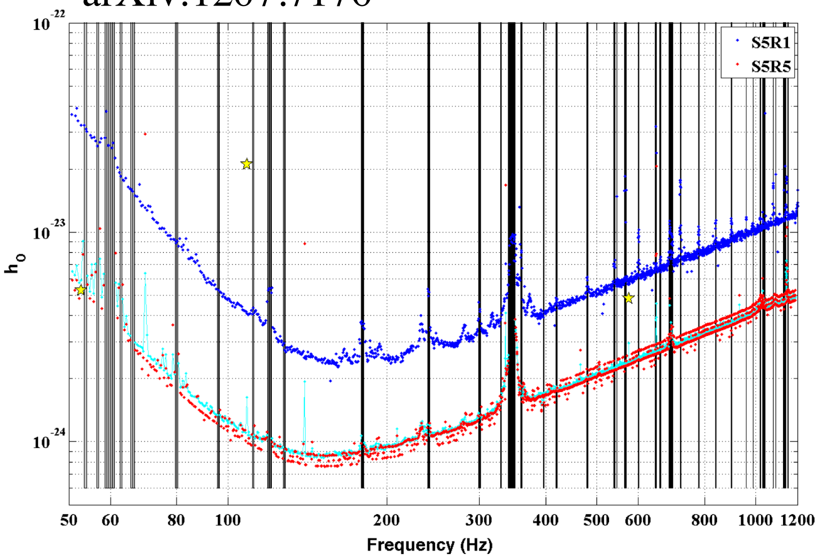

arXiv:1406.4556

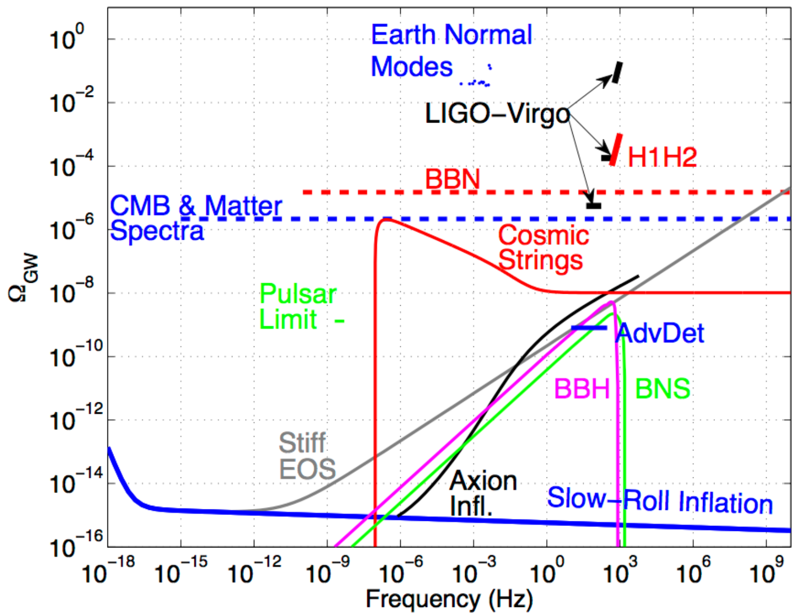

Detector Response

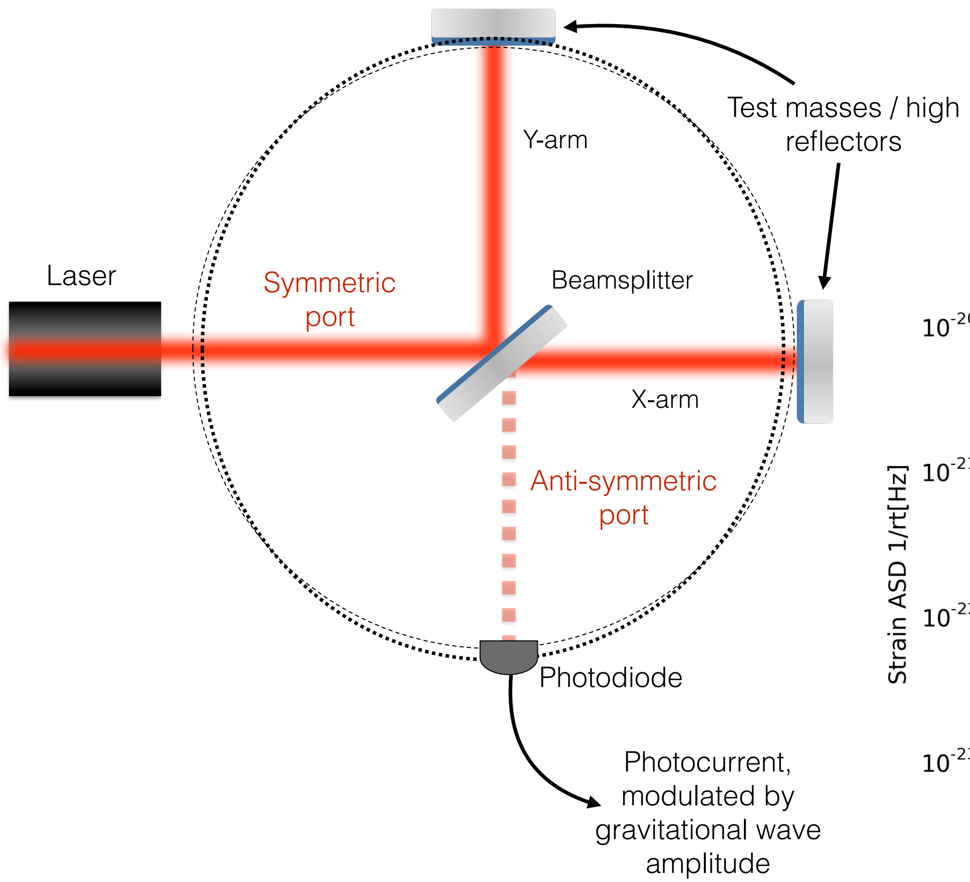

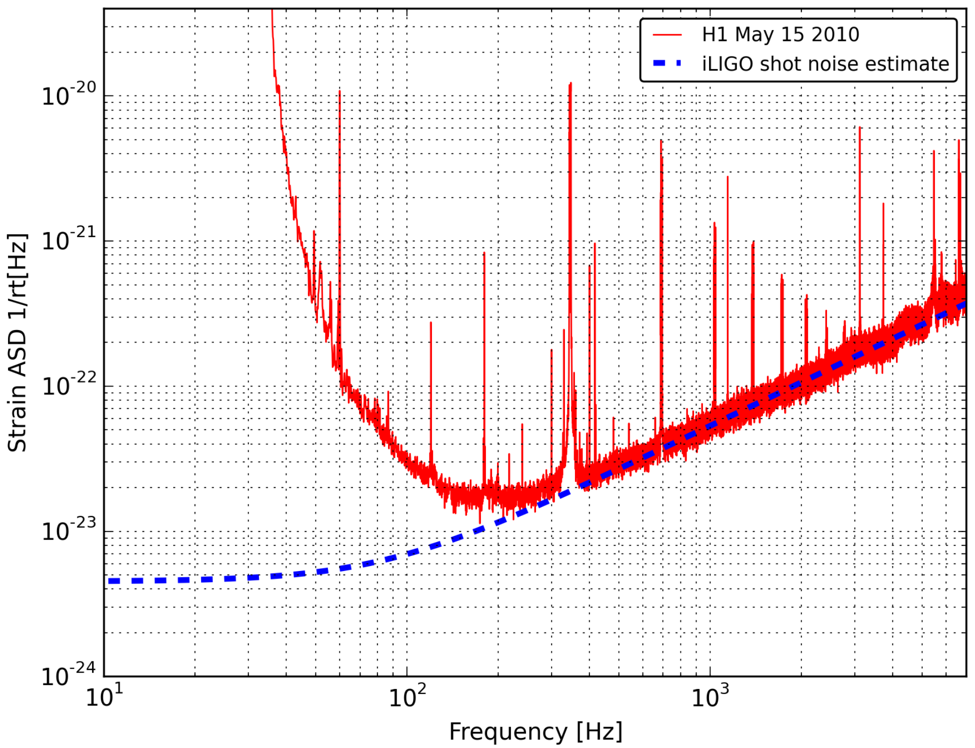

Response function for the initial detector configuration:

$$\frac{\delta P_{AS}}{\delta h} = 8 g_{cr} \frac{\mathcal{F} L}{\lambda} \sqrt{P_{IN} P_{AS}} \left(1 + i \frac{f}{f_{\mathrm{pole}}}\right)^{-1}$$

ALS Laser Alignment in 2012

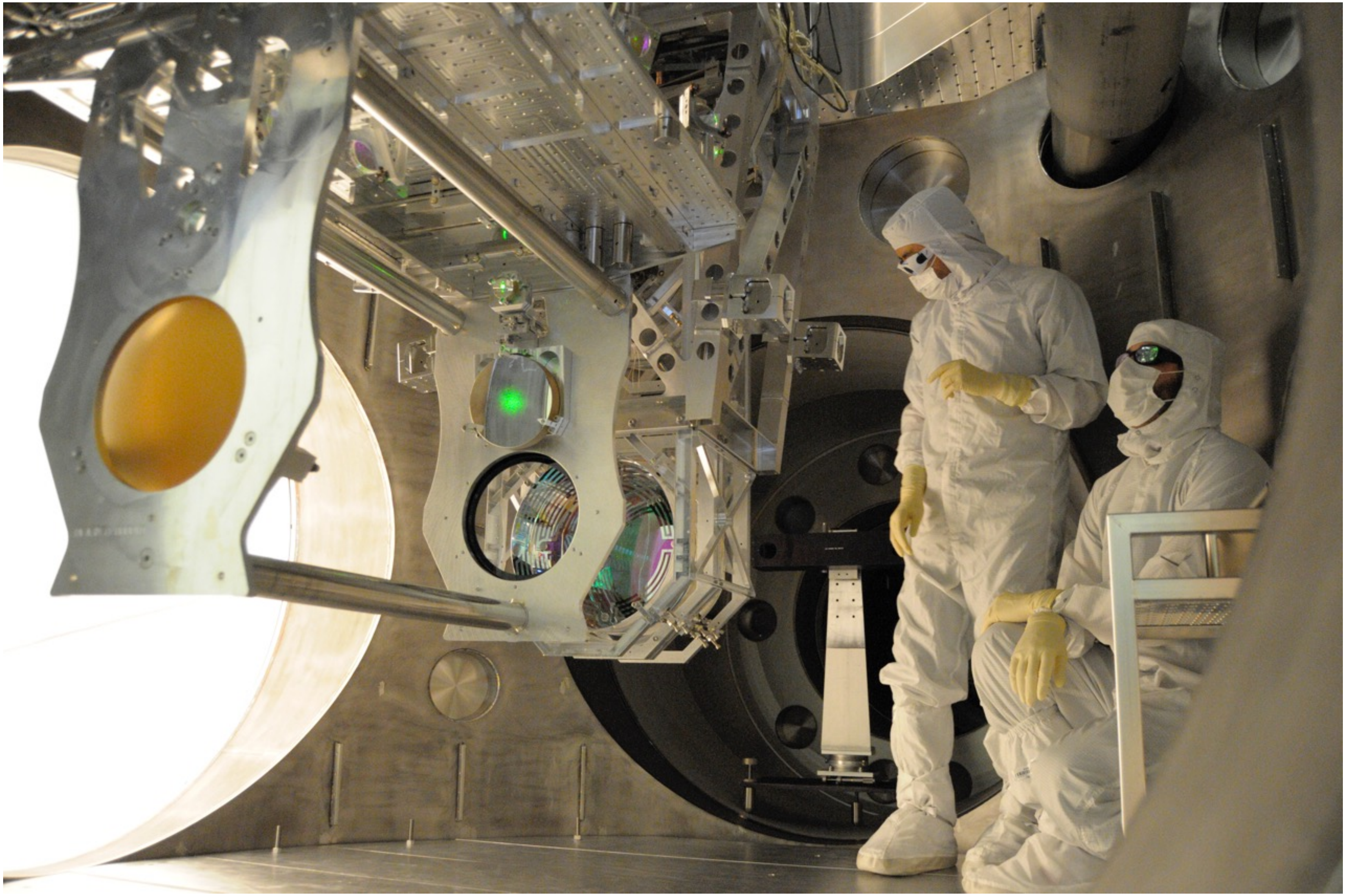

ALS Control

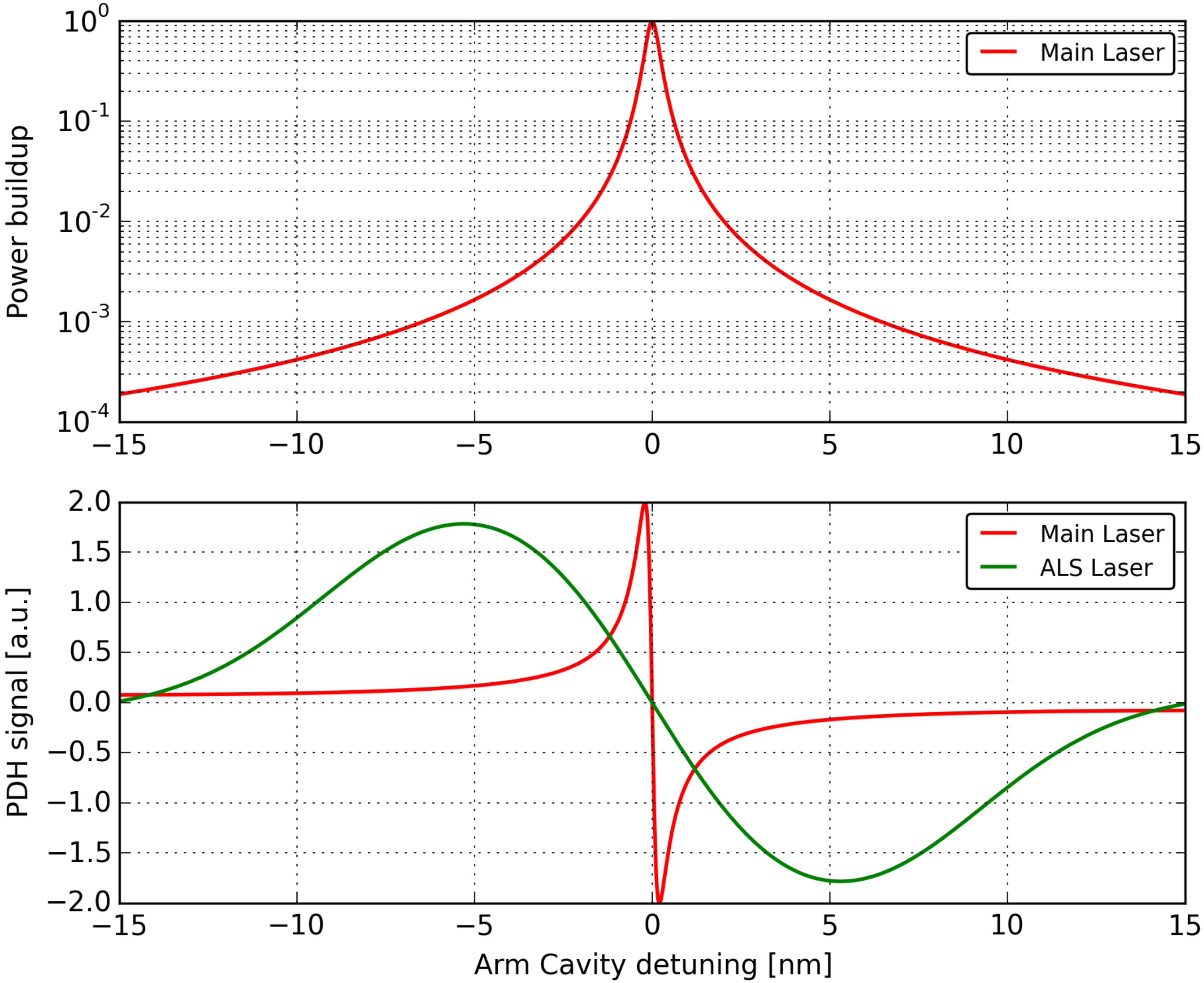

Power buildup
10^{0}
10^{-1}
10^{-2}
10^{-3}
10^{-4}
Main Laser
−15
−10
−5
0
5
10
15
PDH signal [a.u.]
2.0
1.5
1.0
0.5
0.0
−0.5
−1.0
−1.5
−2.0
Main Laser
ALS Laser
−15
−10
−5
0
5
10
15
Arm Cavity detuning [nm]

ALS Fiber Distribution

Pre-Stabilized Laser

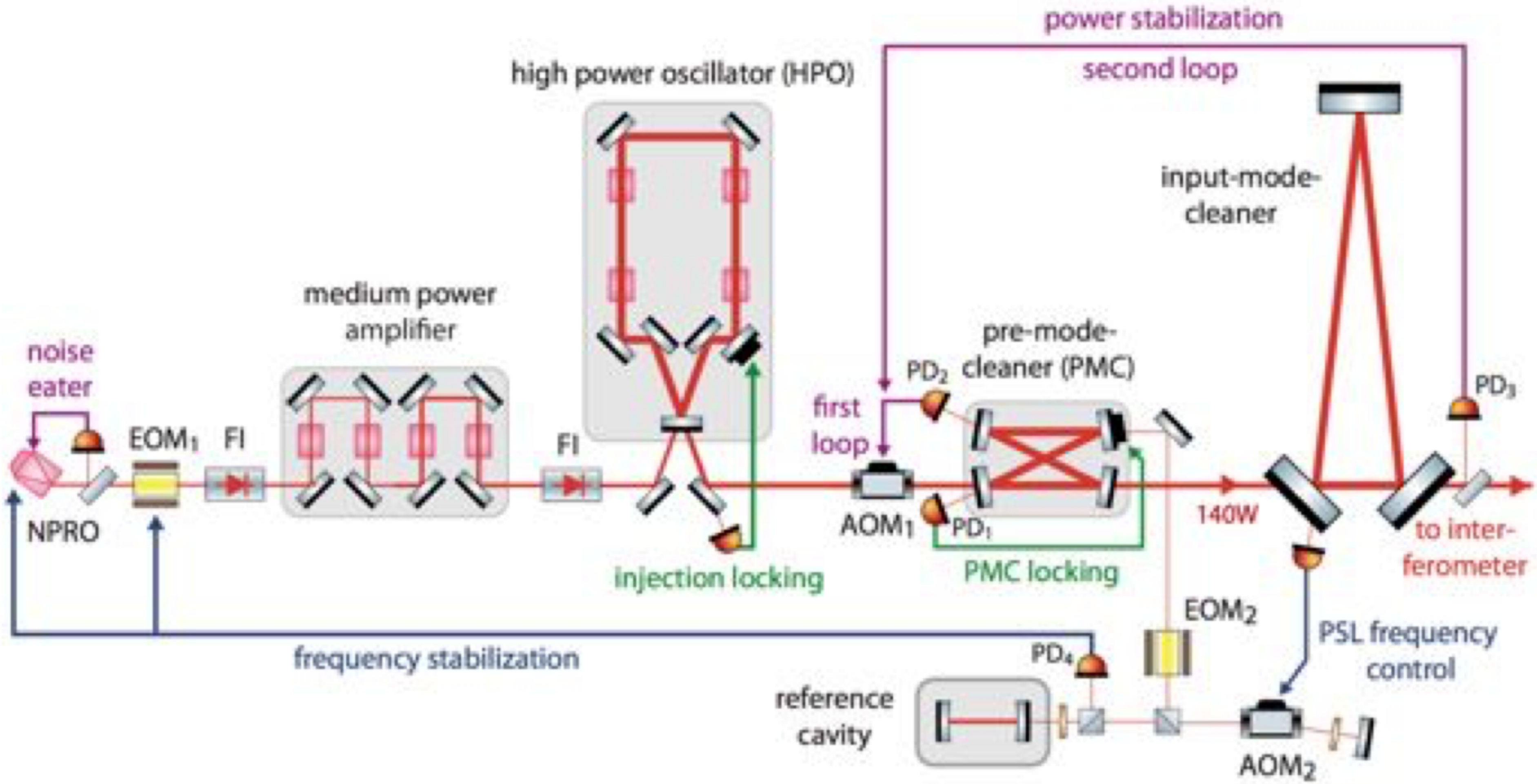

Figure from CQG 32 105102 (2015)
arXiv:1411.4547

Input Optics

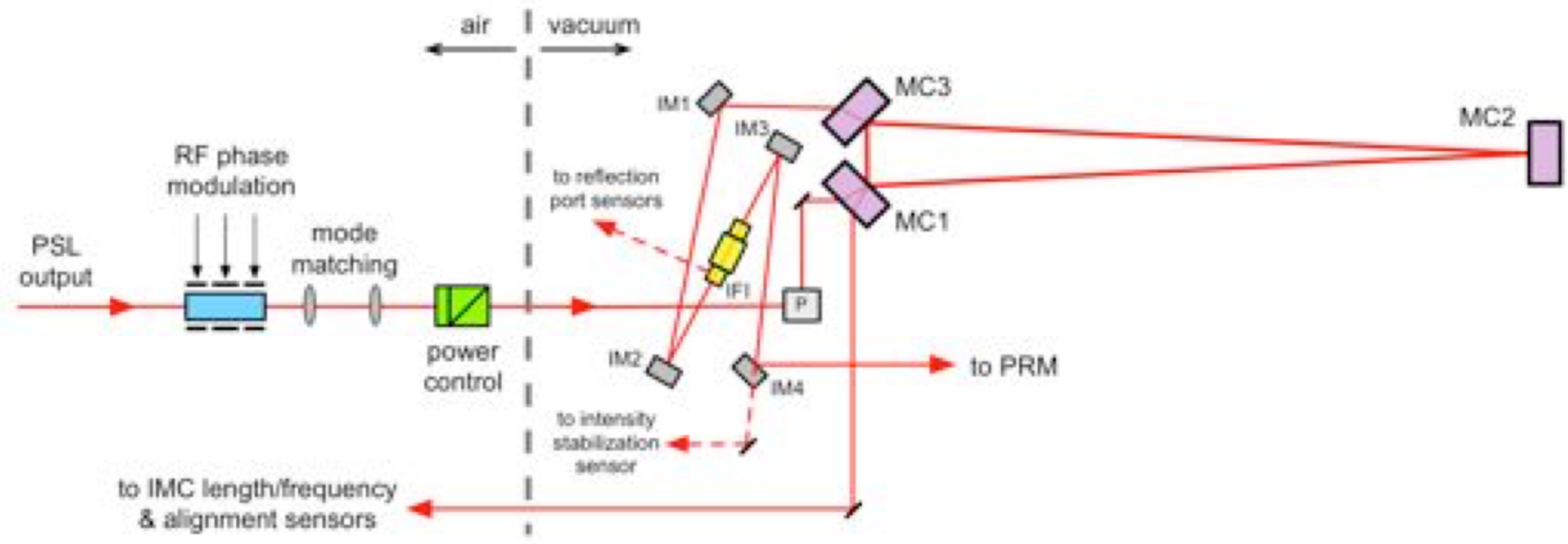

Figure from CQG 32 105102 (2015)
arXiv:1411.4547

More Lock Acquisition

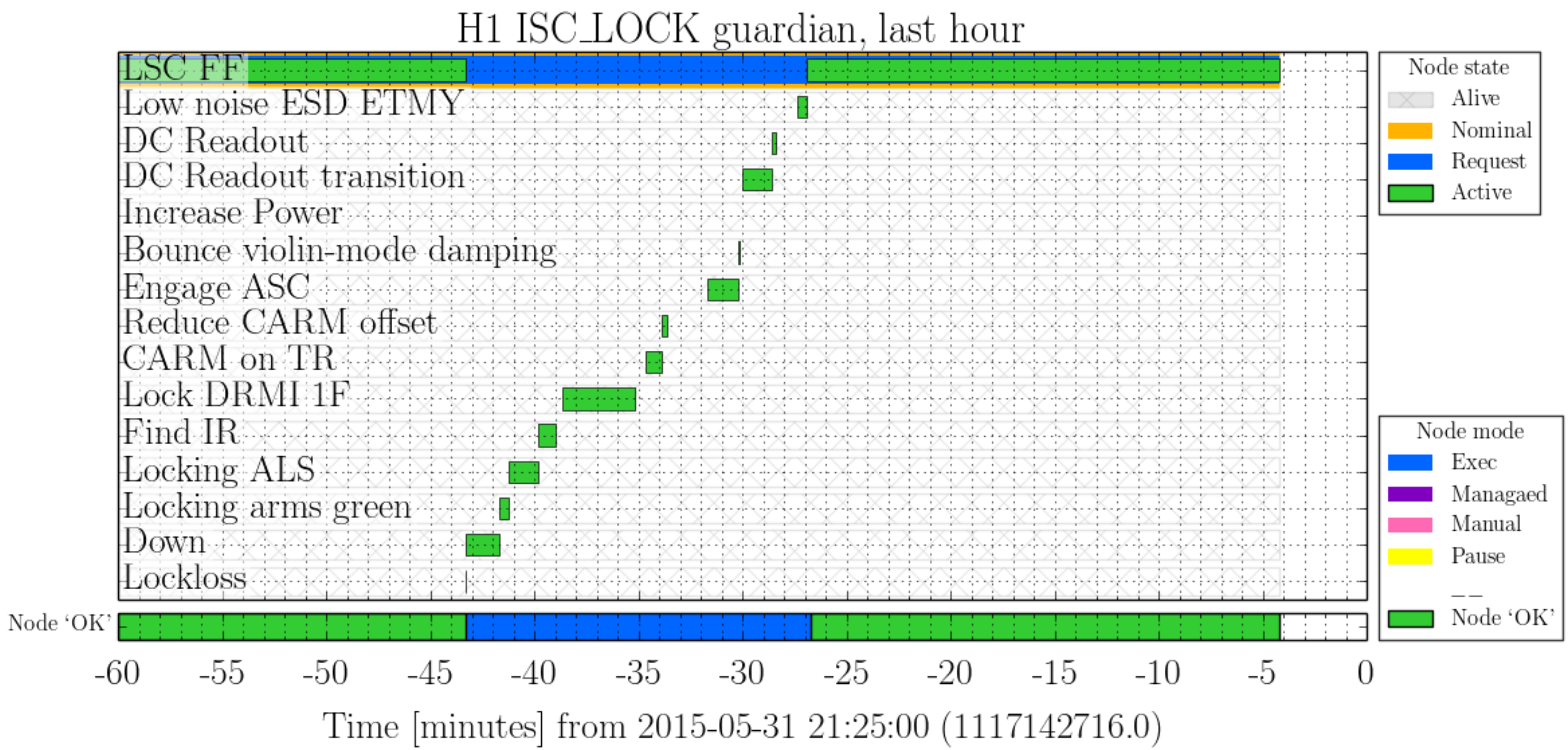

Figure by D. MacLeod

Active Seismic Isolation For In-Vacuum Optical Tables

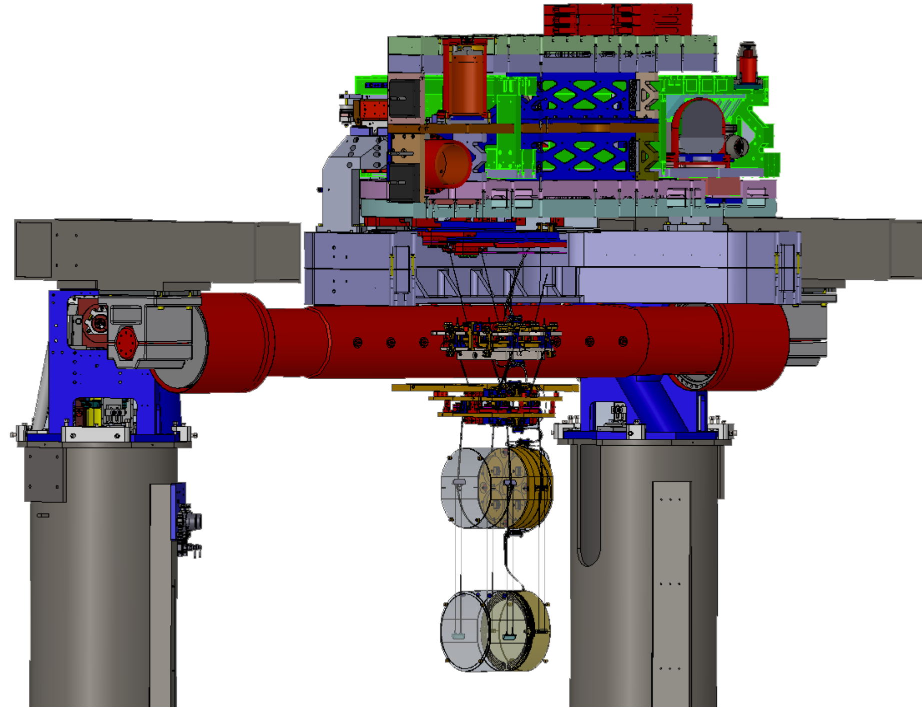

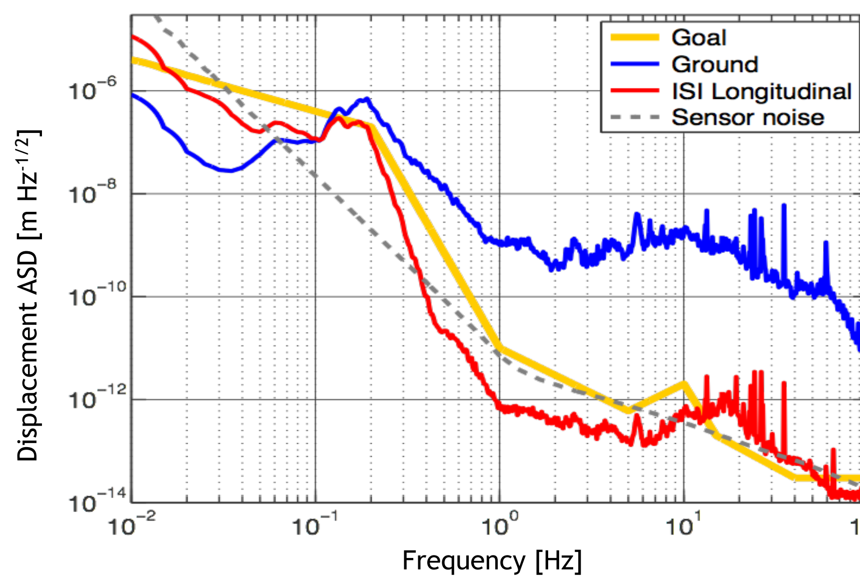

Monolithic Four-Stage Suspensions For Test Masses

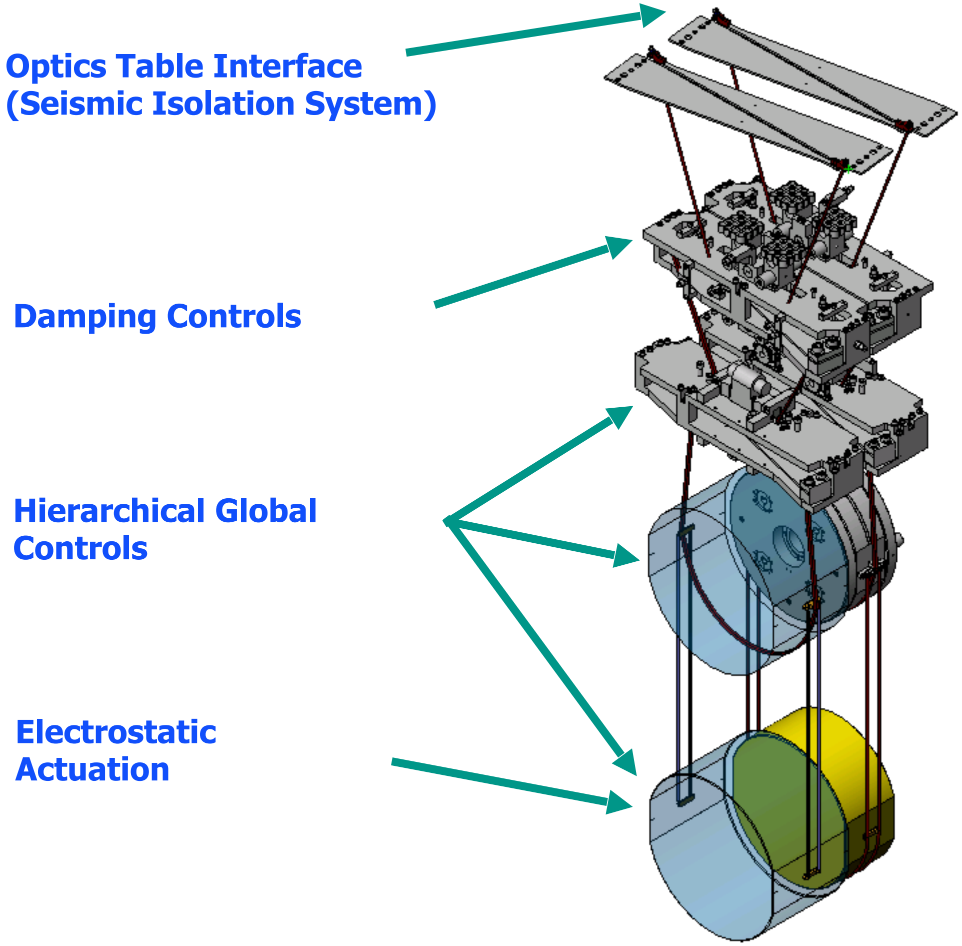

Quantum Noise Reduction: 10x Laser Power, Larger Mirrors

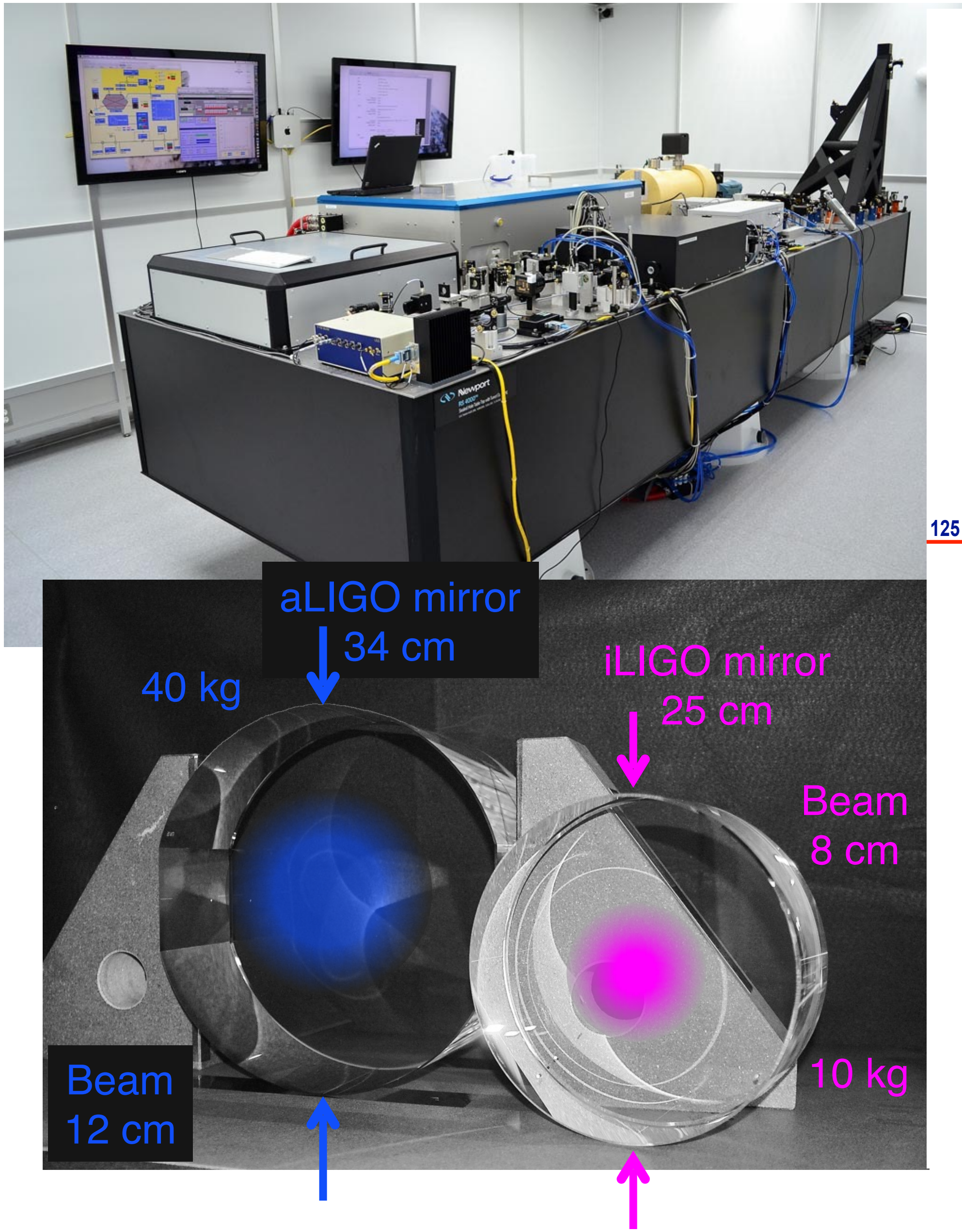

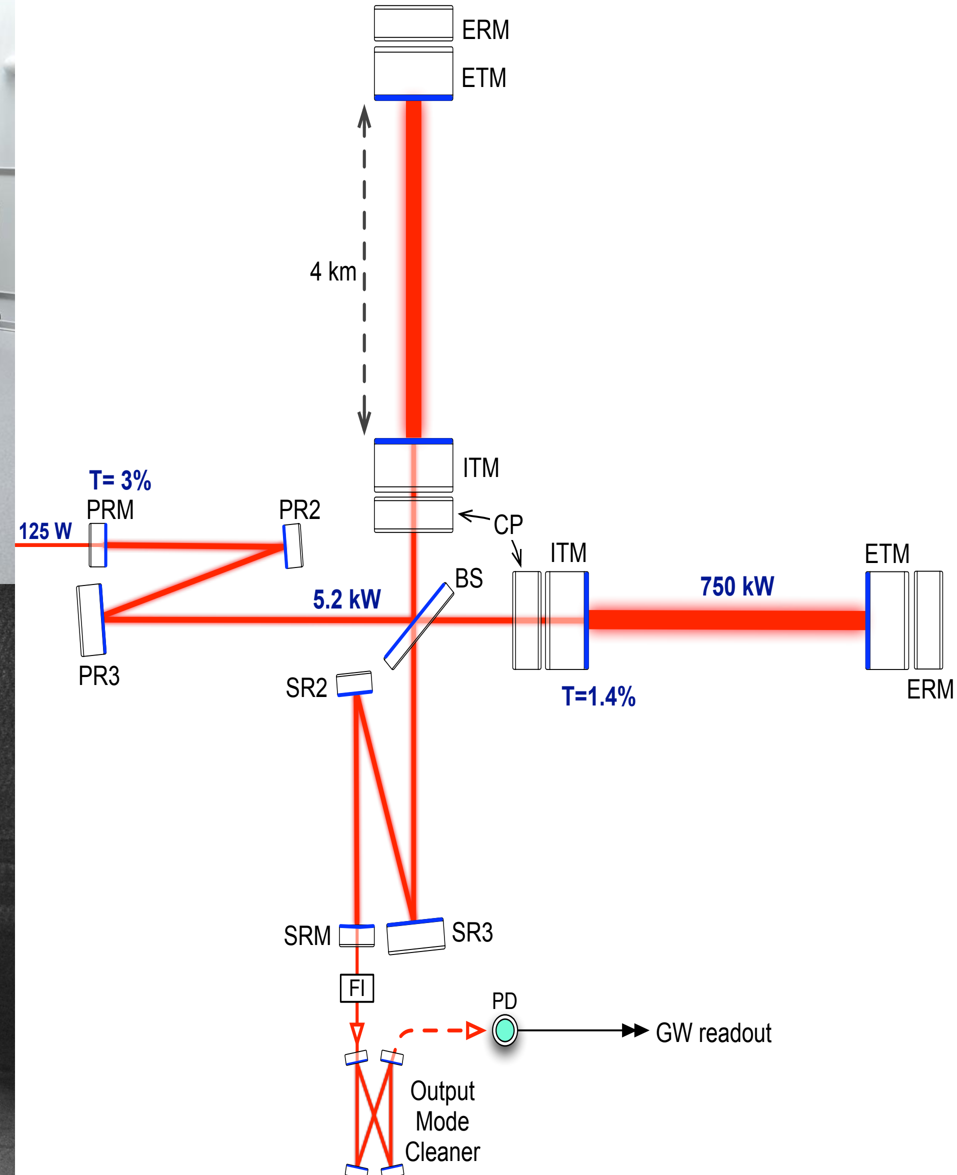

Detuning of Signal Recycling Cavity

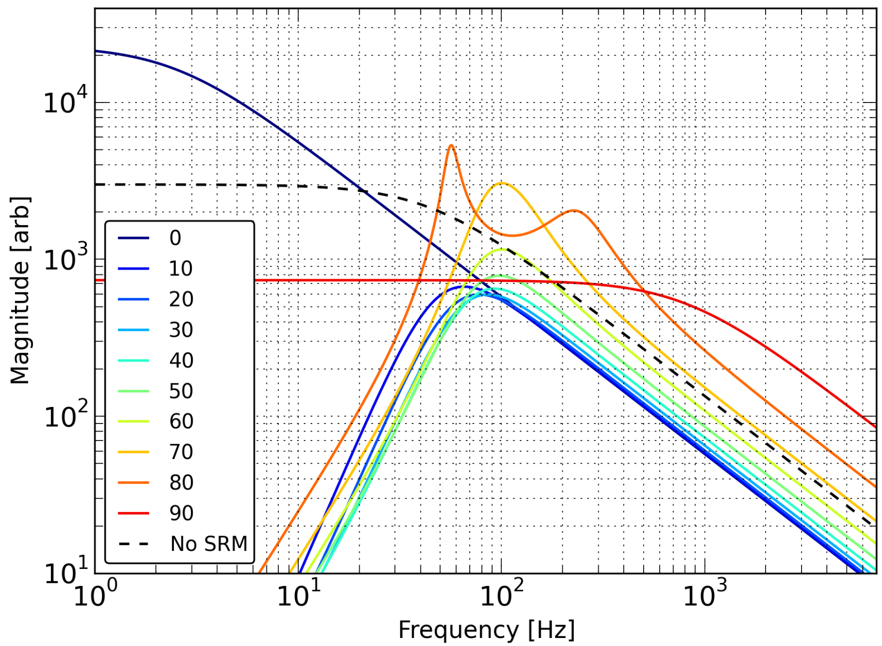

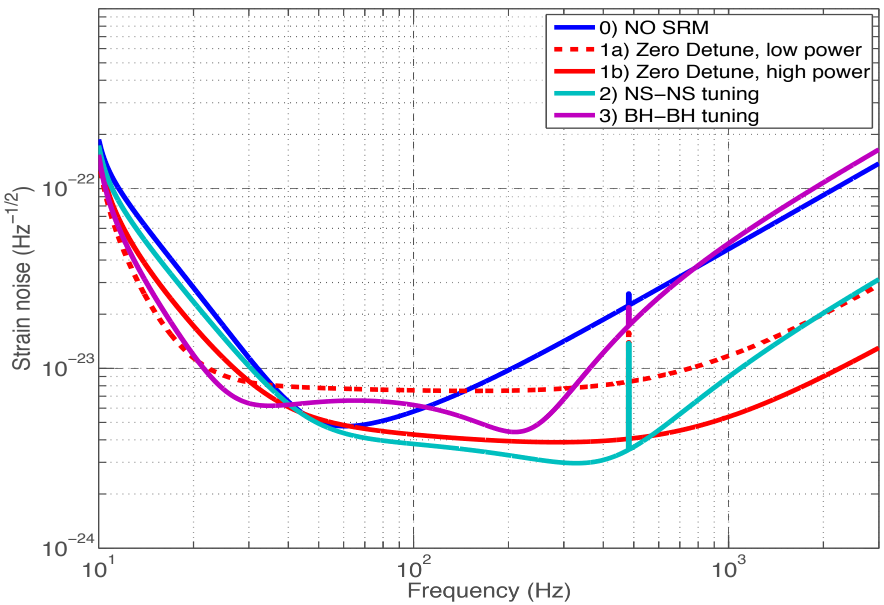

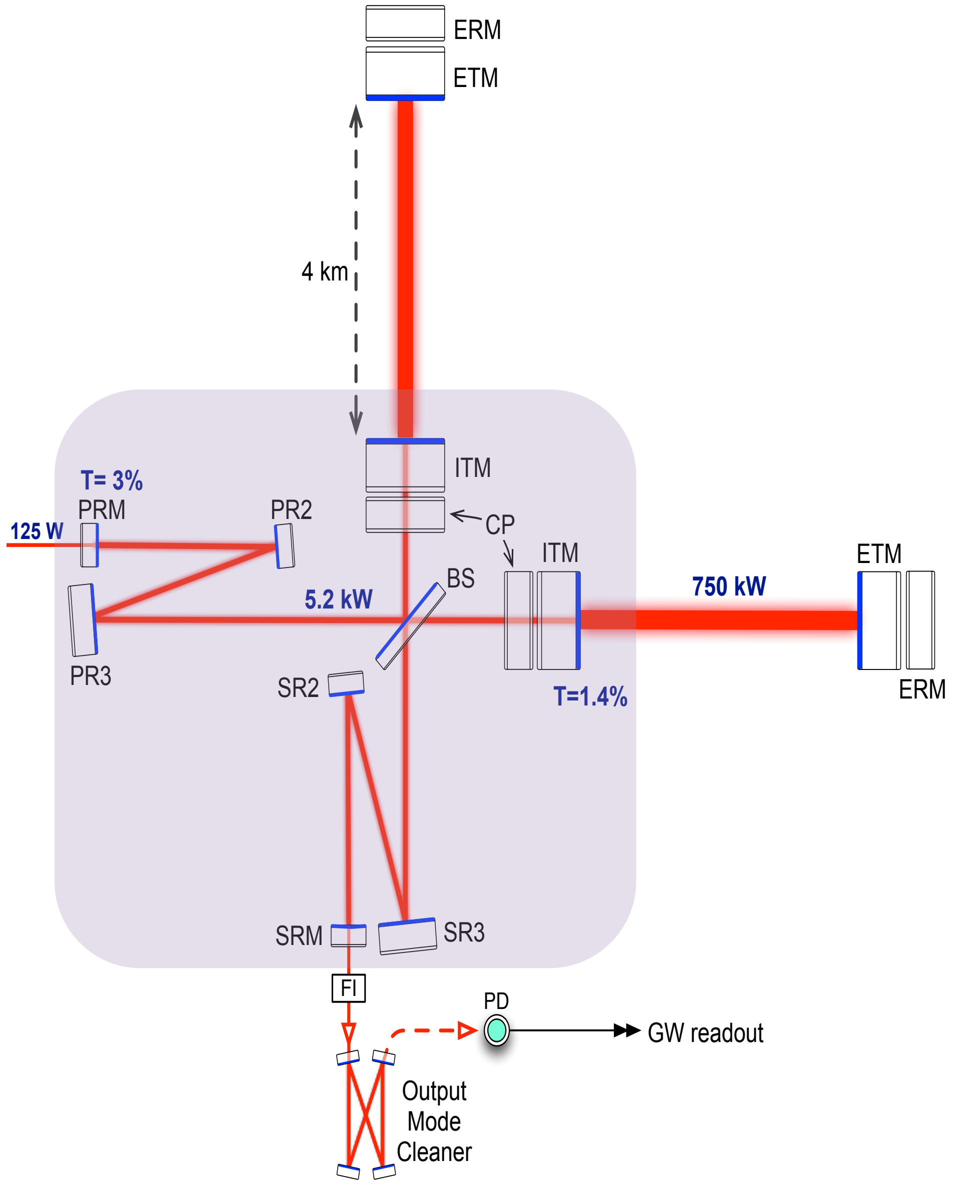

Current Noise Estimation

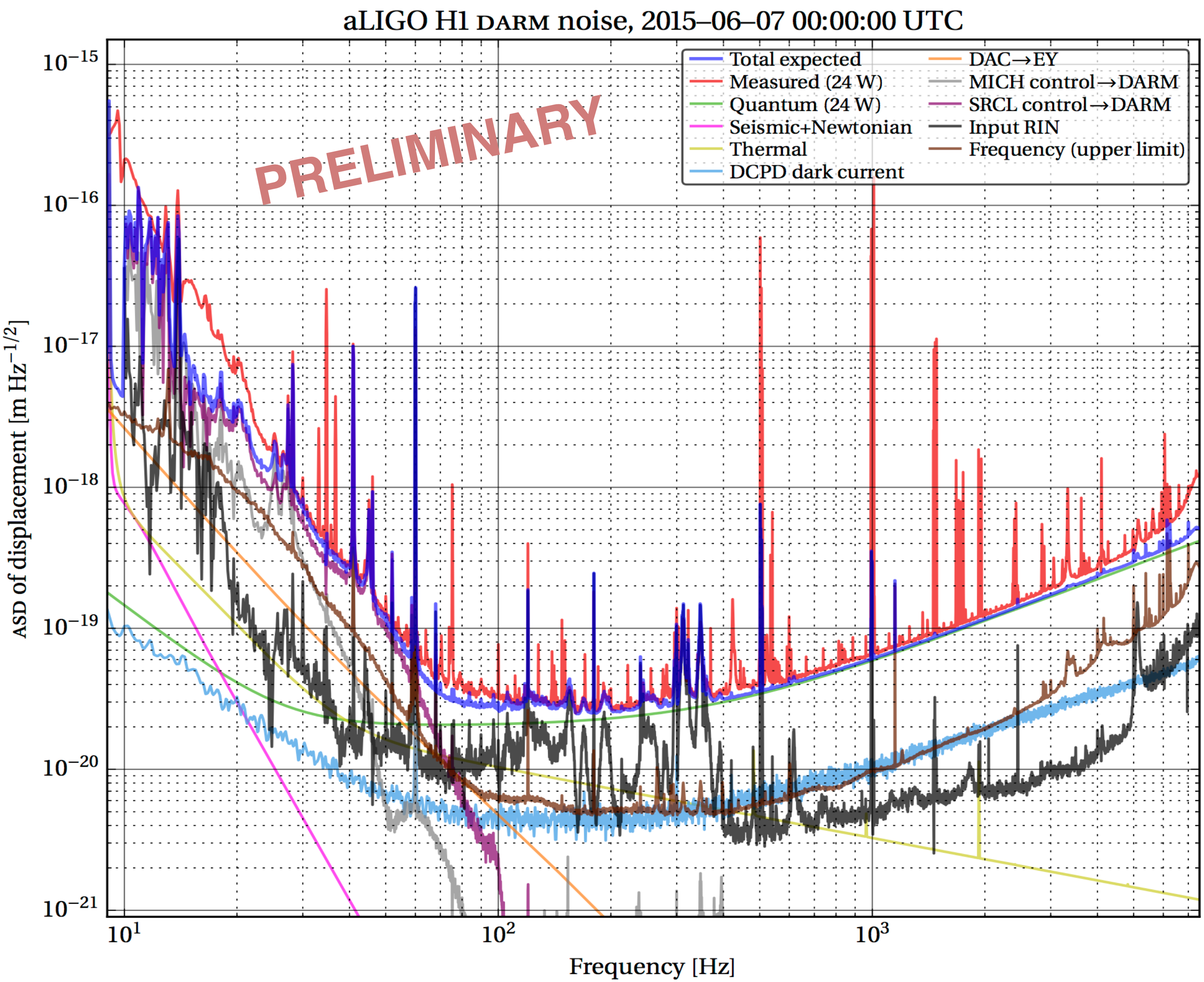

Figure by Evan Hall

Homodyne Detection & Differential Arm Offset

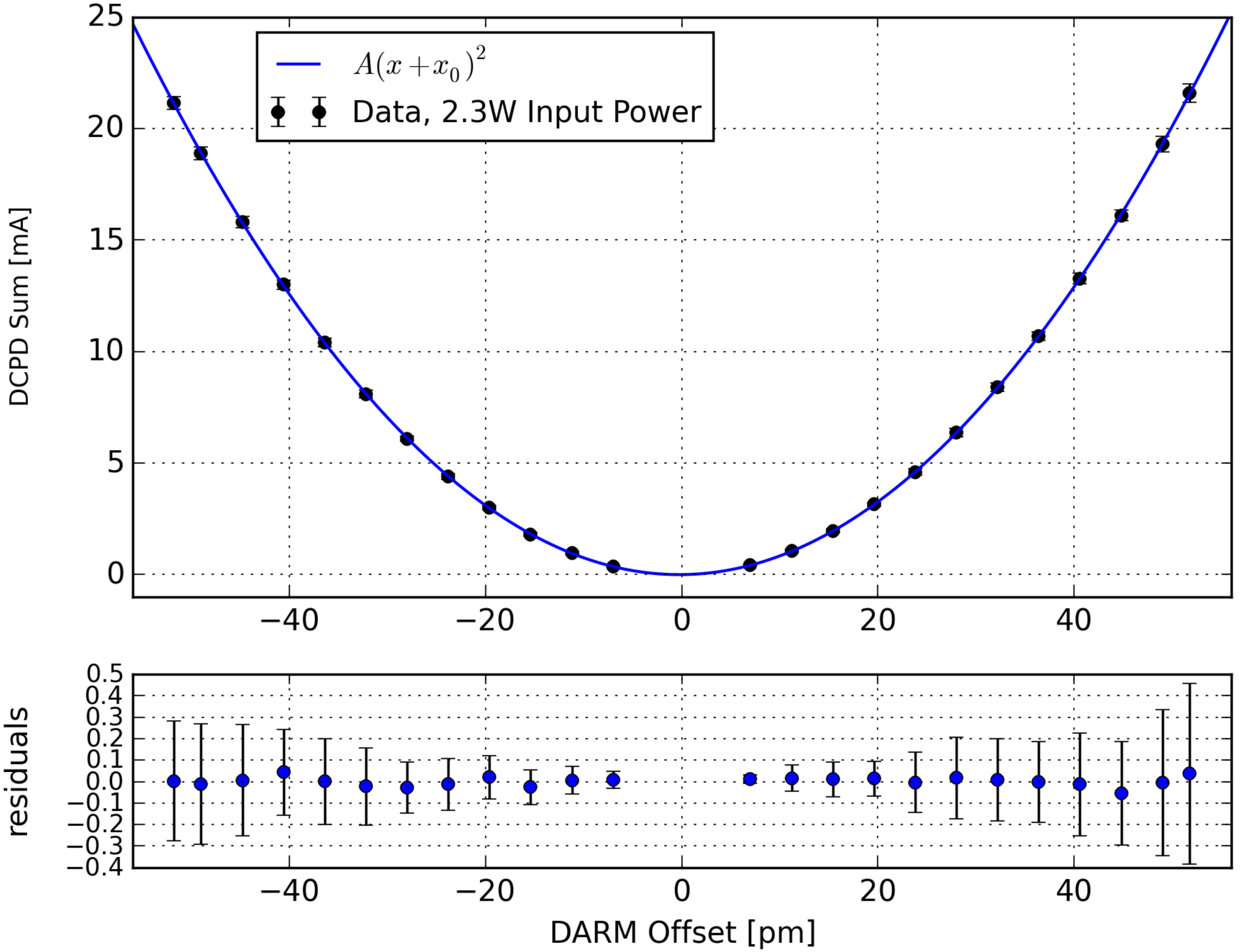

Contrast Defect Measurement

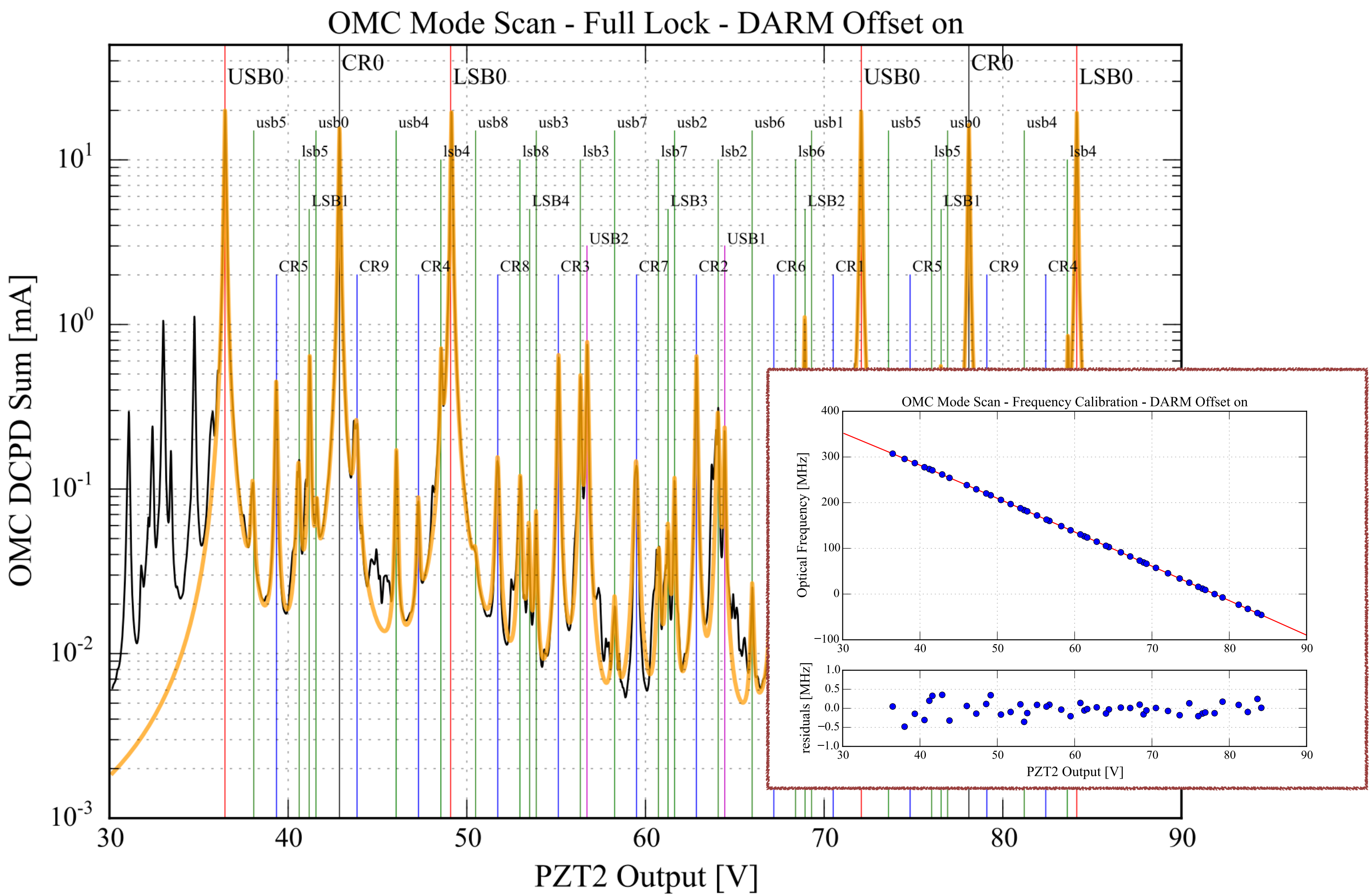

Interferometer Contrast Defect: **140ppm**

Future Plans - O1, Charge Mitigation, PI Dampers, Squeezing

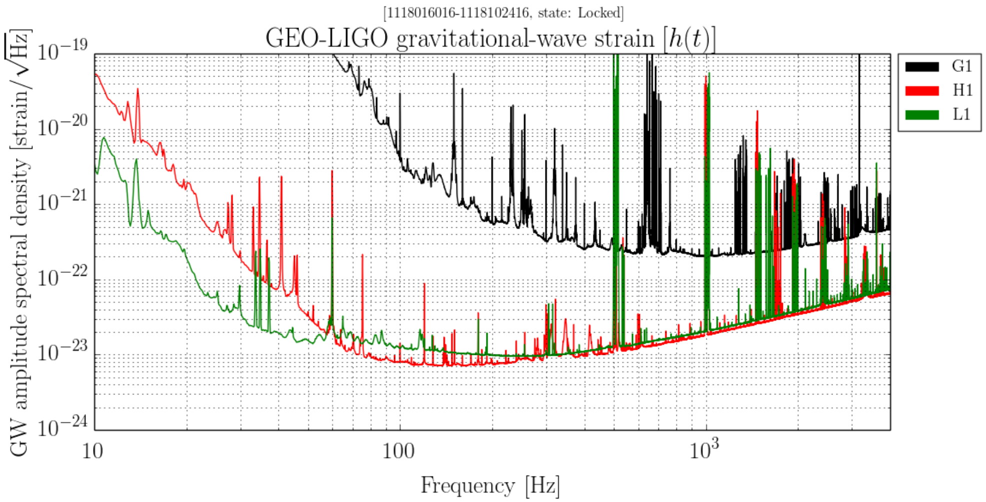

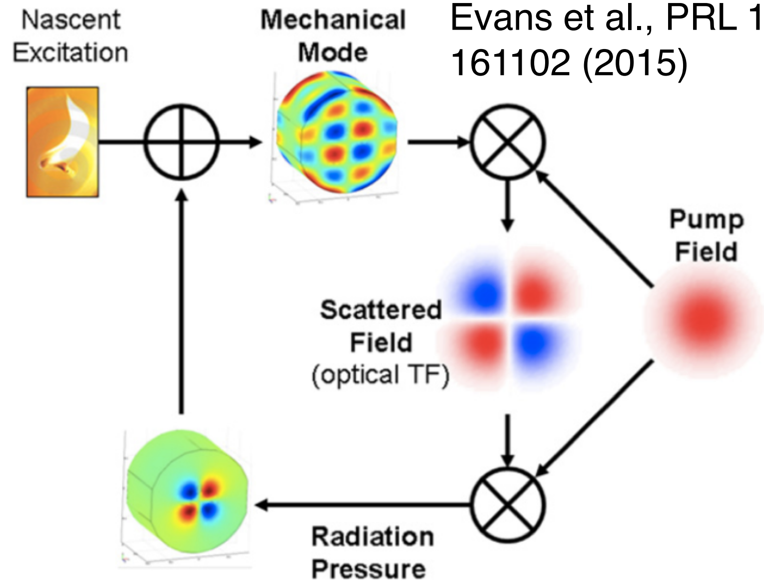

Evans et al., PRL 114, 161102 (2015)

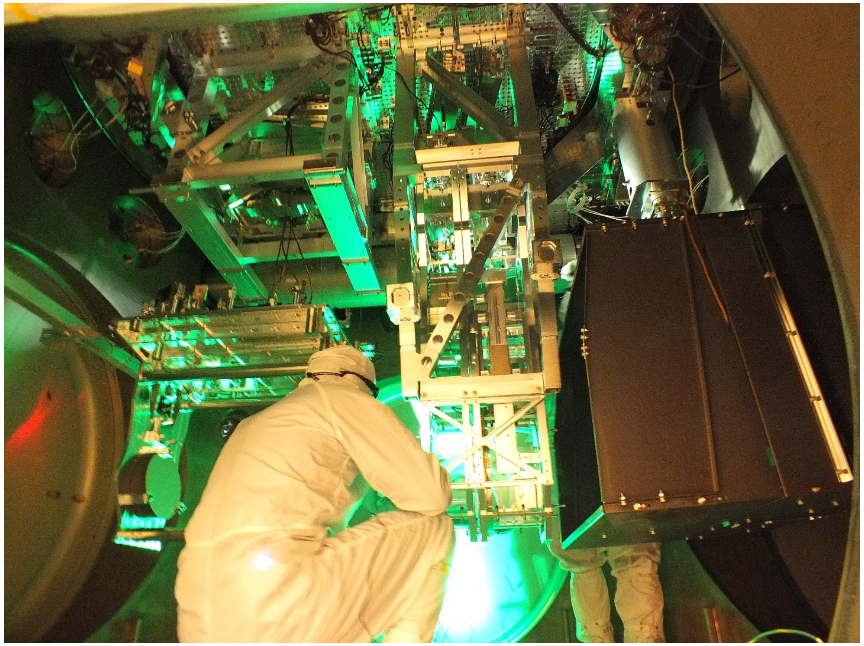

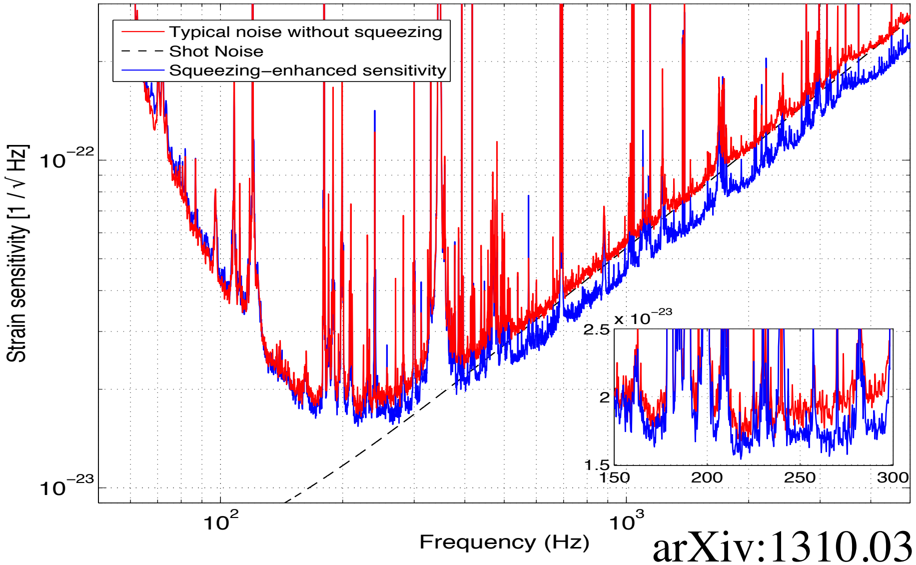

arXiv:1310.0383

Backgrounds of Transient Searches

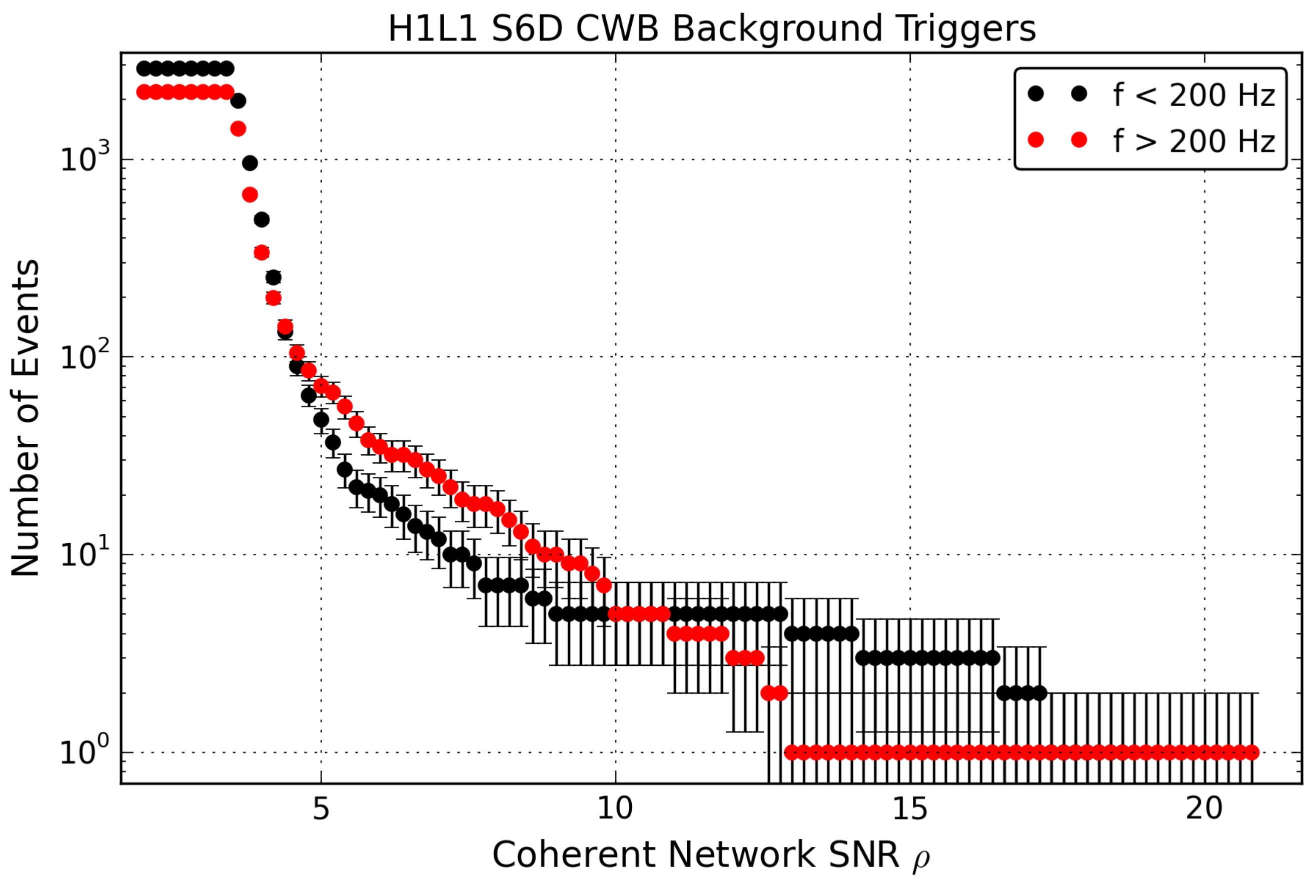

Barkhausen Noise Veto

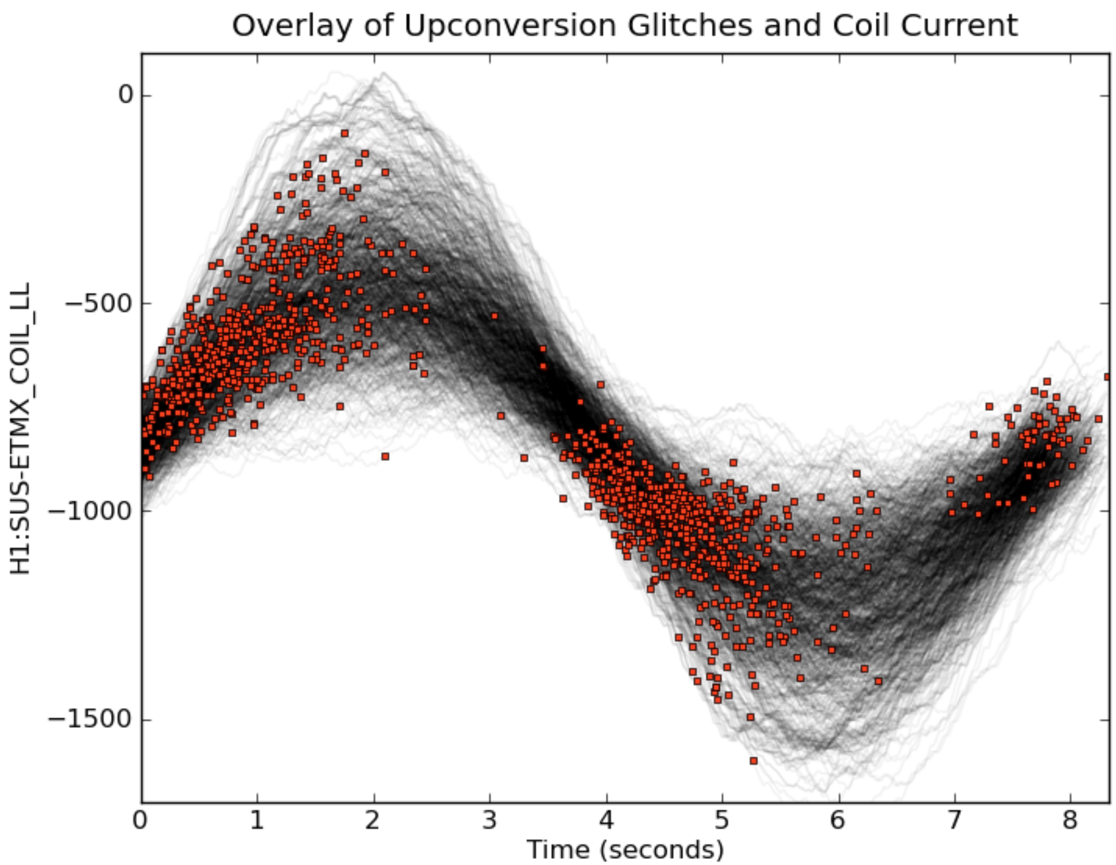

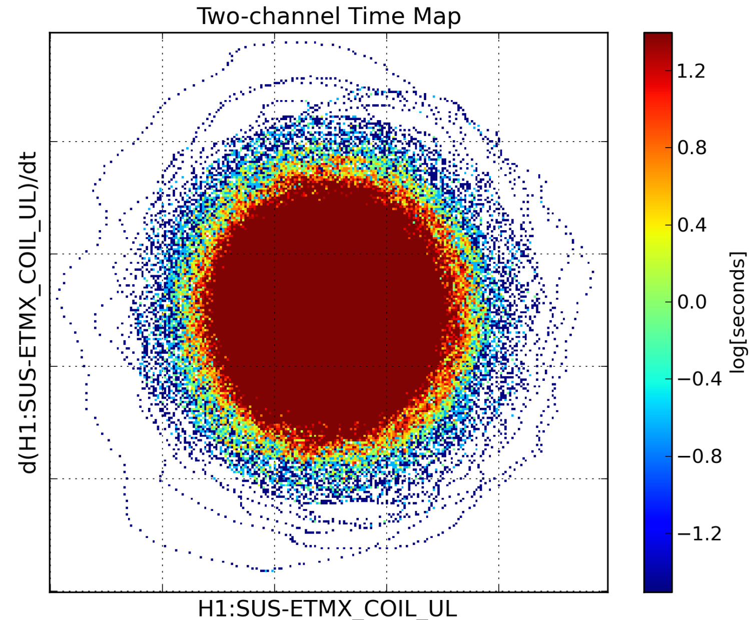

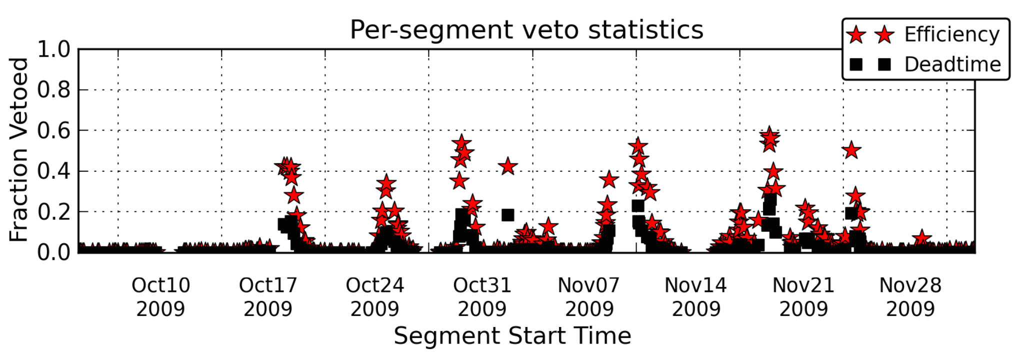

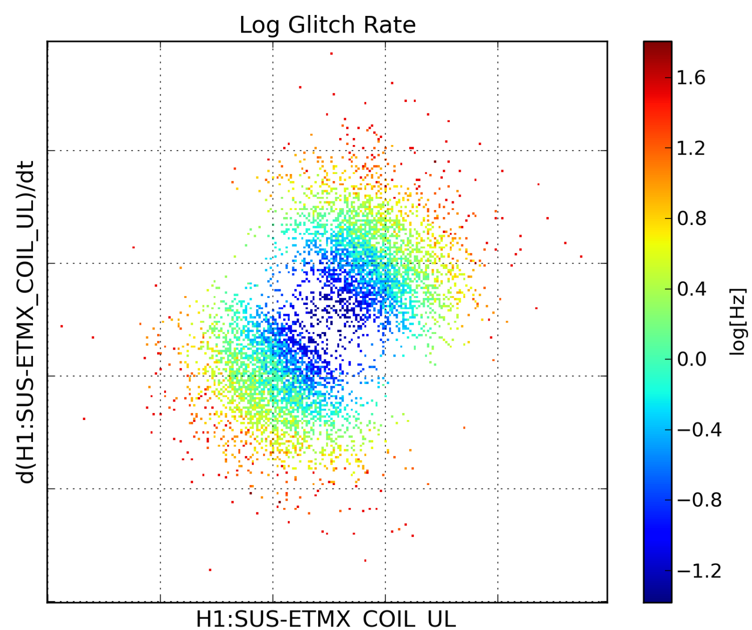

Scattered Light In the OMC Optical Path

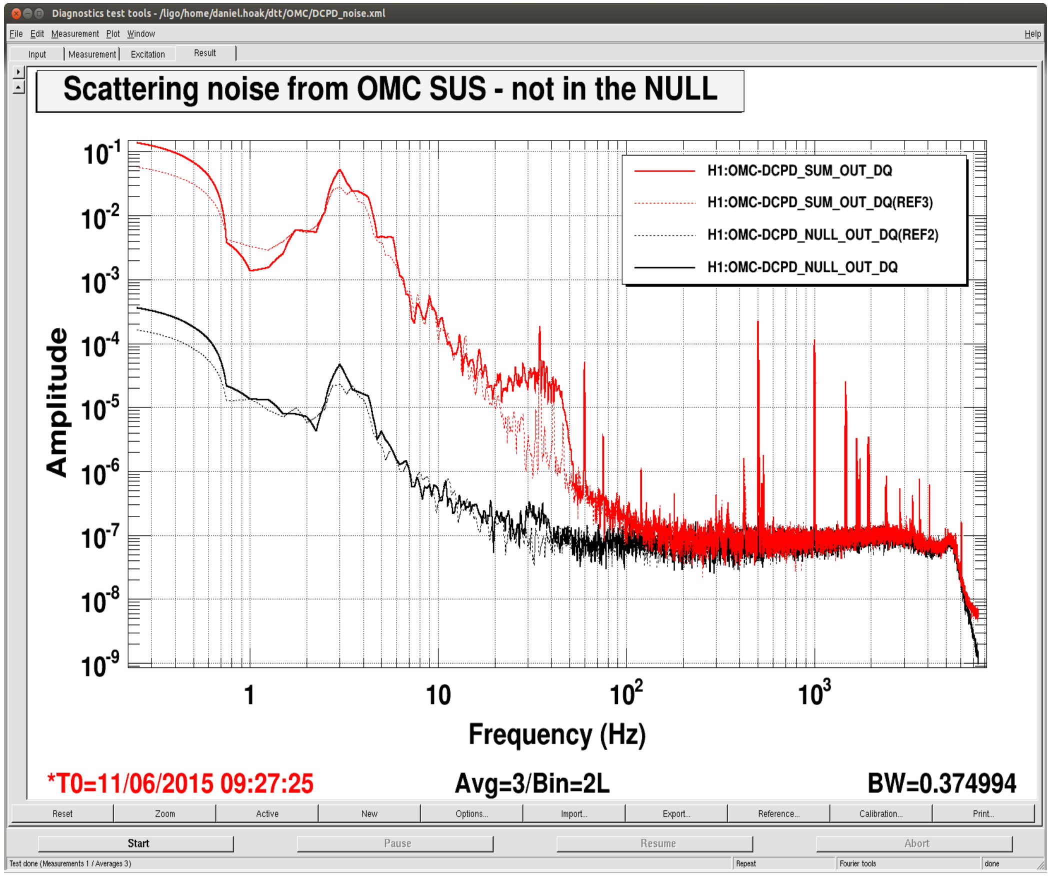

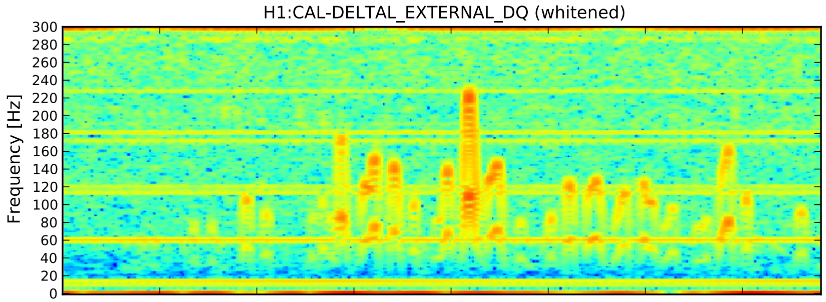

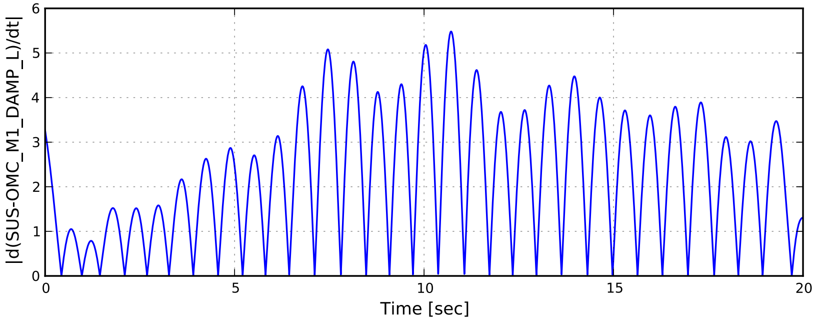

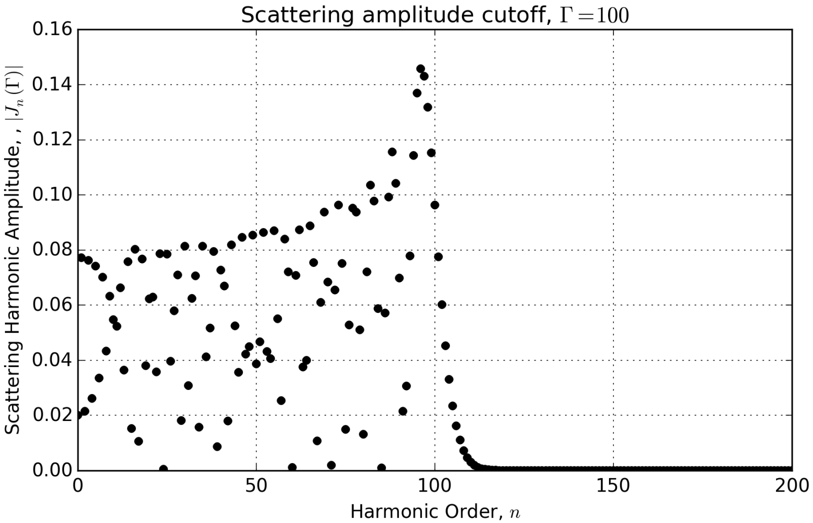

Installing the OMC Shroud

GRB Results from the Initial Detector Era

Many published searches for GW signals with GRBs, using LIGO & Virgo detectors:

- LIGO S2, S3, S4: 39 GRBs, Phys. Rev. D 77 (2008) 062004
- S5-VSR1 Burst: 137 GRBs, Astrophys. J. 715 (2010) 1438
- S5-VSR1 CBC: 22 short GRBs, Astrophys.J. 715 (2010) 1453
- S6-VSR2,3 Burst+CBC: 153 GRBs, Astrophys. J. 760 (2012) 12
- IPN events Burst+CBC: 223 GRBs, Phys. Rev. Lett. 113 (2014) 011102
- Search for long-duration signals: Phys. Rev. D 88 (2013) 122004
- Search for hi-freq GWs with GEO 600: 129 GRBs, Phys. Rev. D 89 (2014) 122004

Best limits on distance to progenitor, using assumptions for the central engine:

~70 Mpc for NS-BH progenitor model, associated with short GRB

~40 Mpc, for narrowband, short-duration burst emitting 0.01 $M_{sun}c^2$ in energy

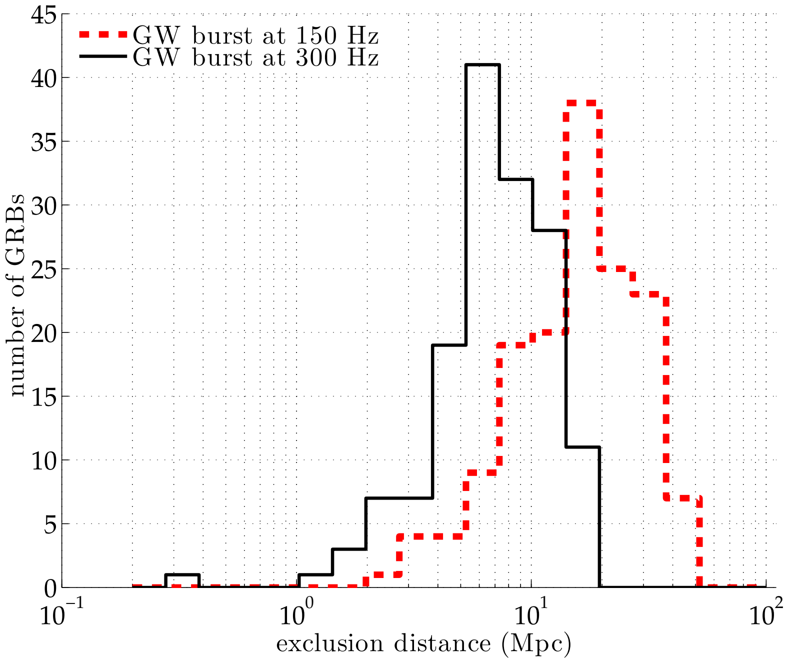

Figure from S6-VSR2,3 search, arXiv:1205.2216

GRB-Triggered Searches with LIGO-Virgo

Upper limits of the searches are calculated in GW-induced strain. Choice of progenitor model leads to a distance lower limit.

Best exclusion distances:

~70 Mpc for NS-BH progenitor model, associated with sGRB

~40 Mpc, for narrowband, short-duration burst emitting 0.01 $M_{sun}c^2$ in energy

We expect a substantial improvement in our limits with aLIGO and adVirgo.

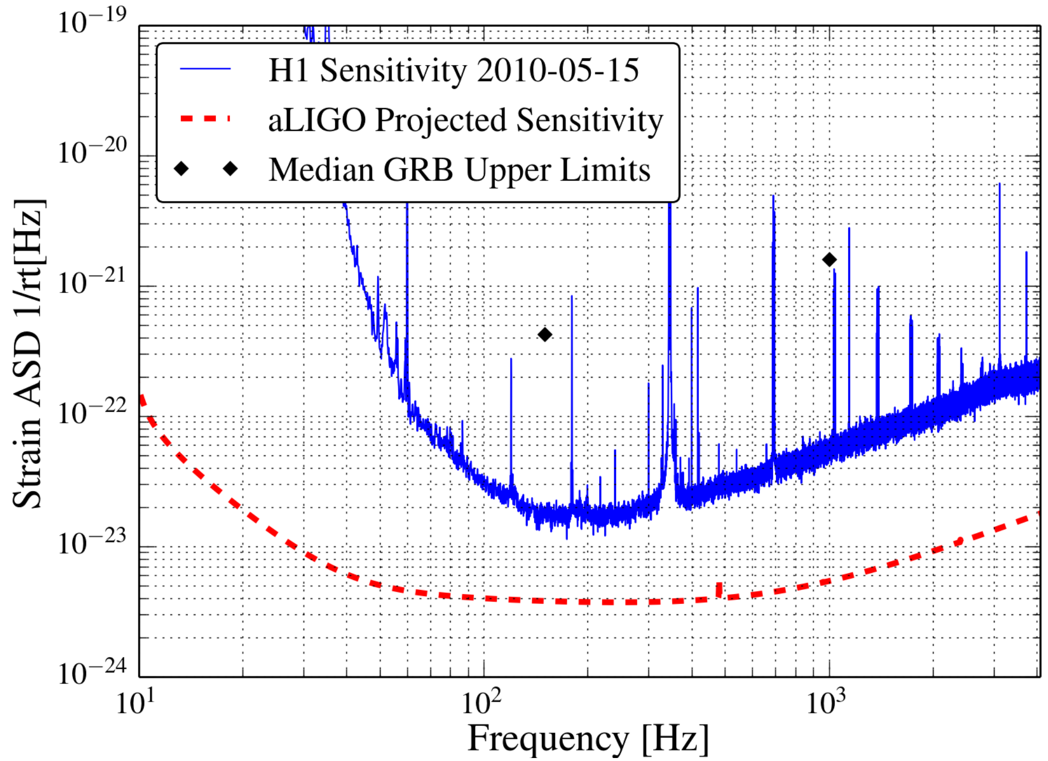

150 Hz UL from S6-VSR2,3 search, arXiv:1205.2216

1 kHz UL from S5-VSR1 search, arXiv:1001.0165

aLIGO noise curve: https://dcc.ligo.org/LIGO-T0900288

Notable Non-detections

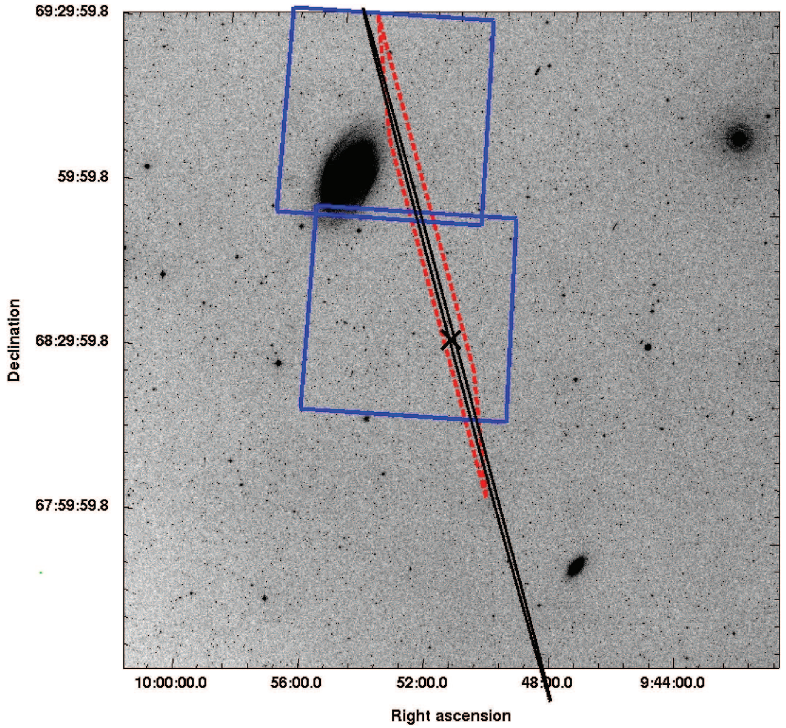

FIG. 1.— The central region of the M81 group, showing the original error trapezium (red dashed line) from the IPN and the refined 3-σ error ellipse (solid black). The blue boxes are the regions studied in the optical. Figure from Hurley et al. (2010) Copyright (c) 2010 RAS.

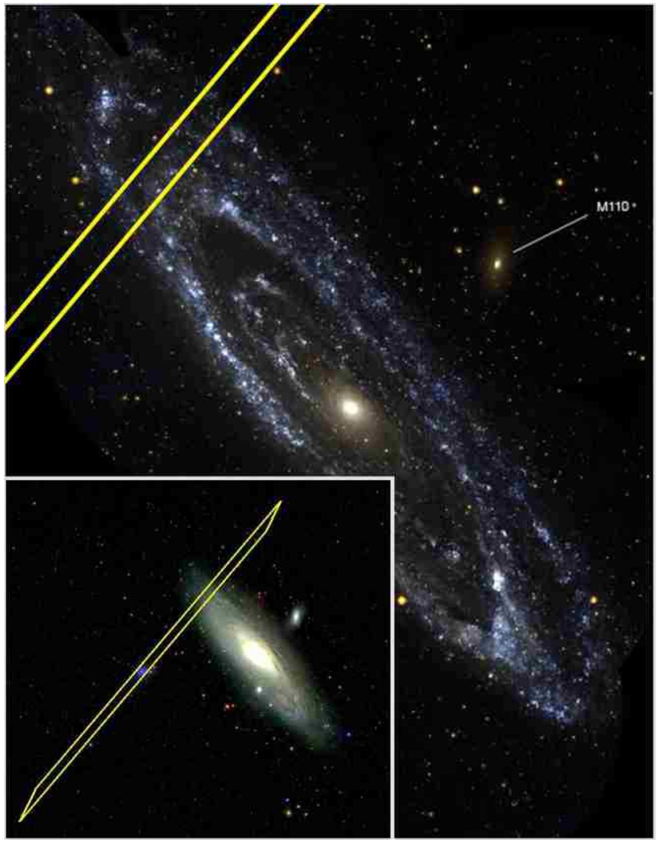

FIG. 1.— The IPN3 (IPN3 2007) (γ-ray) error box overlaps with the spiral arms of the Andromeda galaxy (M31). The inset image shows the full error box superimposed on an SDSS (Adelman-McCarthy et al. 2006; SDSS 2007) image of M31. The main figure shows the overlap of the error box and the spiral arms of M31 in UV light (Thilker et al. 2005).

Short GRBs 051103 (**arXiv:1201.4413**) and 070201 (**arXiv:0711.1163**).
Confident non-detection of BNS associated with foreground galaxy —> either from distant background galaxy or an SGR flare.

Physics Goals for Coincident Detections

Independent measurement of the Hubble expansion using BNS mergers as 'standard sirens':

$$H_0 = c\frac{z}{D_L}$$

$$\begin{bmatrix} h_+(t) \\ h_\times(t) \end{bmatrix} = \frac{A(t;(1+z)\mathbf{M})}{D_L} \begin{bmatrix} (1+\cos^2\iota)\cos(\phi(t)) \\ 2\cos\iota\sin(\phi(t)) \end{bmatrix}$$

Challenges:

- degeneracy between luminosity distance D_L and source inclination
- degeneracy between redshift and chirp mass $\mathbf{M}$

Proposed solutions:

- Use known distribution of neutron star masses as prior on $\mathbf{M}$ (Taylor et al. arXiv:1108.5161)
- Use galaxy catalog as prior on D_L (del Pozzo arXiv:1108.1317)
- Use short GRBs to fix inclination, EM followup observations to measure redshift of host galaxy (Nissanke et al. arXiv:0904.1017)

Can measure H_0 to ~10% with ~dozens of events.

Analysis Procedure

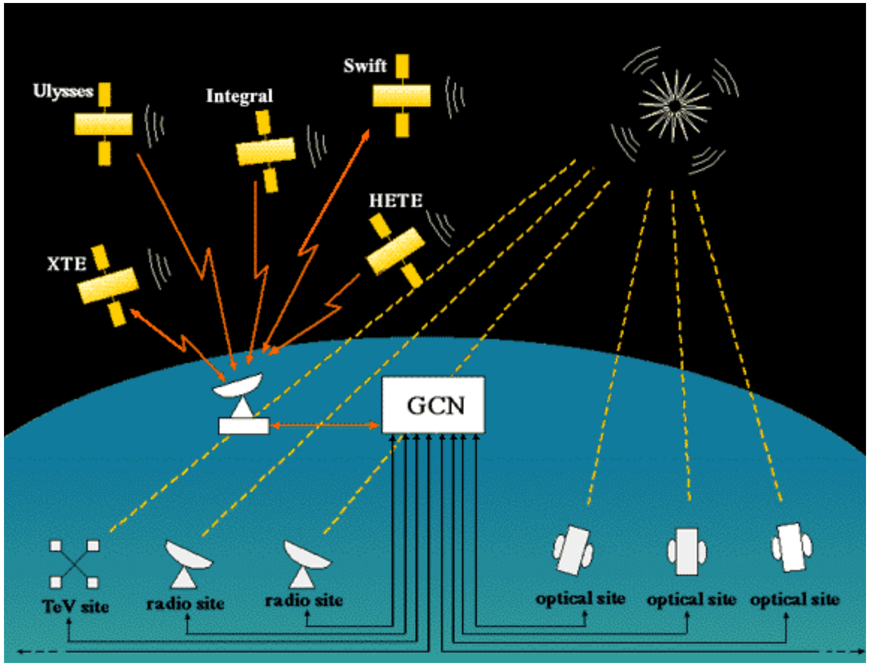

GRB events are collected from the GCN alerts, plus the IPN catalog.

Two complementary analyses are performed:

- A template-based search for modeled signals (BNS, NSBH) from short GRBs
- An unmodeled search for any coherent short-duration coherent, from all GRBs

Data around each GRB are searched with no assumptions for redshift, burst luminosity or spectral hardness. Sources are assumed to have small inclination angles.

Localizations from *Fermi* GBM require a sky tiling procedure to account for the phase delay across the error region.

GRB Sky Localization - What if you miss?

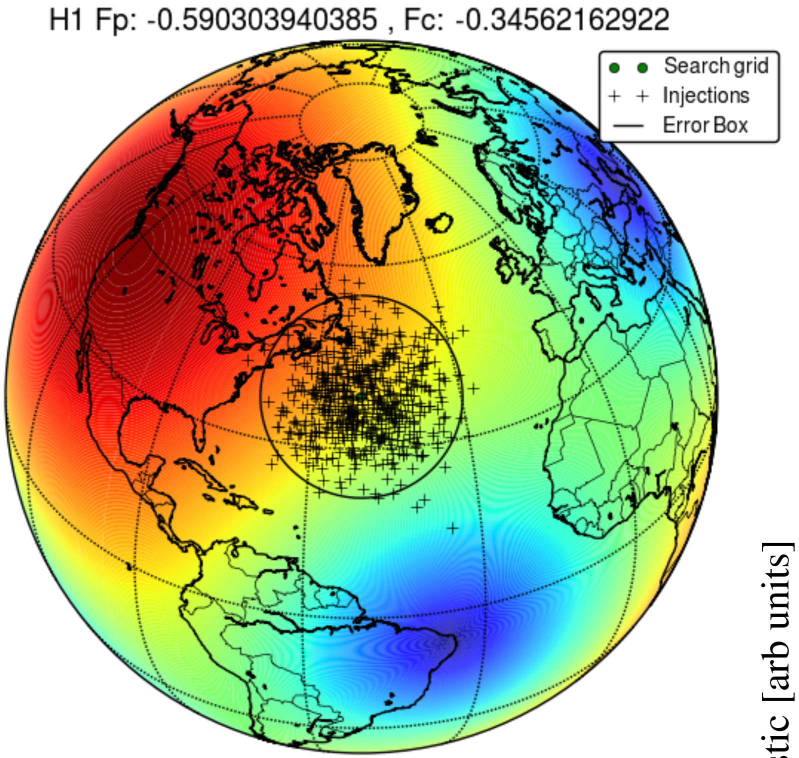

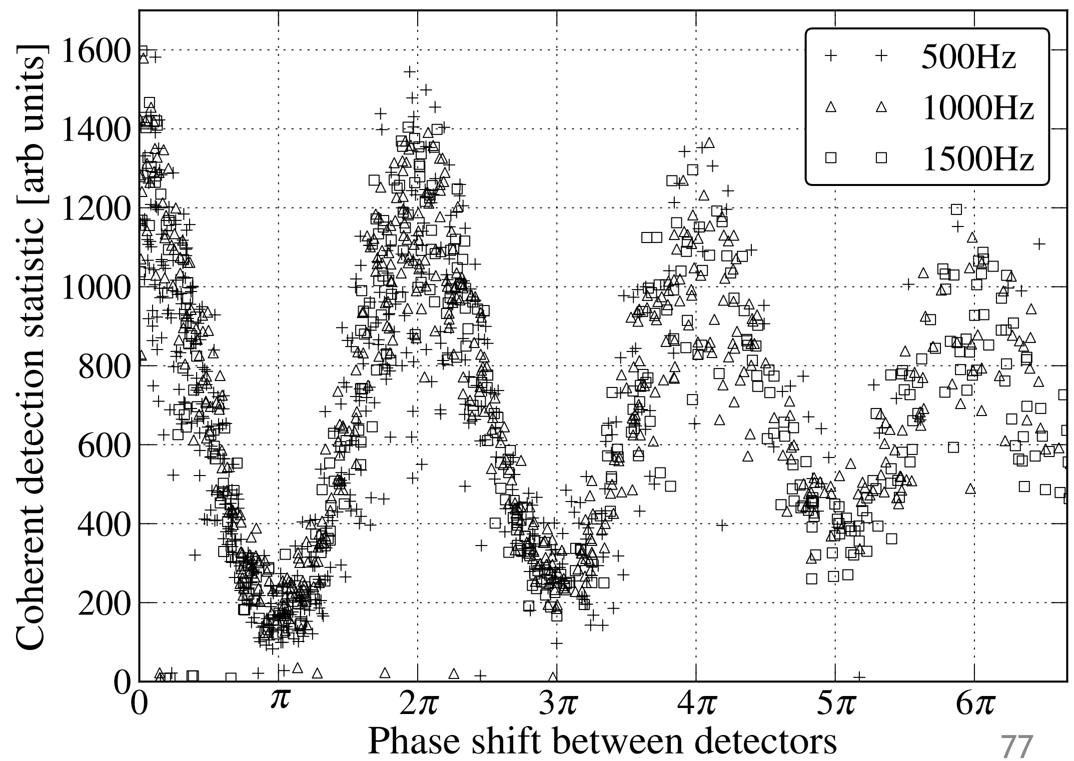

GRB Sky Localization - Check the search grid delay tolerance

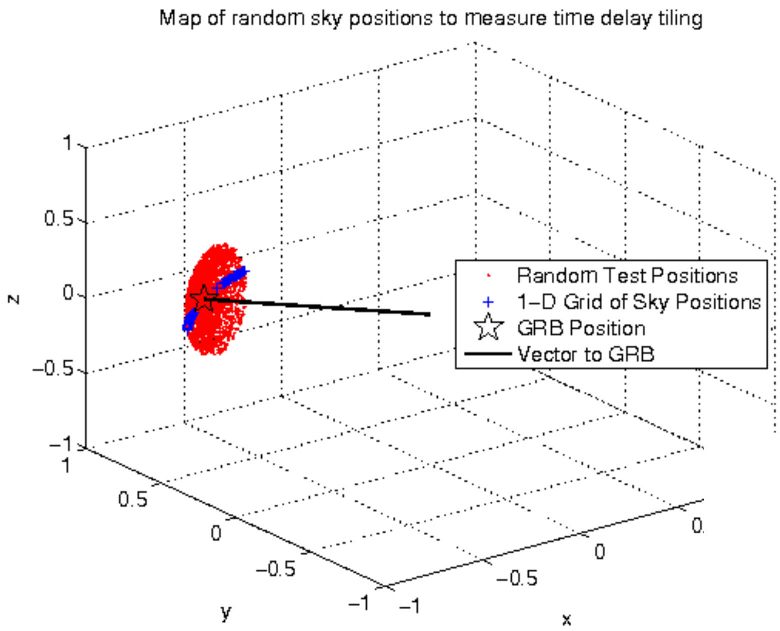

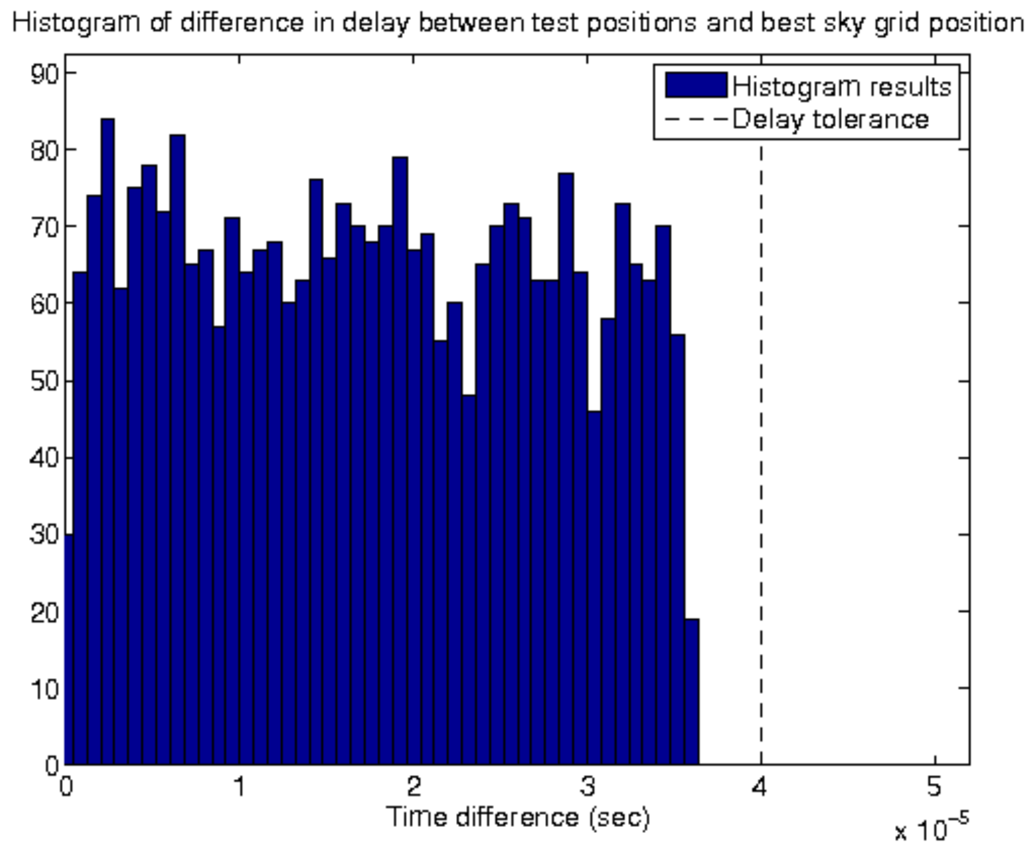

GRB Physics

GRB Discovery

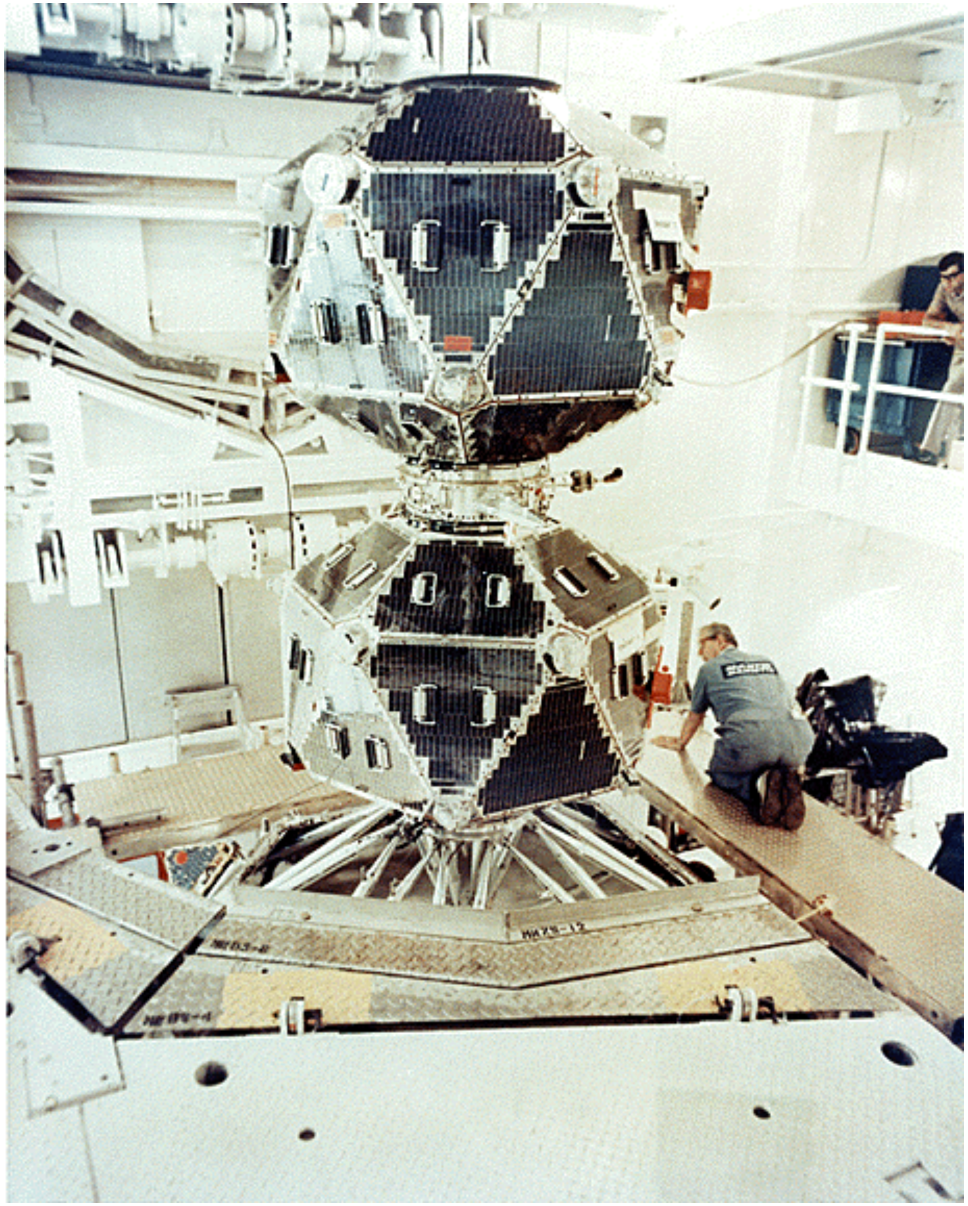

Vela 4A Event – July 2 1967

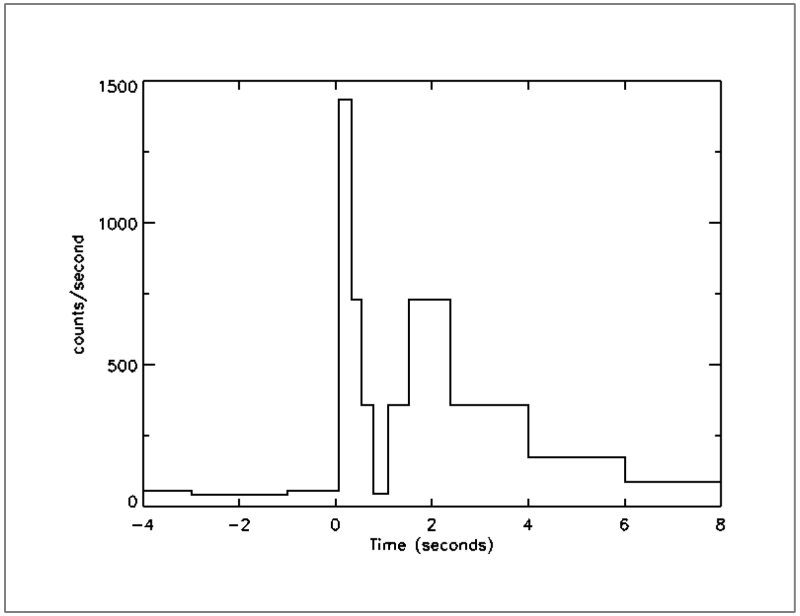

Omnidirectional gamma-ray detectors to verify test-ban treaty.

Addition of more satellites allowed for rough sky localization
(not terrestrial —> declassify!)

GRB Detections

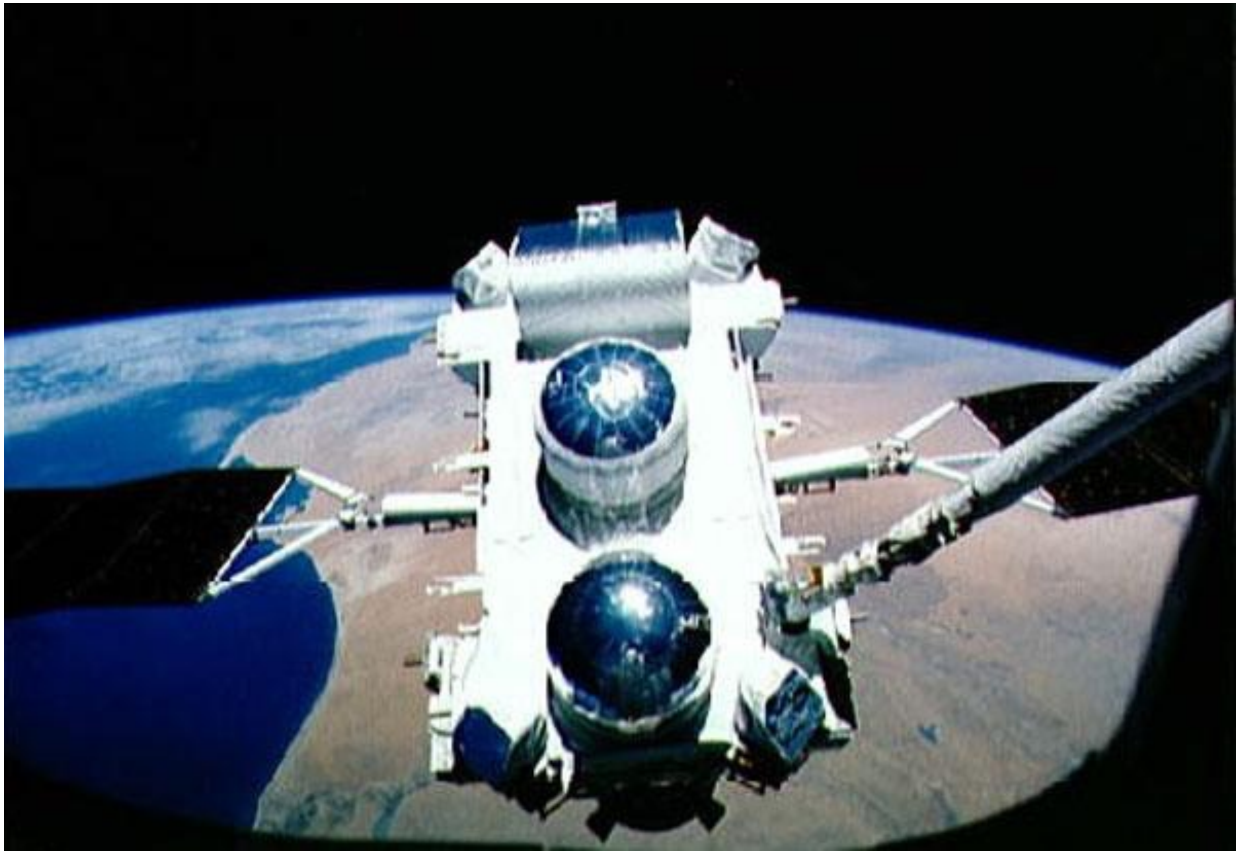

Compton Gamma Ray Observatory (CGRO), with the Burst and Transient Source Experiment (BATSE).

Launched in 1991. BATSE had 4pi sky coverage, 20 to >600 keV sensitivity.

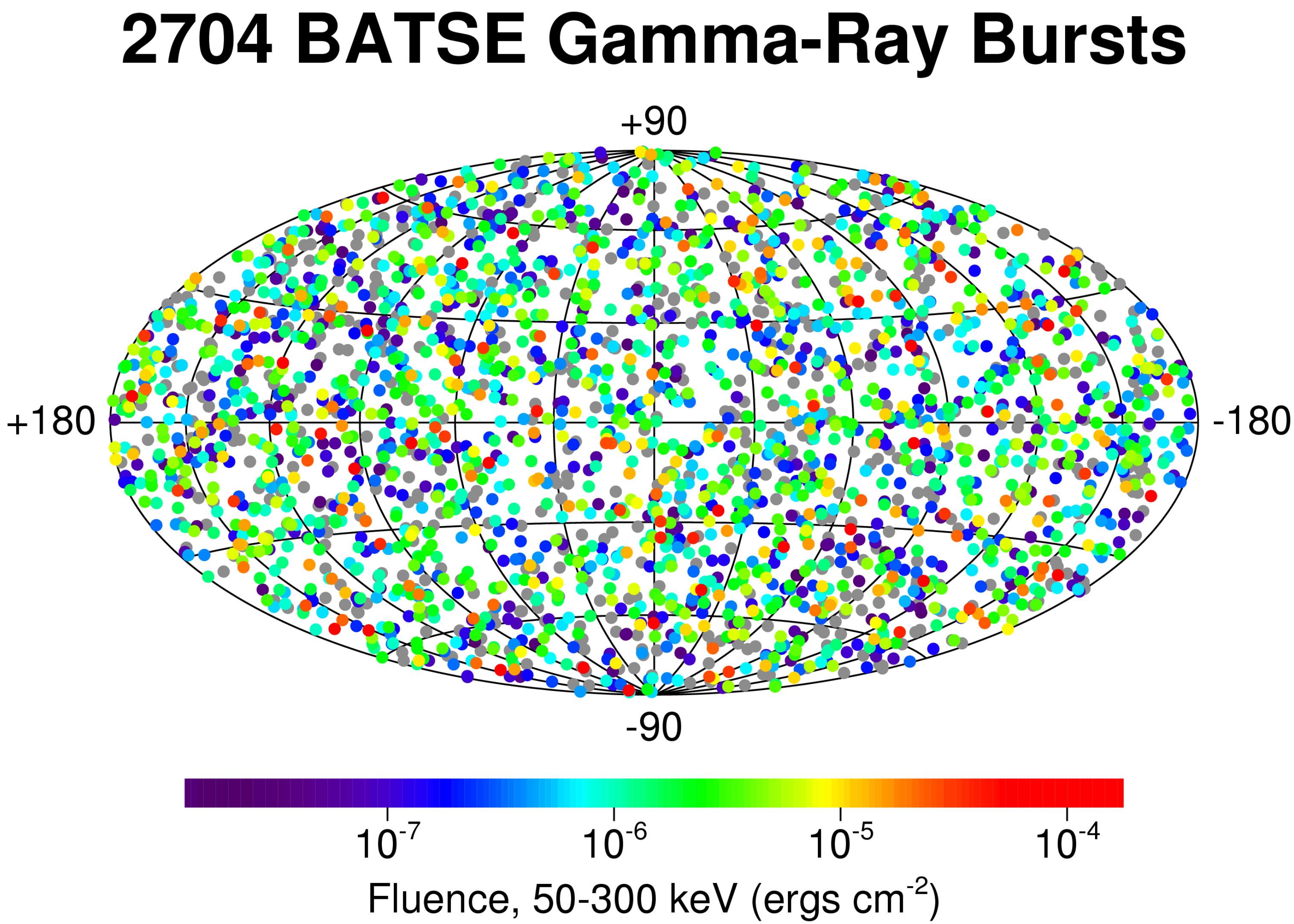
2704 BATSE Gamma-Ray Bursts
+90
+180
-180
-90
10-7
10-6
10-5
10-4
Fluence, 50-300 keV (ergs cm-2)

Short timescale variability

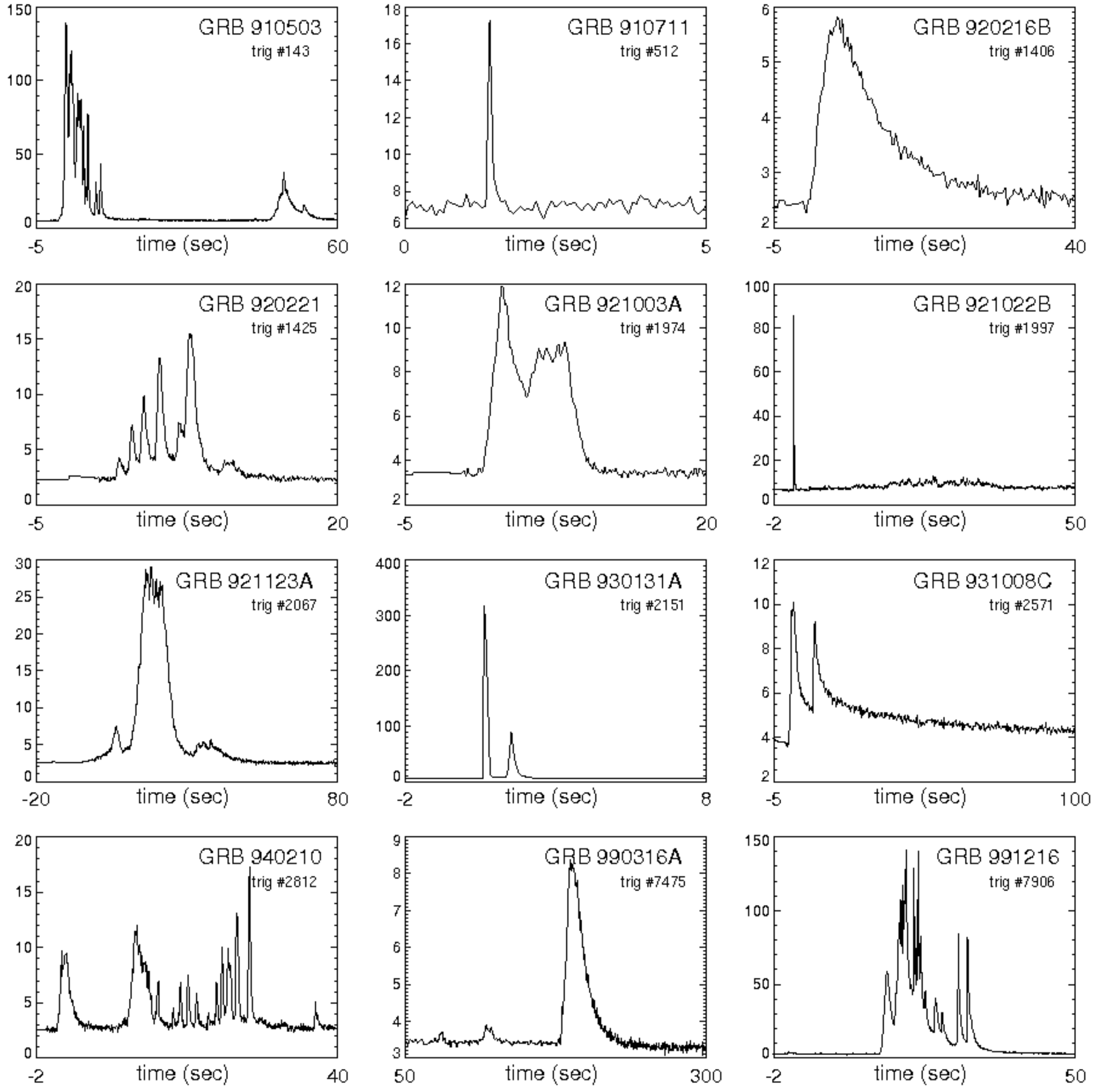

Fourth BATSE Catalog,
arXiv:astro-ph/9903205

Two populations

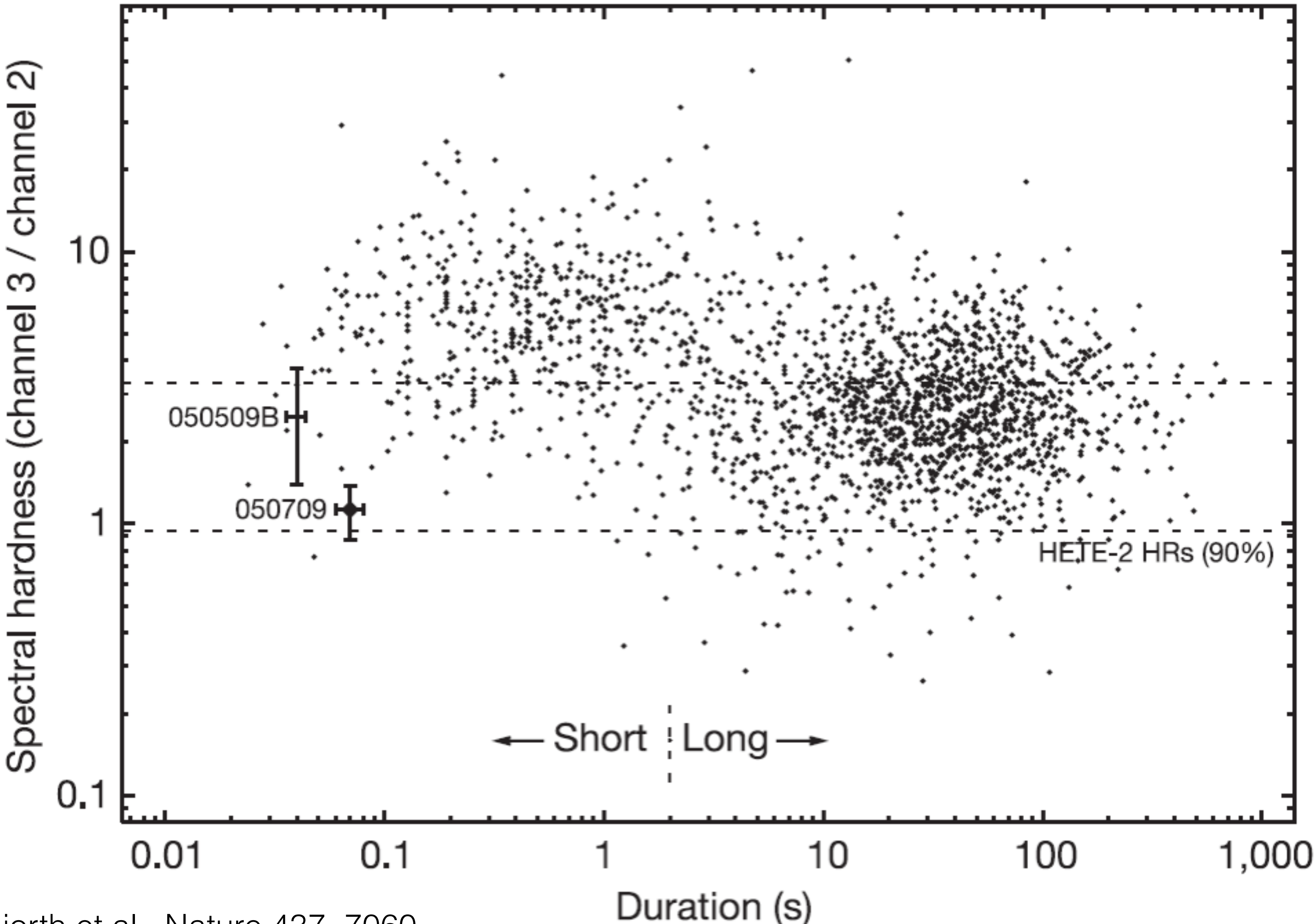

Hjorth et al., Nature 437, 7060

Unambiguous Extragalactic Origin - BeppoSAX mission

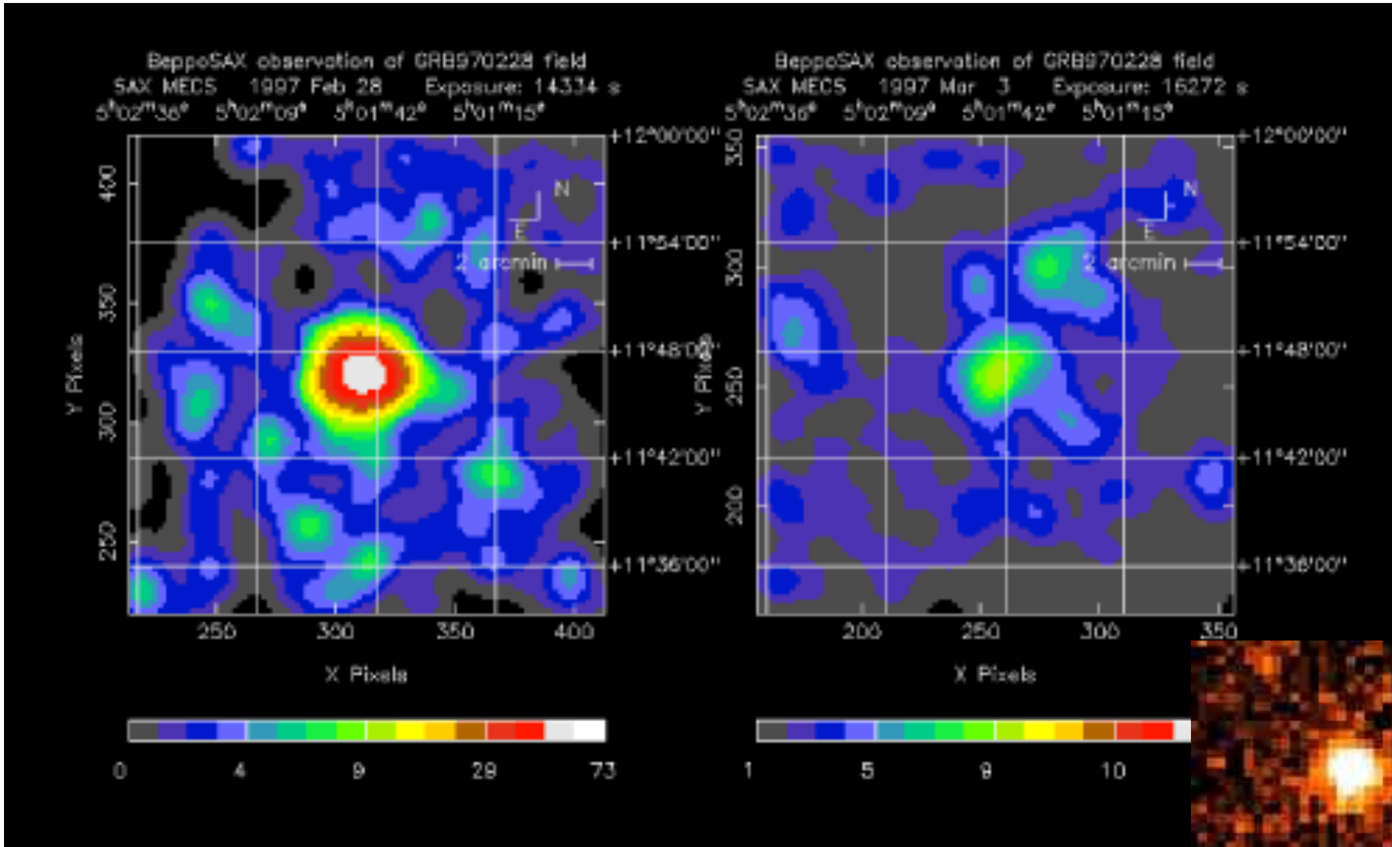

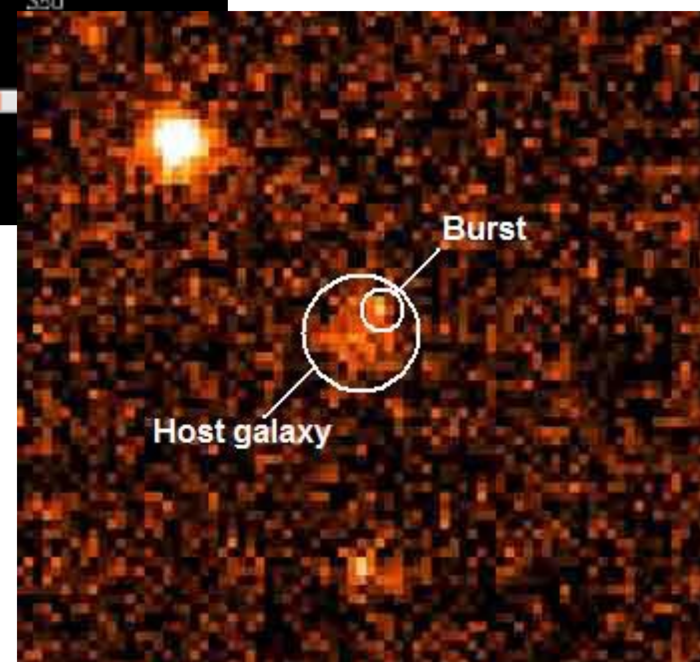

GRB 970228

T_{90} = 80sec

z=0.695 (2.5 Gpc)

Association with Supernovae Type Ib,c

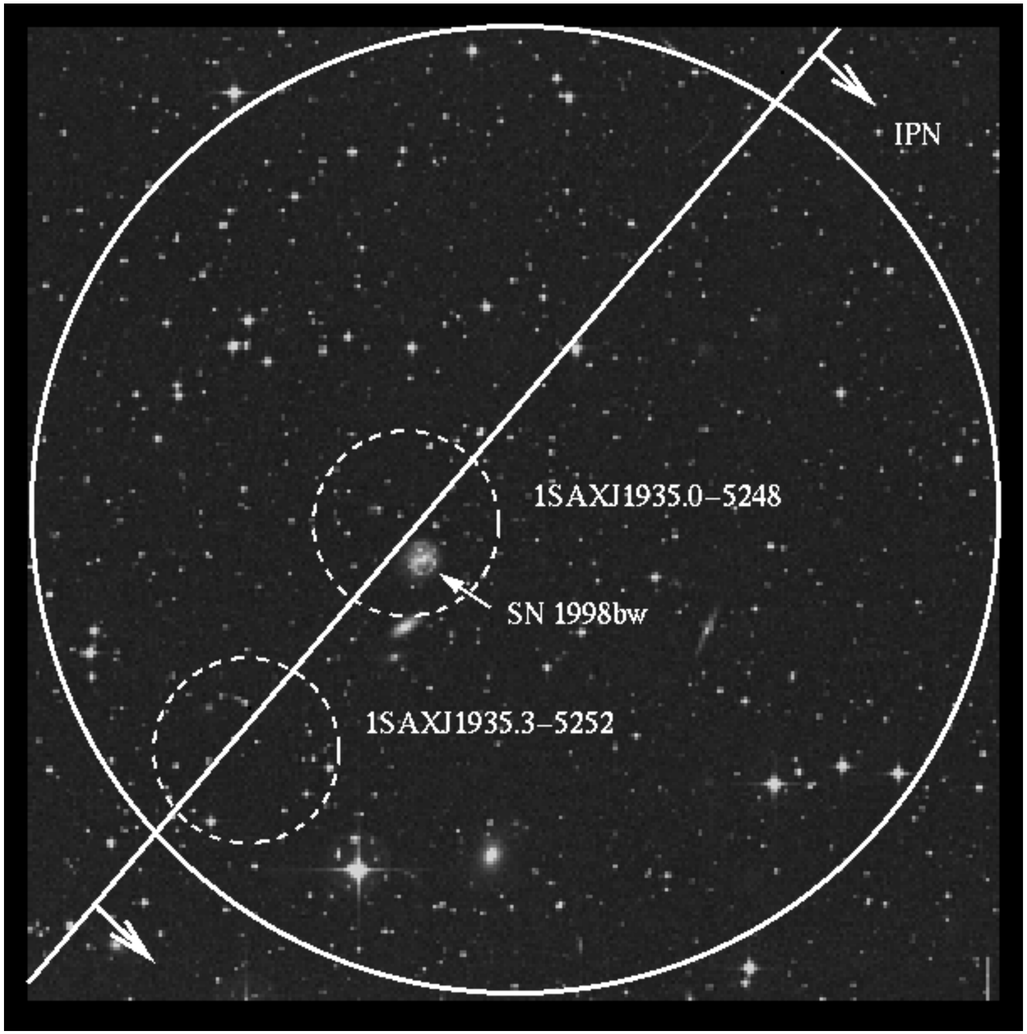

GRB 980425 / SN1998bw (Ic)
T_{90} = 30sec
z=0.0085 (36 Mpc – still the closest GRB on record)

Astronomy 101 Review

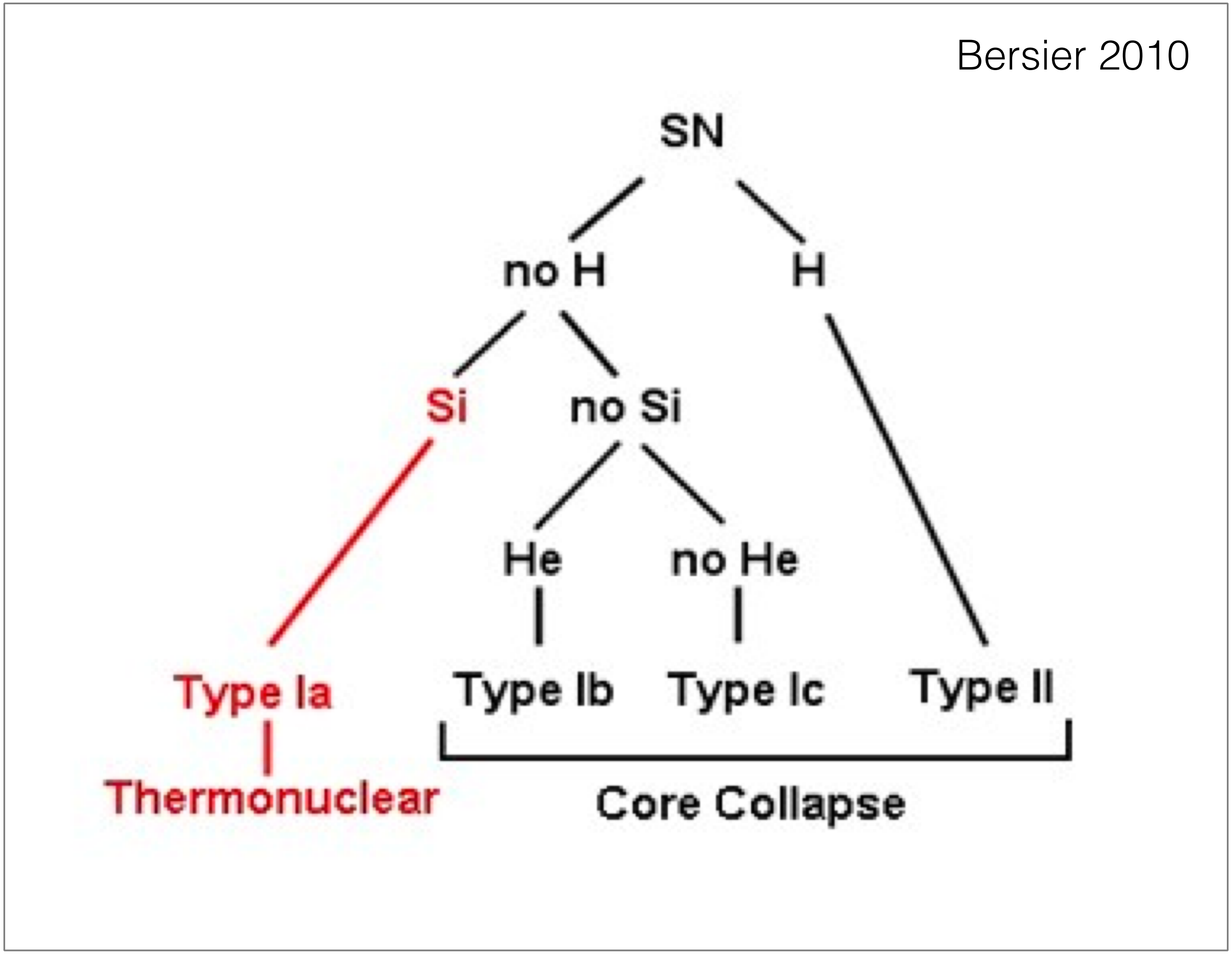

Long GRBs are associated with Type Ib/c supernovae:
core collapse in massive, rapidly rotating stars

Evidence for jets from BNS numerical simulations

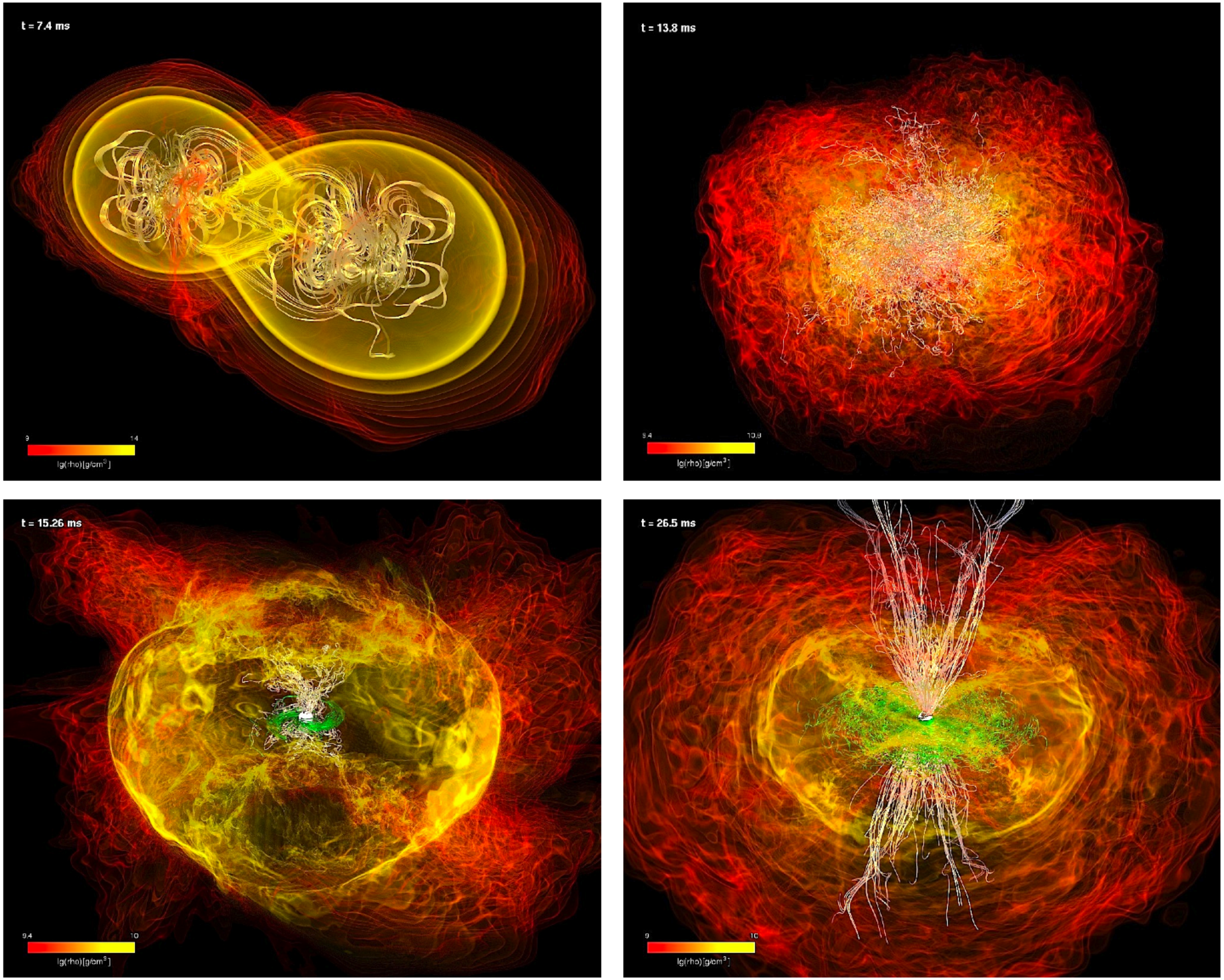

Rezzolla et al. arxiv:1101.4298

Current Gamma-ray Satellite Missions

Swift BAT: arcminute localization

Fermi GBM: several deg localization

Also, the InterPlanetary Network (IPN): high latency, very accurate.

Localizing Gamma-ray Sources

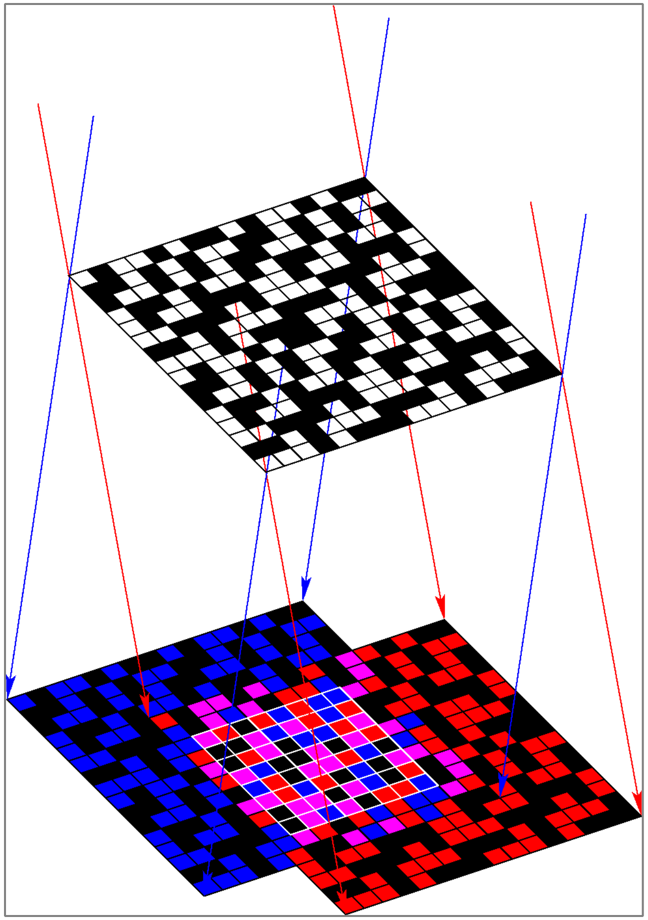

Swift Burst Alert Telescope:
Coded mask, 50% occulted by 5x5mm Pb tiles

Localizing transient gamma-ray sources is a significant challenge. *Swift* relies on rough localization to point x-ray and optical telescopes that search for an afterglow.

Swift – First Localization of a short GRB

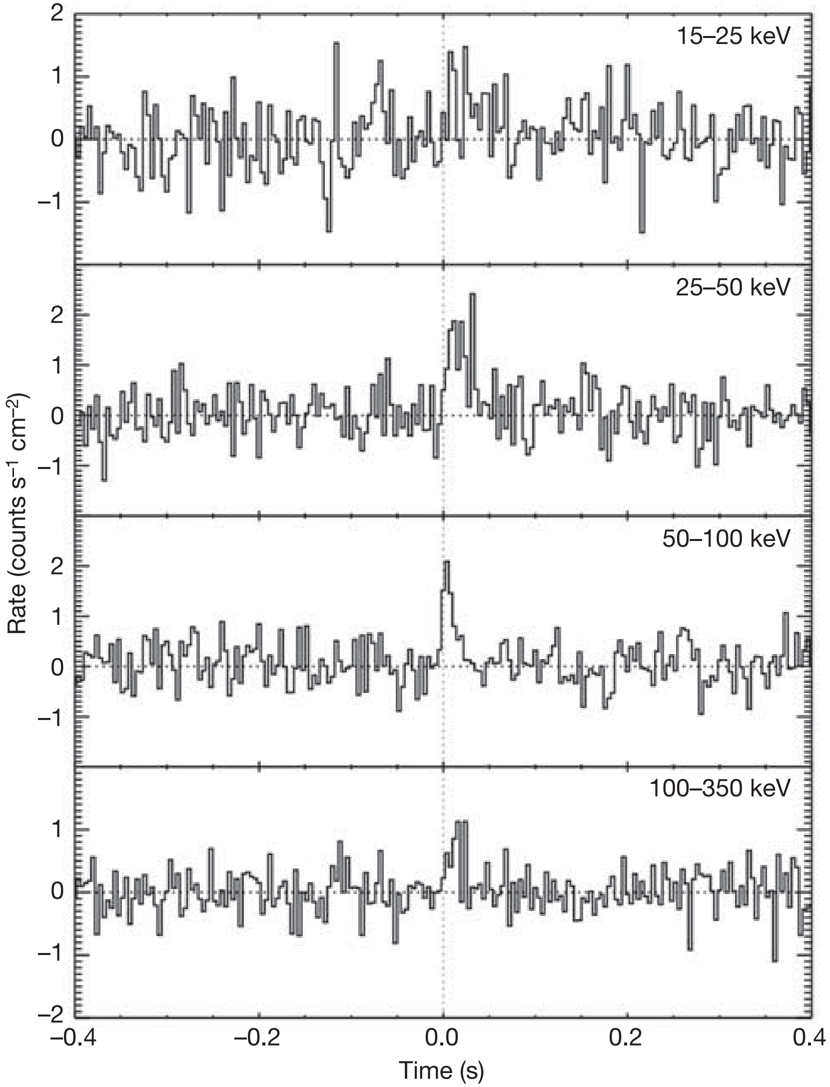

Figure 2 | BAT light curves for the short GRB 050509B, showing the short duration of this GRB. The light curves are given in four photon energy bands with the band identified in the upper right of each panel. The peak has a duration of 40 ± 4 ms (90% containment of counts). There is no

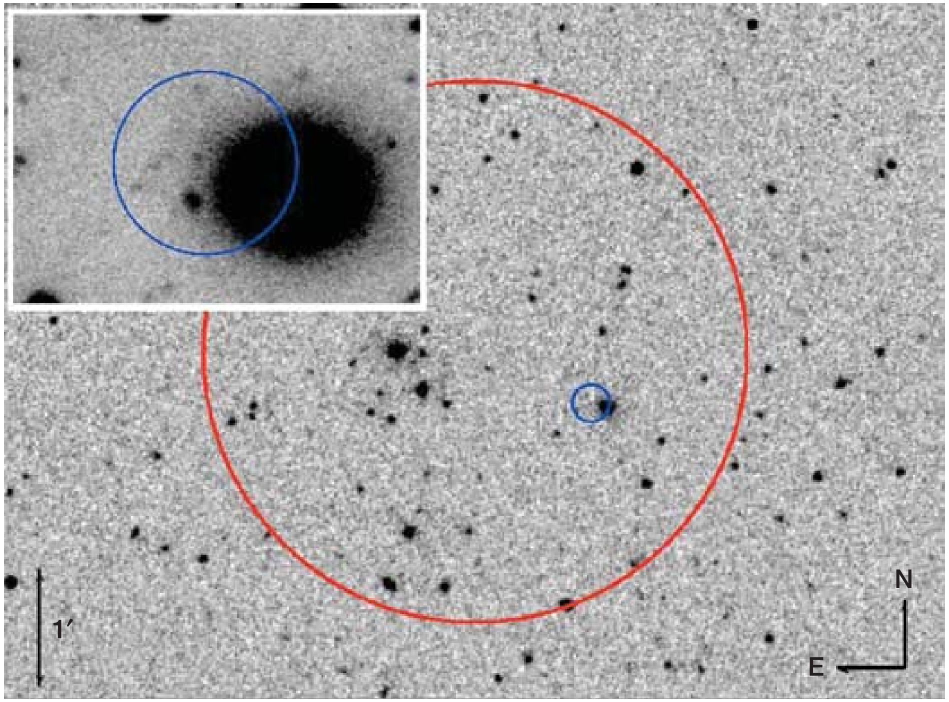

Figure 1 | Optical images of the region of GRB 050509B showing the association with a large elliptical galaxy. The Digitized Sky Survey image.

z=0.225 (900 Mpc)
Gehrels et al., Nature 437, 6

"There may be more than one origin of short GRBs, but this particular short event has a high probability of being unrelated to star formation and of being caused by a binary merger."

Short GRBs – *Swift*-era Localizations

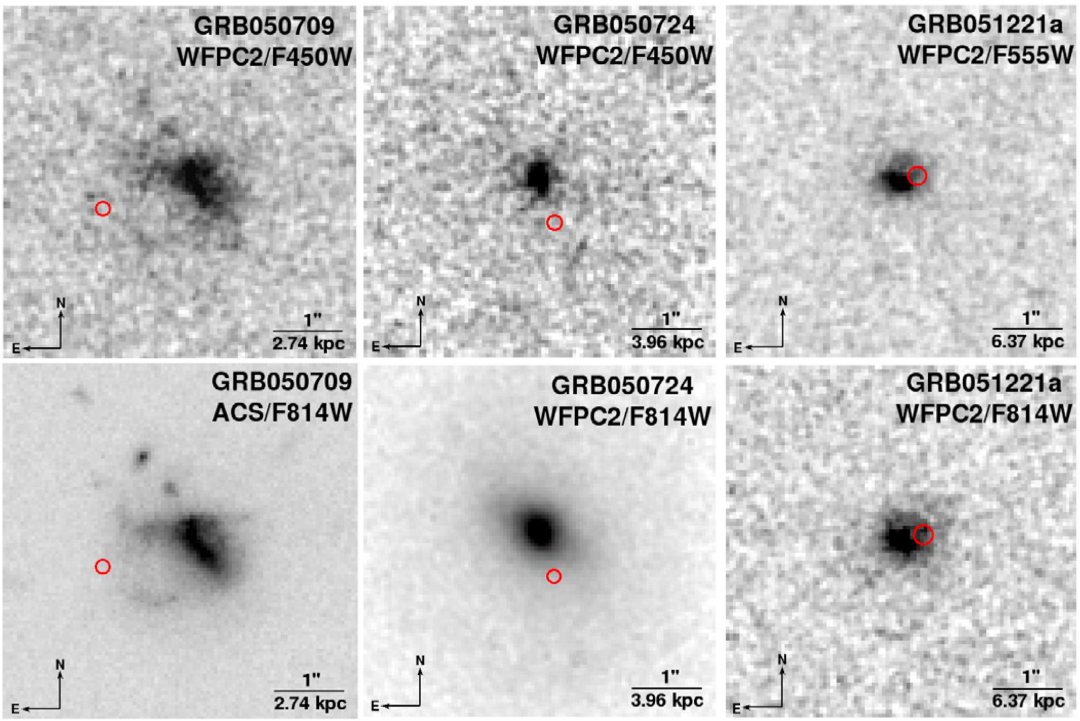

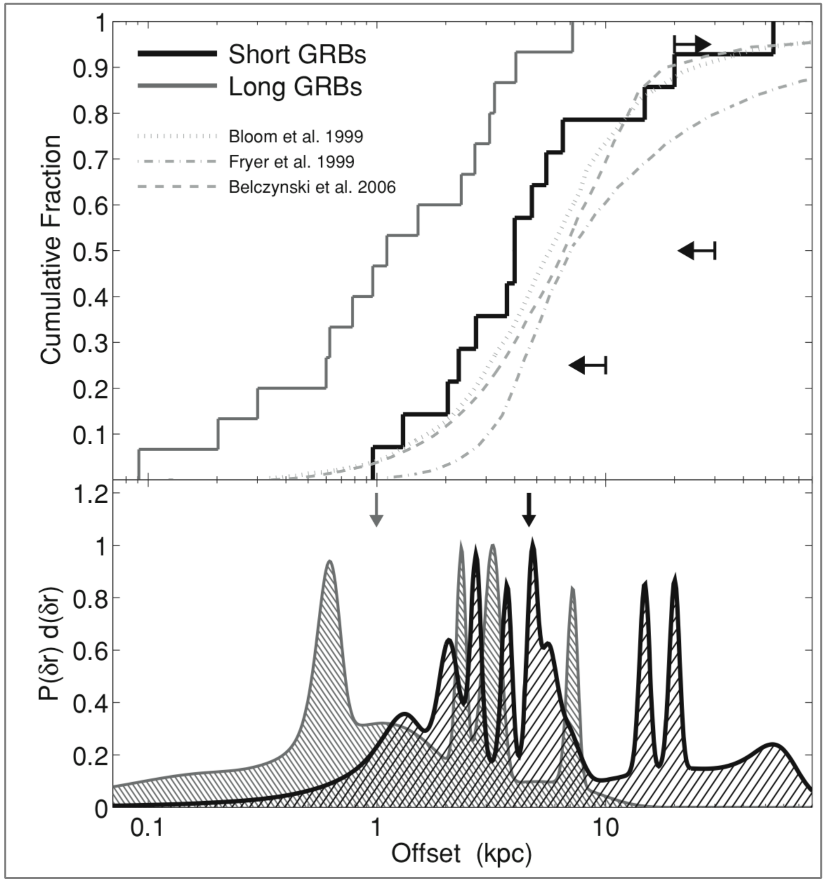

Fong et al., arXiv:0909.1804

The host galaxies of short GRBs are older (elliptical, irregular); sGRBs originate in non-star-forming regions

Short GRBs tend to have larger offsets from the center of their host, consistent with kicks received in formation of NS-NS binaries.

Short GRBs – *Swift*-era Localizations – Redshift observations

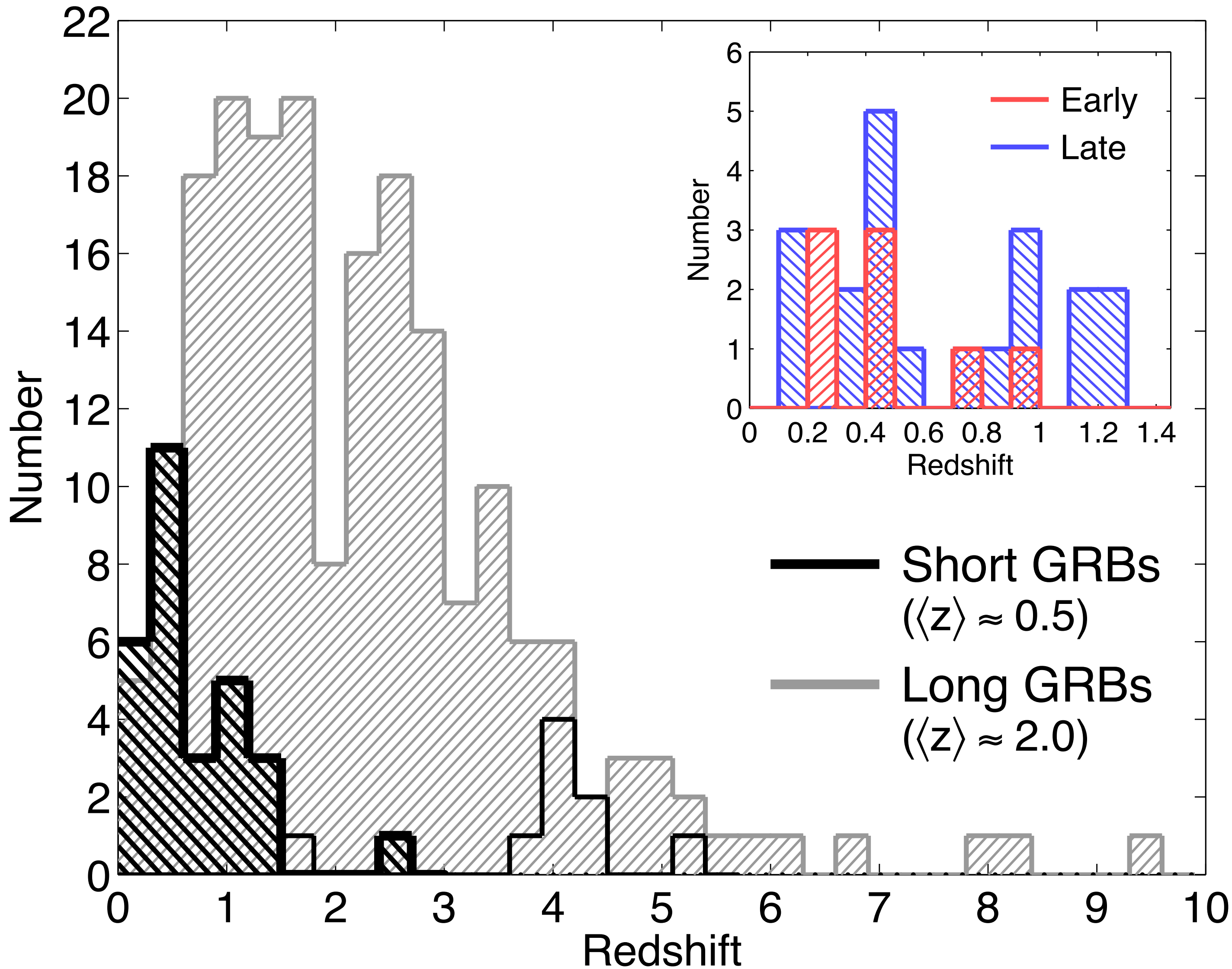

Berger, arxiv:1311:2603

Short GRBs – No SNe Association, to Deep Limits

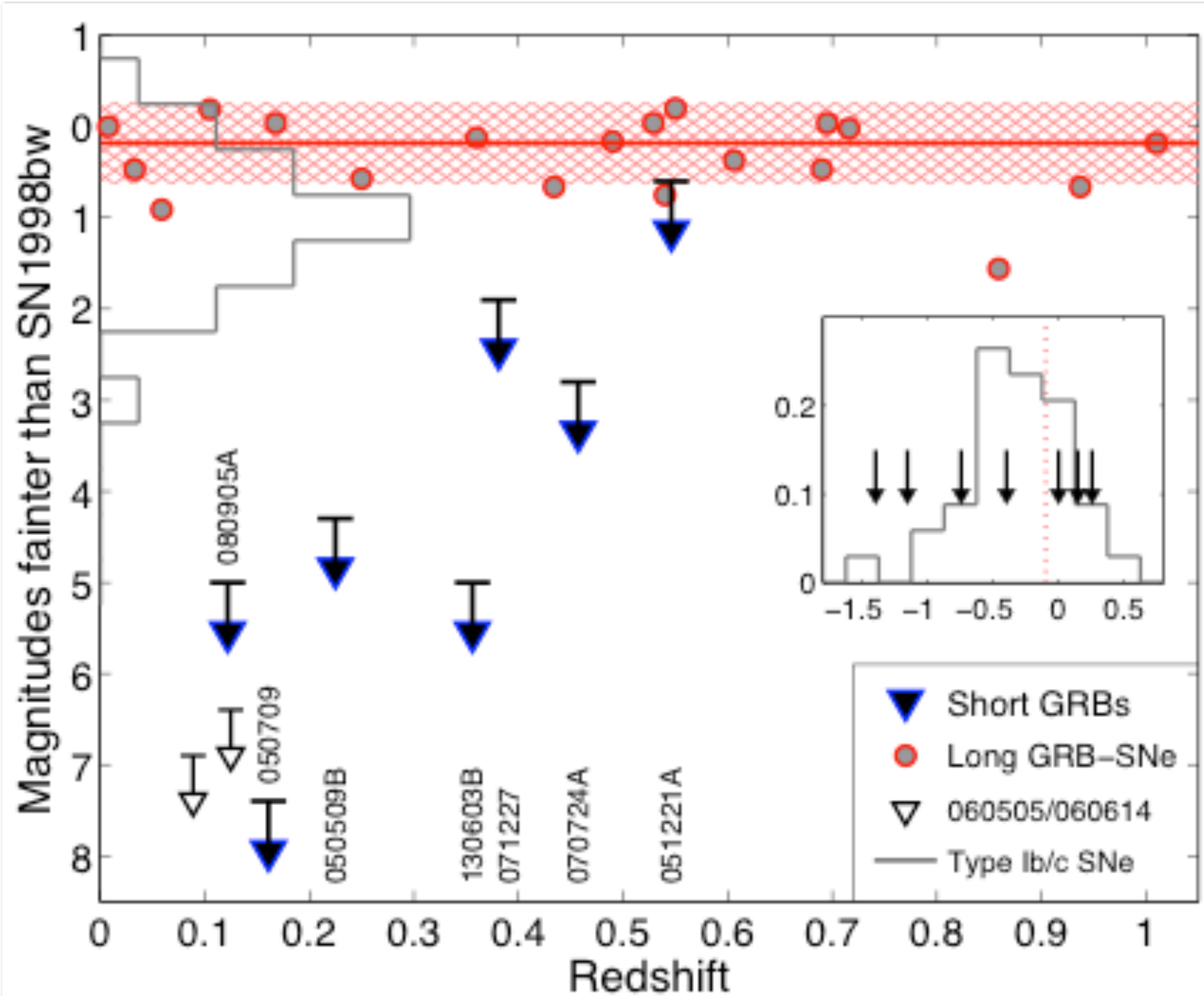

Berger, arxiv:1311:2603

The Fireball Model

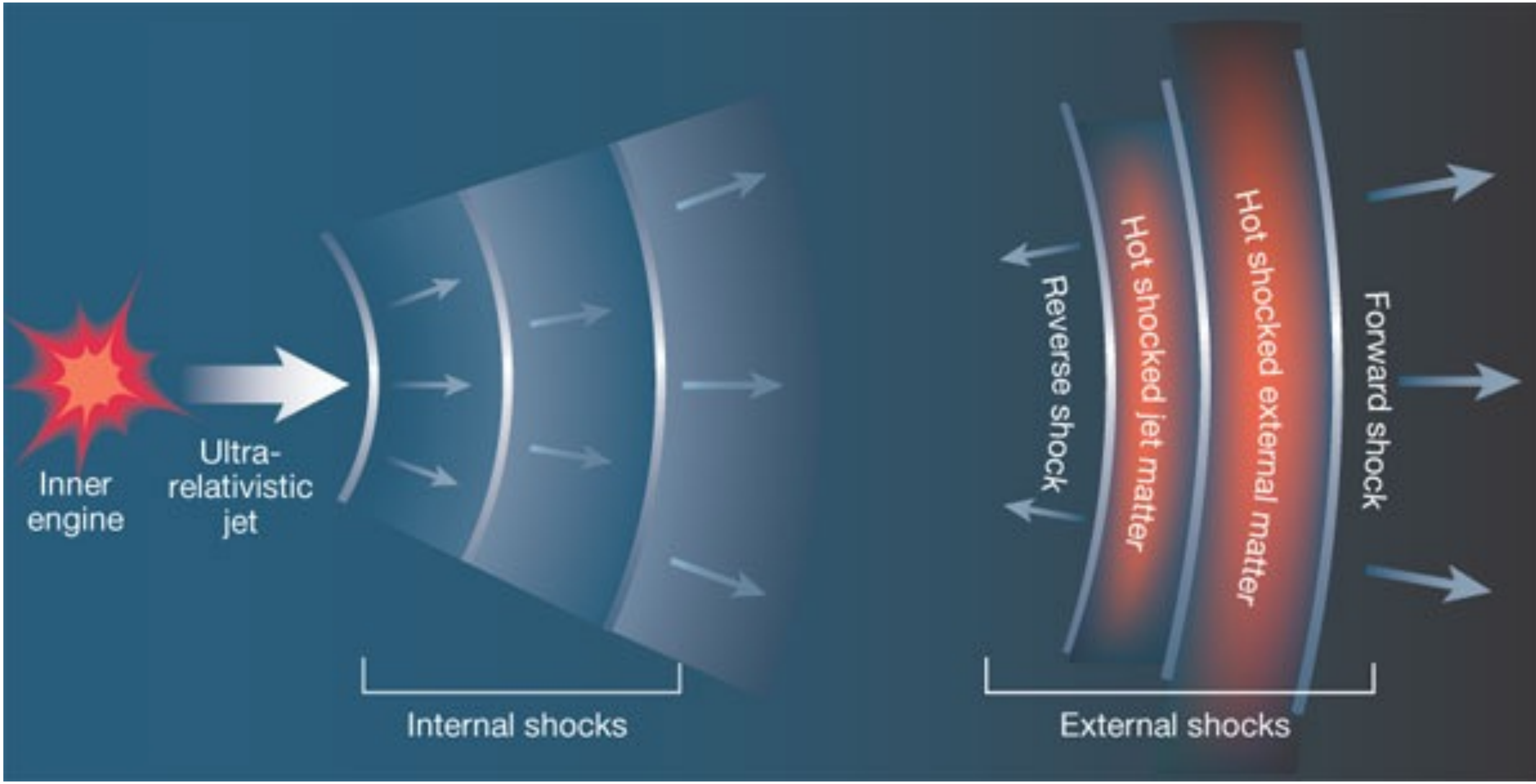

Explains a number of observed features: millisecond structure, afterglows, prompt optical flashes. Is agnostic regarding the central engine.

Relativistic Beaming

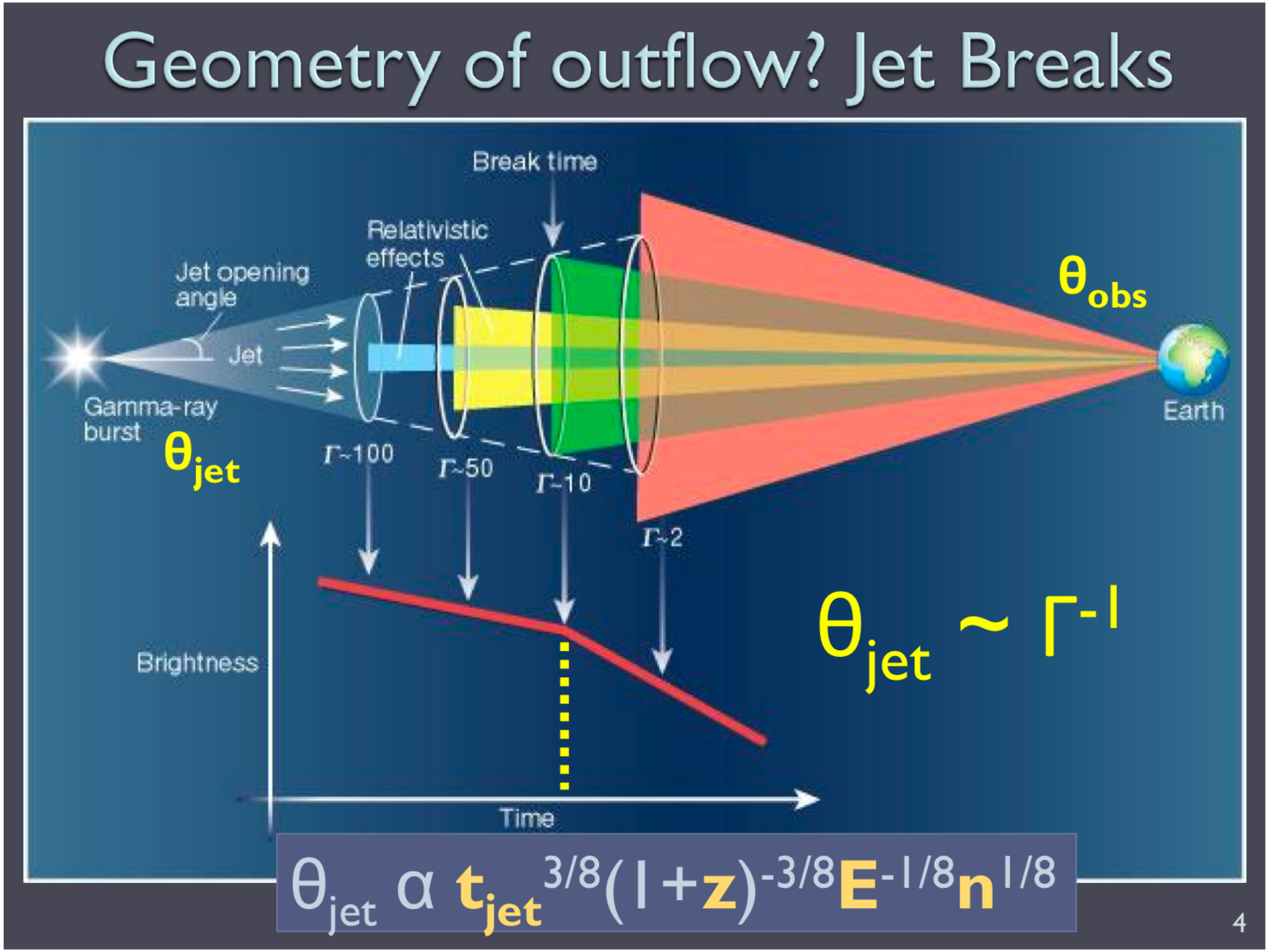

Courtesy W. Fong

Jet Breaks

Jet breaks are a geometric effect – should be seen across all wavelengths/ frequencies ("achromatic").

A crucial parameter when calculating rates.

$$\theta_j = 0.13 \left(\frac{t_{j,d}}{1+z}\right)^{3/8} \left(\frac{n_0}{E_{52}}\right)^{1/8}$$

Berger, arXiv:1311:2603

Includes assumptions of the density of the interstellar medium and the adiabatic expansion of the jet (which determines the evolution of the Lorentz factor)

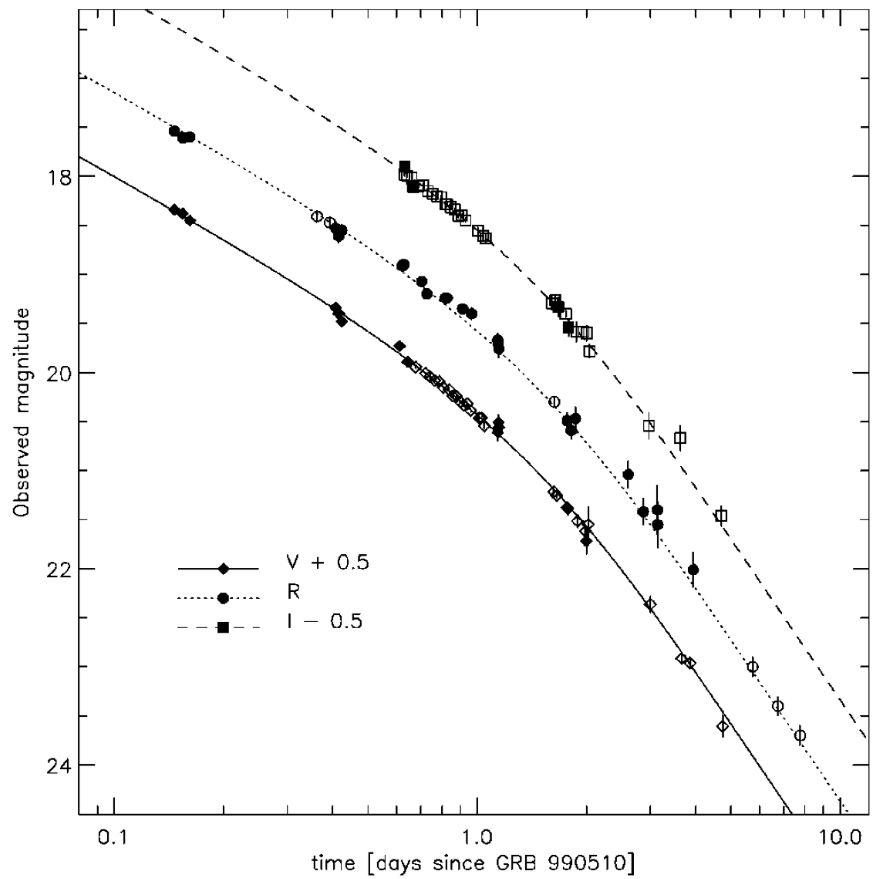

FIG. 8. Optical light curves of GRB 990510. A fit for the observed optical light curves is obtained with $\alpha_1=0.82\pm0.02$, $\alpha_2=2.18\pm0.05$ and $t_*=1.2\pm0.08$ days. From Harrison *et al.*, 1999.

Piran, astro-ph/0405503

Short GRB Rates and BNS/NSBH Populations

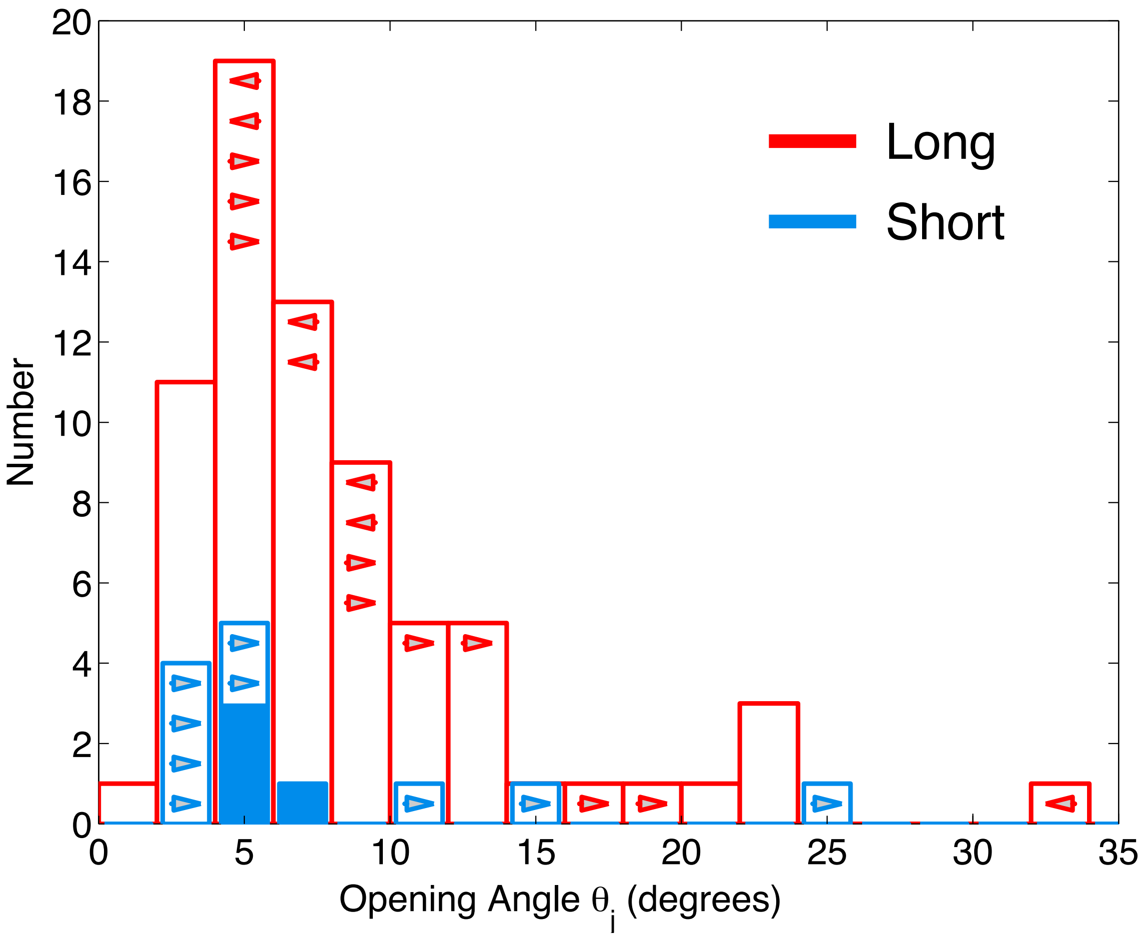

Fong et al. arxiv:1309.7479

5-10deg beaming of short GRBs implies rate of ~300 Gpc^3 yr^-1. This is consistent with NS-NS population studies, *IF* all short GRBs are from binary mergers.

GRB 130603B – kilonova detection

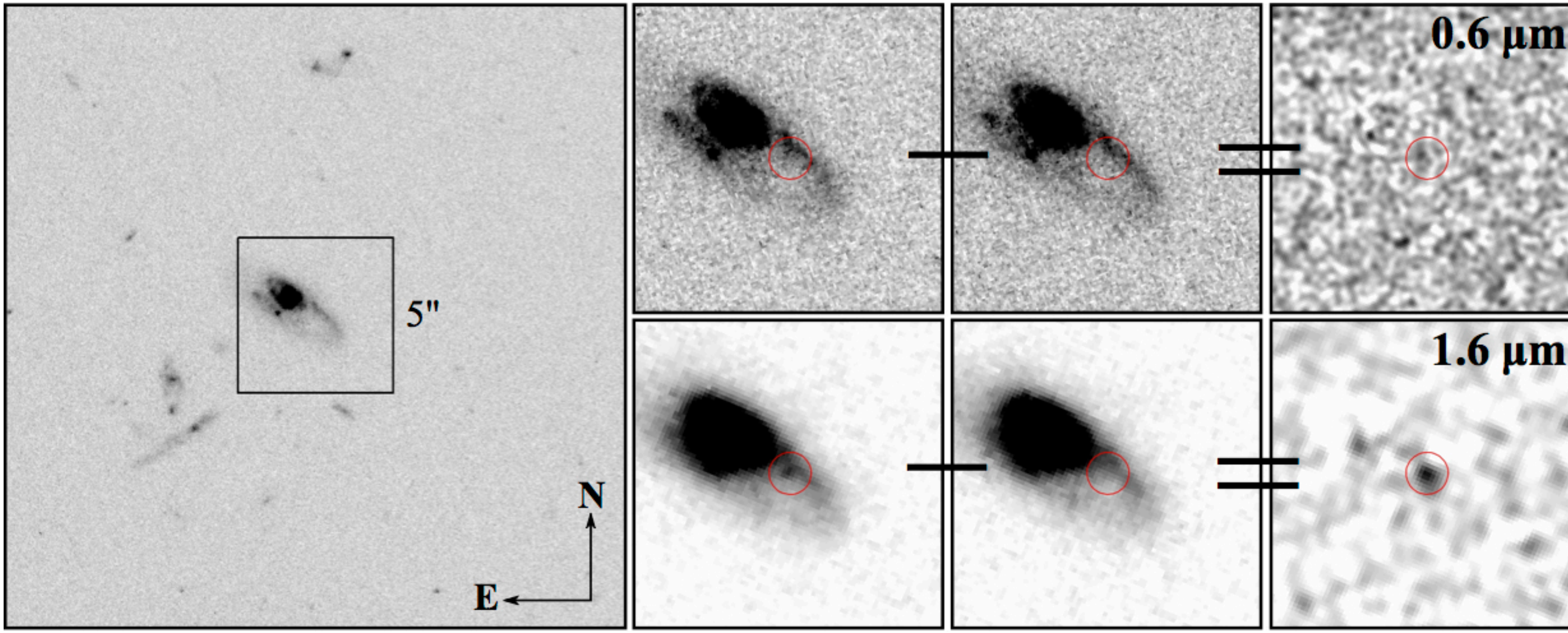

Figure 1 HST imaging of the location of SGRB 130603B. The host is well resolved and displays a disturbed, late-type morphology. The position (coordinates RA_{J2000} = 11

Tanvir et al. arxiv:1306.4971

z=0.356, 1.4Gpc

Kilonova lightcurve

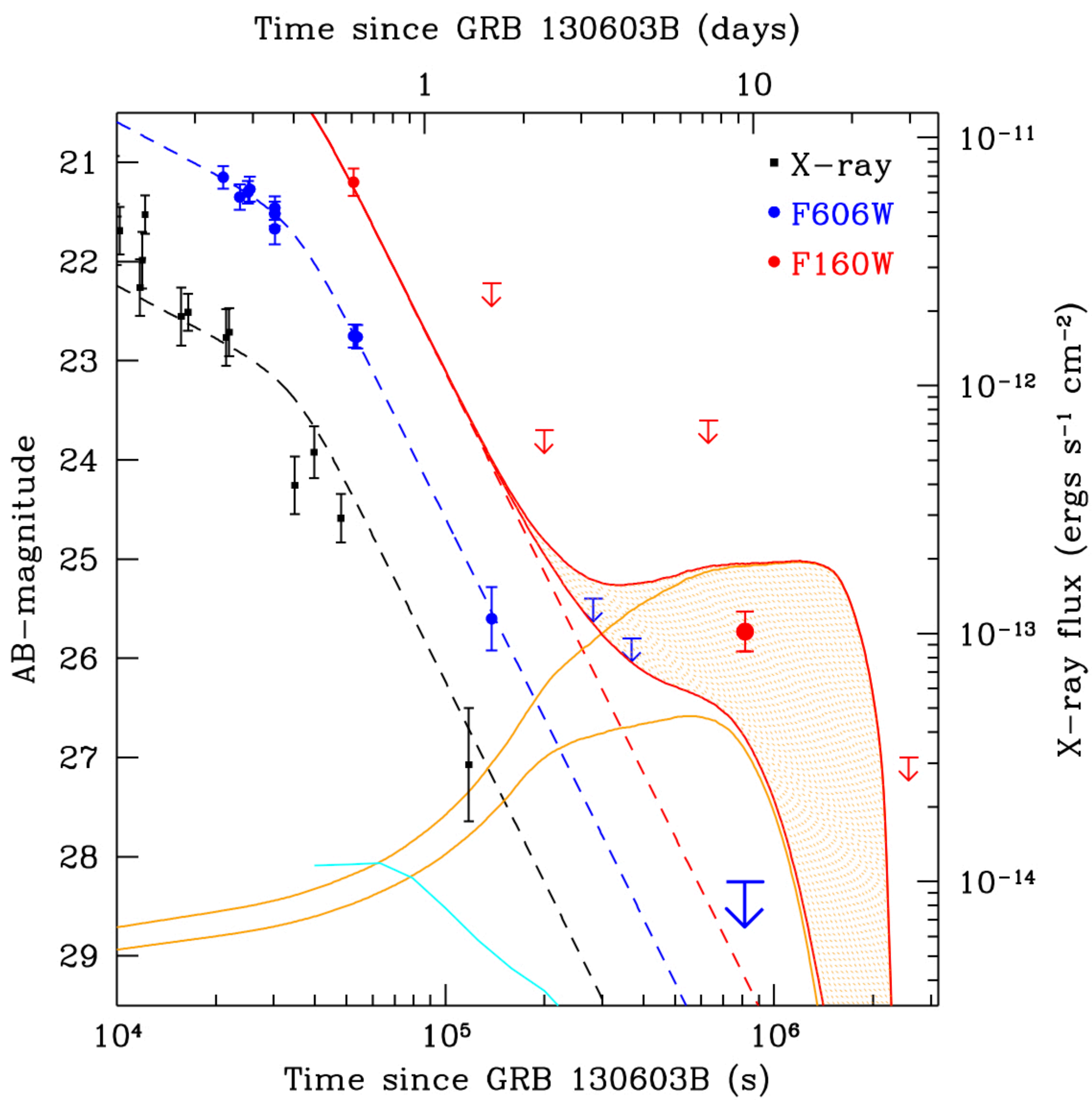

Tanvir et al. arxiv:1306.4971

Kilonova lightcurve

Jet break – implies 6 deg opening angle!

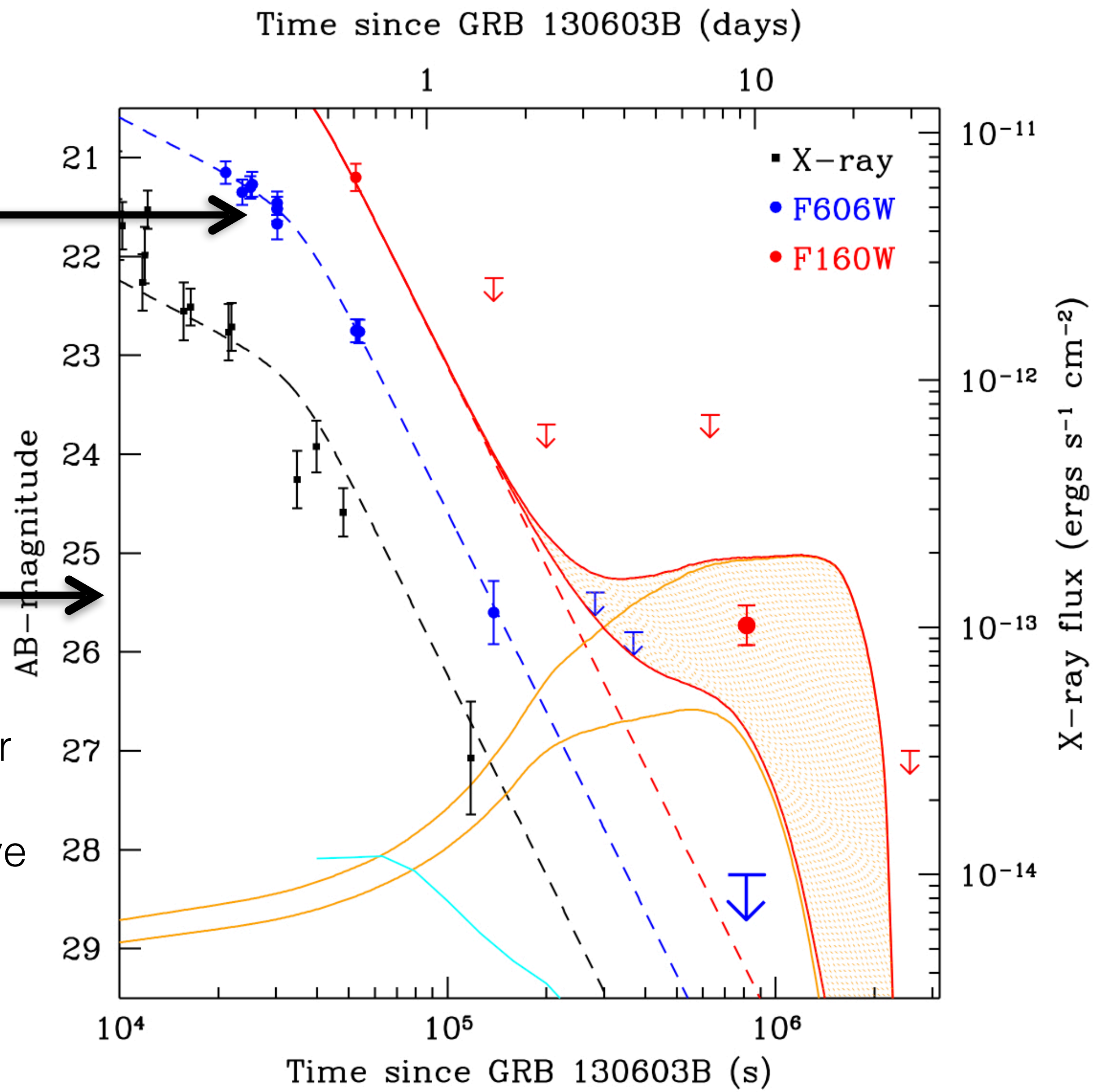

Very faint – needs Hubble or next-generation wide field telescopes to reliably observe

Tanvir et al. arxiv:1306.4971